Investigation of Non-DLVO Forces using an Evanescent Wave Atomic Force Microscope

Clayton T. McKee

Dissertation submitted to the faculty of the Virginia Polytechnic Institute and State University in partial fulfillment of the requirements for the degree of

Doctor of Philosophy
In
Chemistry

Dr. William A. Ducker, Committee Chair
Dr. Mark R. Anderson
Dr. Richey M. Davis
Dr. James M. Tanko
Dr. Roe-Hoan Yoon

June 26th 2006
Blacksburg, Virginia

Keywords: EW-AFM, AFM, evanescent wave scattering, thin film refractive index, steric force, hydration force, hydrophobic force

Investigation of Non-DLVO Forces using an Evanescent Wave Atomic Force Microscope

Clayton T. McKee

Abstract

This dissertation describes new methods for measuring surface forces using evanescent waves, and applications to non-DLVO forces. An evanescent wave, generated at a solid-liquid interface, is scattered by AFM tips or particles attached to AFM cantilevers. The scattering of this wave is used to determine absolute separation between surfaces and/or the refractive index as a function of separation in AFM measurements. This technique is known as evanescent wave atomic force microscopy (EW-AFM). The scattering of an evanescent wave by Si_3N_4 AFM tips is large and decays exponentially with separation from a refractive index boundary. Thus, scattering is a useful method for measuring the separation between a Si_3N_4 tip and sample. This method has been used to measure the absolute separation between a tip and sample in the presence of an irreversibly adsorbed polymer film. Measurement of the film thickness and time response of the polymer to applied loads has also been studied. These measurements are not possible using current AFM techniques. In addition to measurements in polymer systems, the simple scattering profile from Si_3N_4 tips was used to re-examine short range hydration forces between hydrophilic surfaces. Results presented in this thesis suggest this force does not depend on the hydrated radius of the ion between glass and silicon nitride. The scattering generated by a Si_3N_4 tip has also been used to measure the refractive index of bulk fluids and thin films between hydrophobic surfaces. Based on these results, I have shown that a long-range attraction between hydrophobic surfaces is accompanied by an increase in the refractive index between the tip and surface. From this I have concluded that the attractive force, measured in this study, is the result of an increase in the concentration of organic material between surfaces. Finally, I have shown that the scattering profile depends on the material and size of the scattering object. Scattering from silicon nitride tips is exponential with separation. In contrast, the scattering profile from silicon tips, which are similar in size and geometry, is not a simple exponential. The scattering profile of larger spherical particles attached to cantilevers is also not exponential. It is approximately the sum of two exponentials. The functional form of the scattering profile with separation is consistent with the transmission of evanescent light through flat planar films. This result would suggest that a re-examination of the separation-dependence of scattering in TIRM measurements is necessary.

Acknowledgments

I would like to thank my advisor, Dr. William Ducker, for his guidance and support during my PhD. My understanding of surface chemistry is, in no small measure, a result of William's ability to teach, guide, and challenge his students to become scientists. I was lucky to have the opportunity to learn from William.

I would like to thank Bill Lokar and Aysen Tulpar for freely passing on to me, the things they learned during their PhD's. Bill and Aysen are good friends. Thank you for your support during my PhD. To my friends at the University of Melbourne, thank you for making Lori and me feel welcome.

I would like to thank my parents, Dan and Cheri. I could fill a page thanking you for the things you've done to help, at the end of which, I'm sure I would have left out most everything. I will simply say thank you, and I will try not to ask for any more money after this.

Finally, I want to thank my wife Lori. You have shared this with me for all its ups and downs. Your selfless support always kept me going when I wanted to stop. I could not have done this without you. Thank you.

Table of Contents

Chapter 2 Scattering Intensity vs. Separation for Particles in an Evanescent Field…....37

Chapter 3 Measurement of the Absolute Separation between Surfaces ………………..62

List of Figures

List of Tables

Chapter 1

Introduction and Literature Review

1.1 Introduction

Colloidal dispersions and their stability are determined by interactions between individual particles and or groups of particles, where the ratio of surface area to volume is quite large. To better understand the factors that affect the physical properties of a dispersion requires a theoretical and experimental understanding of the distance dependence of the force that exists between two surfaces. Because the forces are very small (μN to nN) and are inversely proportional to some function of distance, experimental measurement is quite difficult. During the last thirty years, many techniques/instruments have been developed to quantify these forces; they include the osmotic stress technique[1-3], the Surface Forces Apparatus (SFA)[4], the Thin-Film-Balance[5-7], the Force Balance[8], the Atomic Force Microscope (AFM)[9, 10], and Total Internal Reflectance Microscopy(TIRM)[11, 12], to name a few. This thesis describes development and application of a new instrument that is used to further the fundamental understanding of colloidal forces. This instrument can be used to monitor both the absolute separation and refractive index between two microscopic surfaces (output similar to SFA) by combining instrumental analysis techniques of the AFM and TIRM. This instrument has been termed an Evanescent Wave Atomic Force Microscope (EW-AFM)[13]. I have used the EW-AFM to study non-DLVO forces (hydrophobic, steric, and hydration forces) between Si_3N_4 and glass substrates in aqueous solutions. The EW-AFM uses scattered evanescent light as a tool to characterize surface forces. Therefore, in addition to the study of non-DLVO forces, I have conducted a detailed study on the interaction of colloidal-sized particles interacting with evanescent waves.

This introduction includes a review on the theoretical framework to which experimentally measured forces are compared. In addition, the surface force apparatus, the atomic force microscope, and total internal reflection microscopy have been reviewed. These three instrumental techniques provide the background and serve as a point of comparison to the design and application of the Evanescent Wave Atomic Force Microscope.

1.2 Theory of Surface Forces

The force between two surfaces is defined by a change in the free energy, V as a function of separation, h.

$$F = -\frac{dV}{dh} \tag{1.1}$$

The negative sign ensures that positive quantities are repulsive. Forces can be classified as conservative and non-conservative. Frictional forces for example, are not conserved. The total work done is dependent on the path taken between an initial and final point, and therefore not recoverable. Electrostatic and van der Waals forces are conserved; the force does not depend on the path taken between two points.

Because colloidal particles are not limited to a single geometry, the force between identical materials with varying geometries will be different. Most results are presented as the energy per area (V_A) between two flat sheets. This interaction can be compared to the force between particles with different geometry, through Derjaguin's approximation[14].

$$V_A = \frac{F_{sphere-flat}}{2\pi r} \quad \frac{F_{sphere-sphere}}{\pi r} \quad \frac{F_{cylinder-cylinder}}{2\pi r} \tag{1.2}$$

Where r is the radius of particle and F is the force between the points of smallest separation. The approximation is that both the range of the interaction and the separation is much smaller than the radius of the particle. Because of the direct relationship between F and V_A, they are often loosely interchanged when discussing surface interactions. Note that V and V_A are different; V_A is the derivative of V, when Derjaguin's approximation is valid.

1.2.1 DLVO Theory

The first attempts to predict the interaction between two solid surfaces in simple electrolyte solutions was conducted independently in two different research groups, without the knowledge of the other, at approximately the same time. Derjaguin and Landau in Russia[15], and Verwey and Overbeek in Amsterdam[16]. Both groups stipulated that the dominant interactions between two charged lyophobic (hydrophobic) particles in electrolyte solution could be described by the sum of an electrostatic repulsion, and a van der Waals (vdW) interaction. This is now known as DLVO theory (named after the authors,) and is widely used as a first approximation to most forces measured in surface science.

$$\frac{V_{total}}{A} = \frac{V_{electrostatic}}{A} + \frac{V_{vdW's}}{A} \tag{1.3}$$

In practice, DLVO does not accurately describe the forces between all surfaces, although it does well in many cases. In particular, it only applies to lyophobic particles and long range forces. Interesting exceptions to DLVO include long range attractions between hydrophobic surfaces [17, 18], strong short range repulsions between hydrophilic surfaces[19-21], and steric forces[22, 23].

1.2.1.1 Electrostatic Double-Layer Forces

The electrostatic force between surfaces can be attractive or repulsive; it depends on the surface charge density and surface potential of each surface, and the physical properties of the medium separating the two surfaces. When surfaces are immersed in water, the high dielectric constant of the water causes surface groups to dissociate, which results in a charged interface (alternatively, selective adsorption of ions from solution can charge a surface). An example of this is the dissociation of silanol groups at the surface of a silica substrate. The dissociation of the surface silanol groups creates a diffuse layer of oppositely charged ions, whose concentration decreases as a double exponential with distance away from the solid-liquid interface.

$$c_x = c_o \exp\left(\frac{-ze\psi_x}{kT}\right) \tag{1.4}$$

$$\psi_x = \psi_o \exp(-\kappa x) \tag{1.5}$$

Where c_x is the concentration at a distance x from the solid liquid interface, c_o is the concentration of ions in bulk, z and e are the valency and charge of the ion, ψ_x is the surface potential at a distance x, and finally k and T are Boltzman's constant and the temperature. Equation 1.5 describes how the surface potential ψ, varies as a function of distance, and the inverse debye length κ, to be discussed in the next paragraph. Equation 1.5 is valid when surfaces exhibit a low potential (<50 mV). A schematic representation of dissociated ions next to a surface is shown in figure 1.1. This diffuse layer of ions is termed the double layer[24].

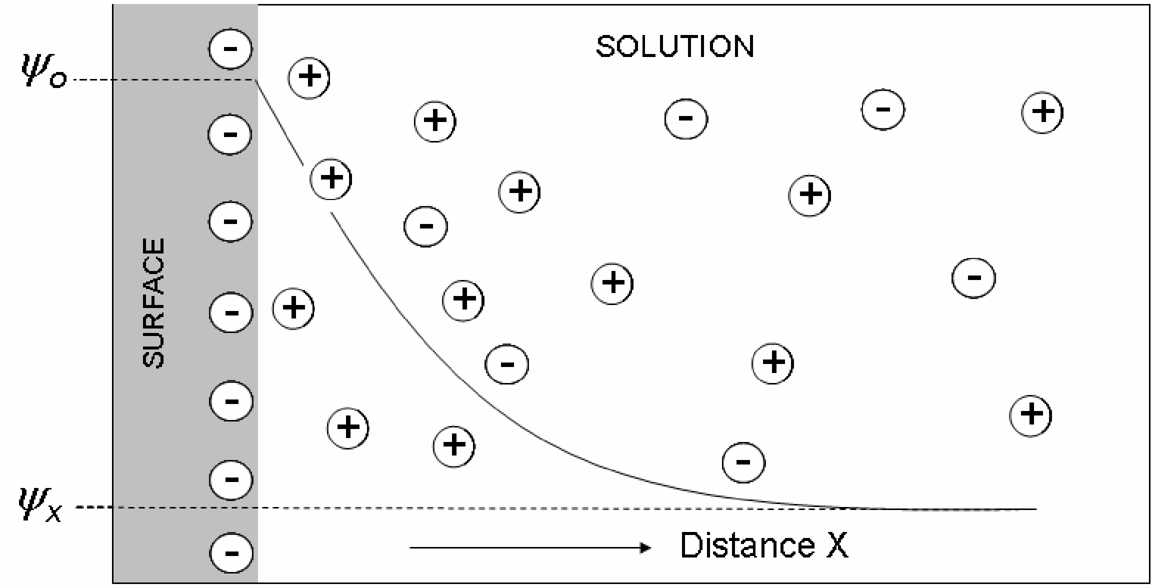

Figure 1.1. Schematic of a diffuse double layer of oppositely charged ions, whose concentration decreases to that of the bulk as a function of distance. The surface potential ψ_o*, decays exponentially as a function of distance, x.*

When double layers from opposing surfaces of equal charge overlap, a repulsive force results between the two surfaces and is described by:

$$\frac{F}{A} = 64kTc_o\Gamma_o^2 \exp(-\kappa h) \tag{1.6}$$

$$\frac{V}{A} = -\frac{64kTc_o\Gamma_o^2}{\kappa}\exp(-\kappa h) \tag{1.7}$$

Where k is Boltzmann's constant, T is the temperature, c_o is the concentration of ions in the bulk, and h is the separation. Γ_o gives a measure of how the bulk ion charge e, ion valency z, and surface potential ψ affect the force. Finally κ, the inverse debye length, describes how the bulk electrolyte concentration affects the length of the double layer, and is a good measure of the range at which an electrostatic force will appear.

$$\Gamma_o = \tanh\left(\frac{ze\psi_o}{4kT}\right) \tag{1.8}$$

$$\kappa^{-1} = \left(\frac{\varepsilon_r\varepsilon_o kT}{\Sigma(ze)^2 c_o}\right)^{1/2} \tag{1.9}$$

$$\kappa^{-1} \approx \frac{0.3nm}{\sqrt{c_o/M}} \; for\ a\ 1:1\ electrolyte\ in\ water\ at\ 25^o C \tag{1.10}$$

Equation 1.7 is an analytical solution valid for weakly overlapping double layers and for a symmetrical z:z electrolyte. More complex systems require a numerical solution.

Equation 1.7 demonstrates that electrostatic forces decay exponentially with distance and depend on the concentration of ions in the bulk. This equation does not take into account the more complex situation of separation-dependent changes in surface charge density or surface potential. The surface potential/charge density of a solitary surface is a function of the proximity of a second, this is known as surface charge regulation and is described in greater detail in[25]. An extreme case of surface charge regulation can occur when the surface potentials of the same sign on opposing surfaces are very different. On approach the smaller charged surface can change sign and the force switches from repulsive to attractive. As surface charge regulation is hard to measure/quantify, two limiting cases of constant surface charge density and constant surface potential are used when fitting the electrostatic force. Experimentally, the measured force usually lies somewhere between the two extremes.

1.2.1.2 van der Waal's Forces

The second term included in DLVO is the vdW force. The vdW force can be either attractive or repulsive, and is always attractive between identical materials. The vdW force is the result of time-dependent electrical dipoles, and is difficult to calculate between macroscopic materials. A simplifying approximation is to assume that the interaction is a pair-wise additive (Hamaker theory[26]). If one simply sums the force over all pairs of atoms in both solids, the interaction is given by the following simple expression.

$$\frac{F}{A} = -\frac{H_{121}}{6\pi h^3} \tag{1.11}$$

$$\frac{V}{A} = -\frac{H_{121}}{12\pi h^2} \tag{1.12}$$

H_{121} is the Hamaker constant[26] between particles '1' in medium '2', and is a measure of the magnitude of interaction between two surfaces. Because the vdW force is a polarization force, each pair-wise interaction is not independent and a more accurate description must include many body effects. Hamaker constants are most accurately calculated by Lifshitz theory[27, 28], which determines the magnitude of interaction through the frequency dependent dielectric properties of the intervening media.

The total interaction in DLVO theory is obtained by summing the electrostatic and van der Waals contribution. With the electrostatic and vdW potential described under previous mentioned assumptions, the total interaction is:

$$\frac{V}{A} = -\frac{H_{121}}{12\pi h^2} - \frac{64kTc_o\Gamma_o^2}{\kappa}\exp(-\kappa h) \tag{1.13}$$

Equation 1.13 gives both a theoretical frame work to predict and compare experimentally measured forces, and knowledge of how surface interactions can be controlled.

1.2.2 Non DLVO Forces

1.2.2.1 Hydrophobic Force

Initial studies on the forces between mica surfaces with adsorbed surfactant molecules[17, 29], demonstrated the existence an attractive force (termed hydrophobic force) that exceeded the calculated van der Waals attraction between the bare substrates. Subtracting the predicted DLVO force from the attractive force, resulted in an exponentially decaying attractive force, with a decay length of 1.0 nm (subtracting DLVO theory from experimentally measured forces requires a high degree of confidence in extrapolated theoretical fits, which could result in a significant error in the magnitude of the additional force). The authors' initial interpretation was that the *hydrophobic effect*[30] between hydrocarbon chains of the surfactant tails may have been the cause of this additional force. Further work by Claesson[31] and Rabinovich[32] confirmed the existence of this additional attractive force, and showed that the range of the force could be greatly enhanced by increasing the hydrophobicity of the surface. This means the hydrophobic effect alone cannot describe the entire force-separation profile.

Surface hydrophobicity is generally characterized by the degree to which water will wet a surface, through the Young-Laplace equation:

$$\gamma_{sv} = \gamma_{sl} + \gamma_{lv} \cos\theta \tag{1.14}$$

Equation 1.14 describes a droplet on a flat surface, where γ_{xy} is the interfacial tension of the solid-vapor, solid-liquid, and liquid-vapor phases respectively, and θ is the angle created at the three phase contact line. If we look at the specific condition of a water droplet on a hydrophobic solid in air, an interesting condition occurs above a contact angle of 90 degrees. Above 90^{o} there is a driving force to increase the area of the solid-vapor interface at the expense of the solid-liquid interface. This condition has driven to the forefront of hydrophobic force studies, an argument for the existence/creation of air bubbles on hydrophobic surfaces, that can span the distance between opposing surfaces to create the additional attractive force[33-35].

The formation of an air/vapor bubble between two surfaces will obviously lead to a large change in the refractive index. Direct measurement of a change in refractive index consistent with the formation of a bridging bubbles has been observed with the surface force apparatus between *macroscopic* surfaces[18, 31, 36]. These results are generally accepted in the surface science community. The larger debate has now centered on AFM results of the long-range attraction between *microscopic* surfaces. Again, the most popular mechanism suggests the existence of pre-existing bubbles or the formation of a proximity induced bubble[34, 35, 37]. Indirect evidence for small nanobubbles on surfaces has been reported by AFM imaging techniques[38], and the long range interaction seems to depend on the amount of dissolved gas in solution[37, 39]. Additionally, researchers have shown that the long-range character of the force does not depend on salt[40], suggesting a non-electrostatic mechanism. Sadly, these AFM methods are ambiguous at best, because no direct information on the refractive index is available by AFM analysis. Further complicating the topic of the hydrophobic force are published reports that do not confirm the above mentioned mechanism. These include AFM images[41], force analysis[41, 42], and ellipsometry measurements[43, 44]. These discrepancies suggest that AFM measurements alone are not sufficient to elucidate the mechanism of the hydrophobic force.

Additional mechanisms have been proposed to describe the hydrophobic force and include: surface induced water structure[40, 45, 46], proximity induced density fluctuations in the aqueous medium separating two surfaces[46], pH effects[42, 47], and lateral movement of adsorbed surfactant molecules on surfaces[47, 48].

1.2.2.2 Steric Force

The majority of interfaces used in surface force experiments are not molecularly smooth (exceptions include mica, and mercury). The non homogeneous nature (roughness) of surfaces can lead to short range effects which are quite small, and usually affect the adhesion between two surfaces [49]. A more pronounced effect occurs between surfaces with large adsorbed molecules at the solid interface, which in effect increases the inhomogeneity of a surface[22, 50-52]. Polymers can adsorb to an interface through electrostatics or hydrophobic interactions, and adopt conformations that are dictated by the solvent adjacent to the solid. In polymer force studies, solvents are referred to as good or bad solvents. For example, polyethylene oxide (PEO) will adsorb to mica in water, and a long range repulsive force is measured as two surfaces are brought together[53]. Water is a good solvent for PEO, which means that portions of the polymer chain that are not involved in direct interaction with the surface, will be extended into the solvent away from the surface. As two surfaces approach, the conformational freedom of extended polymer chains from opposing surfaces decreases (decrease in available volume), which results in an entropic or *steric* repulsion. If the PEO is in a bad solvent, the adsorbed polymer chains have a stronger affinity for the surface. This means the repulsive force between the surfaces is manifest at a much shorter range. Steric forces can at times exceed both the van der Waals force and the longer range electrostatic force, and so are commonly used as stabilizers for colloidal dispersions[54].

As will be discussed later in the introduction, steric forces are difficult to study using the atomic force microscope, because polymer adsorption results in a deformable surface film. Chapter 3 demonstrates how this problem can be overcome using the evanescent wave atomic force microscope.

1.2.2.3 Hydration Force

During initial SFA measurements between hydrophilic mica surfaces in electrolyte solution[4], a strong short-range repulsion was observed that was in excess of the electrostatic force, and did not depend on the salt concentration ($Ca(NO_3)_2$, $\sim 10^{-4}$ to 10^{-1} M). The force was attributed to the overlap of ordered water molecules directly adjacent to the hydrophilic mica sheets, and termed a hydration or structural force[55-57]. The force was repulsive with a decay length of approximately 1 nm. Pashley[21] continued with research in this field by studying the effects of sodium, potassium, and hydrogen ions on the short-range force. His results indicated that at very low electrolyte concentrations (10^{-6} M, either Na^+ or

K^+), and in acidic solutions, the measured repulsive force between two mica sheets was that predicted by DLVO theory. However, as the concentration of Na^+ or K^+ was increased (10^{-4}M), an additional short range repulsion became apparent. Pashley suggested that exclusion of a layer of hydrated cations could describe this additional force.

Water molecules adopt an ordered orientation around ions in solution due to ion-dipole interactions[58] (with the water molecule's dipole moment directed towards the positive ion in solution). The amount of water and the degree of order depends directly on the size of the ion. An example of this is the hydration of group I metals. Moving down group I, from Li^+ to Cs^+, the radius of hydration decreases as the size of the ion increases. Therefore, the range of the force between two hydrophilic surfaces with adsorbed hydrated cations should decrease moving from Li^+ to Cs^+. Pashley demonstrated this between mica surfaces, and suggested the hydration force depends on the force of dehydrating the cation ("secondary hydration"), and a primary force associated with removing the dehydrated ion ("primary hydration"). Pashley's results were consistent with measurements on the stability of latex dispersions in the presence of group one metals[59] and has since been used describe the stability of silica suspensions at high salt concentrations[60, 61]. Similar studies with the atomic force microscope have shown that these short range repulsions exist between AFM cantilever tips and mica substrates[62, 63], and similarly depend on the hydrated radius of the cation.

The short range force has been measured between a range of materials including: silica[64], titanium dioxide[65], lipid bilayers[1] and proteins[66]. Since it is detectable between such a diverse collection of materials, a single hydrated ion model may not be sufficient to explain all experimental results. Other theoretical models include: polarization of water molecules by surface dipoles[67-69], breakage and formation of hydrogen bonds[70], and changes in the dielectric constant of the medium between two surfaces[71]. These different models have been reviewed and compared to an experimental measurement of the force between two silica surfaces in the presence of concentrated NaCl, using an AFM[72]. The authors conclude that the most likely cause of the short range repulsion between two silica surfaces is the rupture and formation of hydrogen bonds between surface silanol groups and adjacent water layers. It is interesting that a majority of the models predicted a greater range for the short range force than was experimentally measured in this paper.

1.3 Techniques for Measuring Surface Forces

The following sections will describe in brief detail three different techniques that are employed to measure the force between both macroscopic and microscopic surfaces. Each section will focus on how the separation and force are determined, and advantages and disadvantages of each technique respectively.

1.3.1 Surface Forces Apparatus

Measurement of the forces between *macroscopic* surfaces in solution using the Surface Force Apparatus (SFA) were first published in 1978[4, 73]. The instrument is a modification of an earlier instrument [74, 75] which was used to measure the force between two crossed cylinders of mica, with interferometric determination of separation. Figure 1.2 is a schematic of the SFA. The separation between two cross cylinder of mica (other materials such as silica[76], saphire[77], and mercury[78] have also be used) is controlled by course screws and a

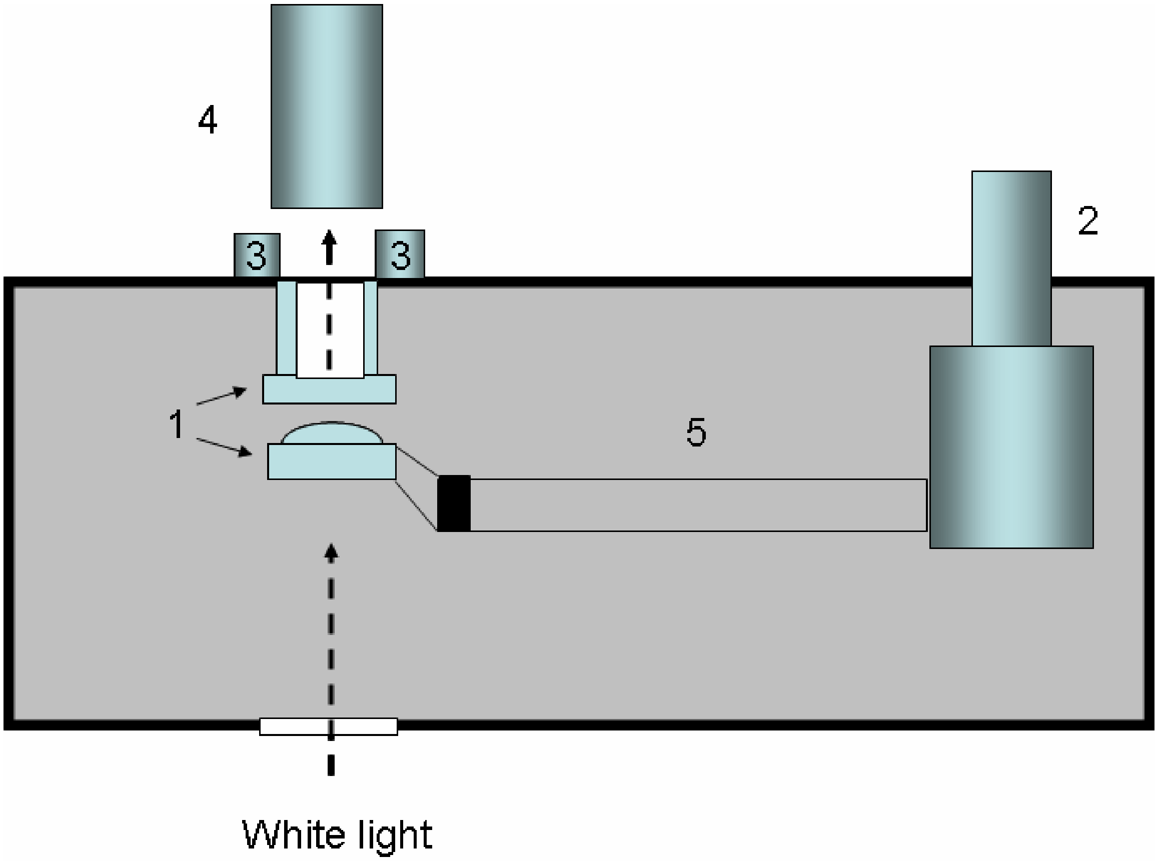

Figure 1.2. The separation between two cross cylinders of mica (1), is controlled by course screws (2) and a piezo electric crystal (3). White light is passed through two cross cylinders of mica and collected by a spectrometer (4). The force is determined through a spring attached to the lower mica sheet (5).

piezo electric crystal. The piezo allows the distance between the two surfaces to be controlled with sub-nanometer resolution. The cylinders are held 90^{o} to one another, with one being fixed and the other attached to a spring. White light is shown through the mica surfaces and collected by a spectrometer. As the separation between the surfaces change, constructive interference of the light is observed, and is used to determine the separation between the two mica surfaces.

1.3.1.1 Measurement of Separation

The separation between two surfaces in an SFA measurement is determined by monitoring the constructive interference of specific wavelengths of light between two approaching surfaces. These interference bands are termed fringes of equal chromatic order[79] (FECO). The wavelengths of constructive interference depend on the separation between the surfaces (h) and the thickness of the mica sheets (T). The thickness is obtained by measuring the wavelength of the FECO fringes when the surfaces are in contact. A significant advantage of the SFA is that the wavelength of interference at zero separation ($h = 0$) can be used as a reference throughout the experiment. A second advantage is that the shape and position of the interference fringes can be used to determine the refractive index of the medium between the two surfaces, and the radius of the cylinders. The radius is necessary to normalize the force between the two cylinders to an energy per area between flat sheets through Derjaguin's approximation[14].

1.3.1.2 Measurement of Force

At large separations, when no force is present, the piezo electric crystal decreases the separation between the two surfaces by a known distance (ΔX), which is compared to the change in distance determined by the interference fringes ($\Delta X'$). At close range separations when a force occurs, $\Delta X \neq \Delta X'$, because the spring deflects. The deflection is multiplied by the spring constant to give the force between the two surfaces assuming Hooke's Law for the spring.

$$F = kx \tag{1.15}$$

$$x = \Delta X - \Delta X' \tag{1.16}$$

The SFA has been used to measure and confirm the predicted force by DLVO, between macroscopic surfaces in simple electrolyte solutions[4]. Results from the SFA have also confirmed the existence of additional forces which include: repulsive hydration forces, steric forces, and long range attractive hydrophobic forces.

1.3.1.3 Advantages and Disadvantages of SFA

The surface force apparatus is a versatile instrument that can be used in liquids, vapors, and vacuum. The SFA has the advantage of obtaining direct measurements of separation and refractive index of the intervening medium simultaneously. Limitations include having to use *macroscopic* (cm), transparent smooth samples. This limits direct application of the results to a few macroscopic materials, and cannot be used directly for colloid particles. Finally, because there is such a large surface area of the sample under study, it is extremely difficult to conduct contaminant free experiments.

1.3.2 Atomic Force Microscope

Initially designed for imaging, the atomic force microscope creates a detailed image of surface contours on a near atomic scale[9]. The images are constructed by optically monitoring the response of a spring with a sharp tip (R<<60nm) in contact with a surface, as the surface is translated laterally underneath the sharp tip (some AFM's translate the tip relative to the surface). The images are therefore topographical images generated from the force between the tip of the cantilever and surface. If the tip is translated normal to the sample, the spring (cantilever) can be used to measure the force between an AFM tip and sample. Ducker et al., [10] advanced the utility of the atomic force microscope, by attaching microscopic spherical particles to the end of the cantilever, and providing an analysis to determine the separation between two surfaces by accounting for the deflection of the cantilever. This increased the interaction area to colloidal size, and the forces could be measured between surfaces of known geometry.

A general schematic of an AFM with a colloidal particle attached to the cantilever (colloid probe) is shown in figure 1.3. The distance between the colloid probe and sample is controlled by a micrometer, and a piezo electric crystal. When the probe and surface are in close proximity, the piezo electric crystal is

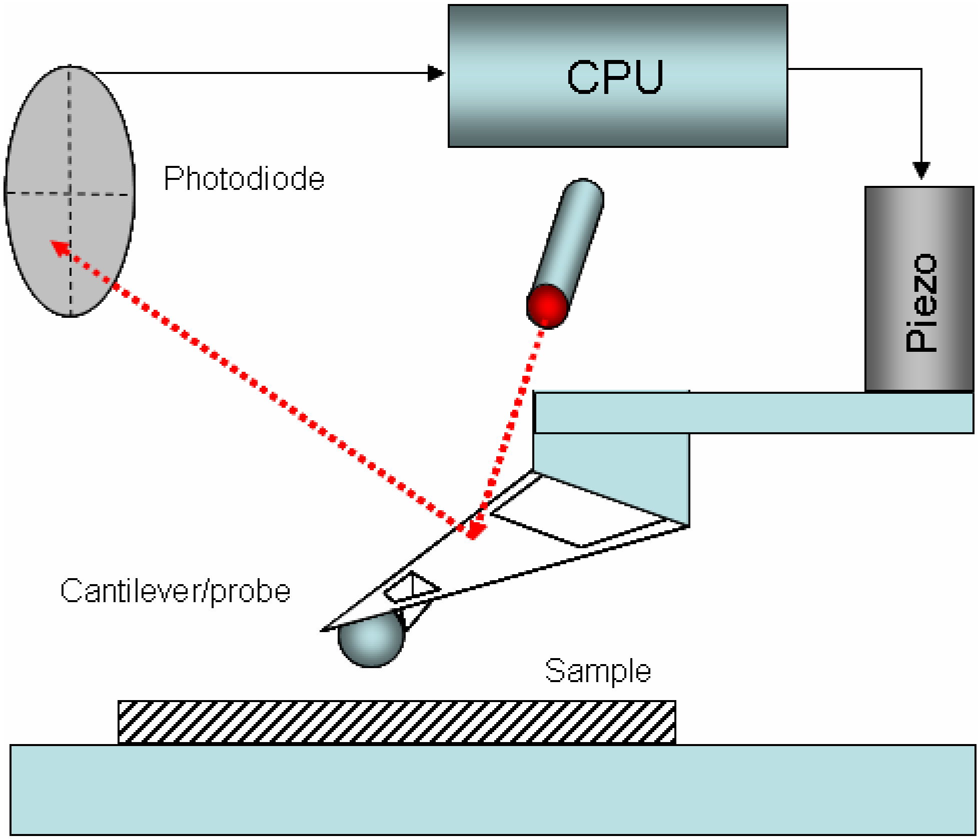

Figure 1.3. The separation between an AFM cantilever tip or colloid probe and sample, is controlled by a piezo electric crystal. Reflected light off the backside of the cantilever is monitored by a split photodiode. This signal is sent to a CPU which in turn controls the position of the piezo.

used to translate either the surface or the tip, towards each other with sub-nanometer resolution. The deflection of the cantilever is detected by a laser, which is reflected off the back side of the cantilever onto a split photodiode. Forces on the tip cause a change in the end slope of the cantilever that in turn displaces the reflected beam across the photodiode. The photodiode outputs a voltage that is proportional to the displacement and thus the deflection of the cantilever. The amount of deflection is regulated by the spring constant of the cantilever, and so a force can be determined.

1.3.2.1 Measurement of Separation

The atomic force microscope does not measure the separation between an AFM tip/probe and surface directly. The separation is calculated from the distance moved by the piezo electric crystal, and the deflection of the cantilever. The distance moved by the piezo electric crystal is measured by a linear variable displacement transducer (LVDT). Not all AFM's incorporate an LVDT, and the distance moved by the piezo electric crystal must be calibrated. The relative separation is simply the distance moved by the piezo, added to the amount of cantilever deflection. The absolute separation between the probe and surface is determined from the point of zero separation between the probe and sample. Zero separation is assumed to occur when there is a very steep gradient in the deflection as a function of piezo displacement. This is termed constant compliance, and the gradient of piezo displacement vs. deflection in this region is used to calibrate the

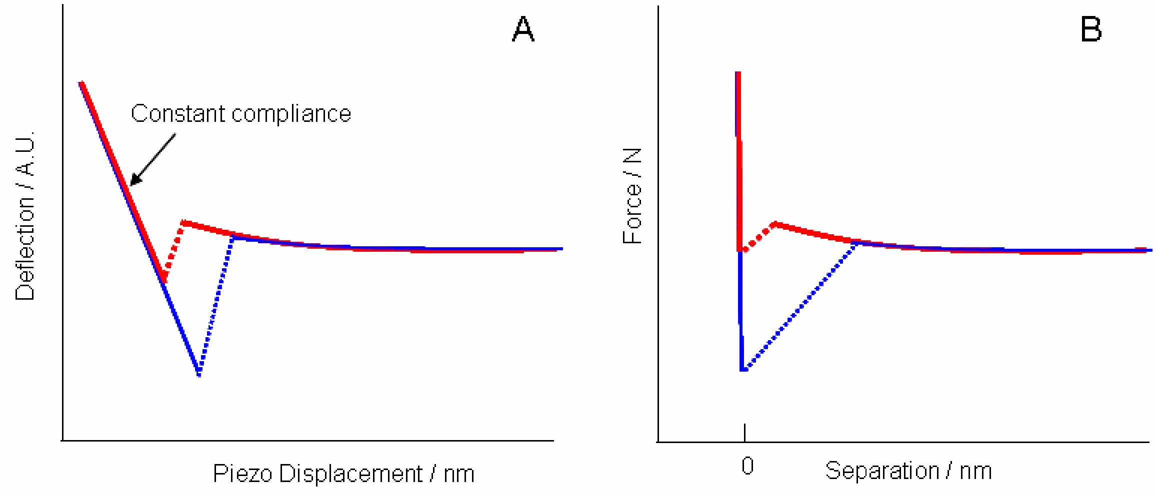

Figure 1.4. (A) Raw deflection of a cantilever approaching (red) and then withdrawing from a surface. (B) Conversion of the deflection vs piezo position, to a force vs. separation.

amount of cantilever deflection prior to contact. This is shown schematically in figure 1.4A. Once the position of zero separation has been chosen, the absolute separation is simply the change in distance moved by the piezo, minus the piezo position at the region of constant compliance, plus the amount of cantilever deflection.

1.3.2.2 Measurement of Force

Once the deflection of the cantilever is known the force is determined through Hooke's law. Figure 1.4B is the conversion of the raw deflection vs. piezo displacement into a force vs. separation.

1.3.2.3 Advantages and Disadvantages of AFM

The AFM has the advantage over the SFA of being able to measure the force between colloidal particles of known geometry. This increases the ability for direct application of surface force measurements to a large range of colloidal dispersions. The AFM can be used in vacuum, air, and liquid, and there is less chance of contamination in comparison to the SFA because the forces are measured between colloidal objects. When studying rigid solids (non deformable) the measurement of separation between surfaces is very accurate assuming the previous mentioned analysis of zero separation.

The disadvantage of AFM is that it does not directly measure the separation between surfaces. Which means that when surfaces are deformable, or an adsorbed film cannot be displaced between an AFM tip or colloid probe and surface, the region of zero separation can be misinterpreted. Researchers involved in the studies of polymer forces must relate the force profiles as a function of relative separation, as the zero of separation is not well defined. In addition, direct measurement of physical properties, such as the refractive index, are not available in current AFM designs. This means that a range of different experiments must be conducted to elucidate the mechanism of a force. The interpretation of these additional experiments is at times ambiguous at best. An excellent example of this is the proposed mechanism that may cause long-range attractions between hydrophobic surfaces in water. This force, between colloidal sized objects, has been attributed to proximity induced bubble formation. This conclusion has not been reached by direct measurement of a refractive index change; rather it has been inferred by observing the force under different conditions such as in degassed water, or in hydrocarbon solvents.

1.3.3 Total Internal Reflectance Microscopy

In a technique known as Total Internal Reflectance Microscopy (TIRM)[11, 12], a spherical particle is floated above an interface to obtain a potential energy-separation profile. The free floating particle (micron sized) migrates towards a flat interface under Brownian and gravitational displacement. If a sufficient electrostatic force is present between the particle and surface, the particle will access a range of separations away from the surface. The displacement of the particle is observed by introducing an evanescent wave between the particle and sample surface. This evanescent light which is scattered by the particle is collected by an objective/photomultiplier tube in the far field. This is shown schematically in figure 1.5.

Evanescent waves are an electromagnetic disturbance generated at an interface where light has undergone total internal reflection. Total internal reflection of light occurs when light propagating through a medium is reflected at

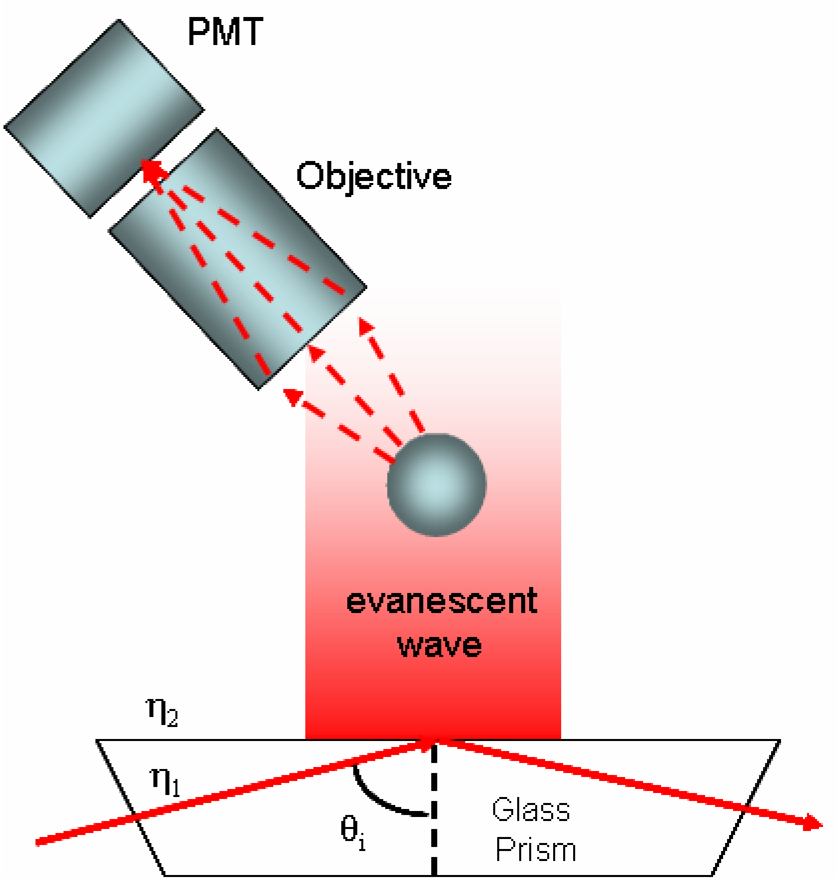

Figure 1.5. Schematic of TIRM. A spherical particle scatters light from an evanescent wave created at a glass-solution interface. The scattered light is collected in the far-field above the scattering particle by an objective, and is transferred to a photomultiplier tube or photon counter.

an interface of a less dense medium above a critical angle, described through Snell's law.

$$\eta_1 \sin\theta_1 = \eta_2 \sin\theta_2 \tag{1.17}$$

$$when\ \theta_2 = \pi/2$$

$$\theta_{critical} = \arcsin\frac{\eta_1}{\eta_2} \tag{1.18}$$

The evanescent wave decays into the less dense medium, and the intensity of the evanescent wave, I_E, decays exponentially with distance, z, according to the following equations[11]:

$$I_E = I_o^z \exp\left(\frac{-z}{\delta_{wave}}\right) \tag{1.19}$$

$$\delta = \frac{\lambda}{4\pi\eta_2\beta} \tag{1.20}$$

$$\beta = \sqrt{\left(\eta_1/\eta_2\right)^2 \sin^2\theta_i - 1} \tag{1.21}$$

Where I_o^z is the intensity of the wave at zero distance ($z = 0$) away from the surface, δ is the decay length of the wave, η_1 and η_2 are the refractive index of the incident and transmission medium respectively, and θ_i is the incident angle of light. For example, at 532 nm and an incident angle of 75^o at a glass-water interface, the decay length of an evanescent wave is 70 nm. Thus the characteristic decay length of an evanescent wave is much smaller than the wavelength of light, and it can approach the length scale of colloidal forces.

1.3.3.1 Measurement of Separation

When a spherical particle, with a refractive index contrast to the transmission medium, is introduced into the zone of an evanescent wave, that particle will scatter light. In TIRM it is assumed that the intensity of the scattered evanescent light is proportional to the intensity of the evanescent wave and so obviously depends on the separation (*h*) between the interface of total internal reflection and the scattering particle.

$$I_h = I_o \exp\left(-h / \delta_{scatter} \right) \tag{1.22}$$

Where the decay length of the scattered wave $\delta_{scatter}$, is the same as the decay length of the evanescent wave in equation 1.20. This theoretical relationship was first proposed by Chew et al.,[80] under the condition where the particle is sufficiently far from the interface of total internal reflection, such that the boundary conditions of the wave are not altered. Experimental validation of this relationship has been performed by Prieve and Walz[81] for the case when the incident angle was close to the critical angle, but the error in the measurement was quite large. Later in my thesis I challenge the validity of equation 1.22.

1.3.3.2 Measurement of Force

Because the colloidal particle under study is a free floating object, a range of separations between the sample and particle will be accessed due to Brownian motion of the particle. If a sufficient repulsive barrier exists between the particle and surface, the particle will experience random motion within a potential well near the sample. If the particle moves from this equilibrium position away from the surface, gravity will push the particle back. If the particle moves towards the surface, the repulsive force will push the particle back towards its equilibrium position. These oscillations are measured over a statistically large period of time by observing changes in the intensity of the scattered evanescent wave. A Boltzman distribution is used to equate these changes in intensity to an energy. A potential energy-separation profile can then be generated assuming an exponential scattering profile. Differentiating the energy with respect to separation results in a force vs. separation profile.

1.3.3.3 Advantages and Disadvantages of TIRM

The primary advantage of TIRM is that the particle is not attached to a spring. This allows very sensitive detection of the force between a freely rotating particle and surface (0.01 pN); it is also the primary drawback. A stable position between the particle and surface is necessary to generate the potential energy profile, which means the force must be measured in solution. If a sufficiently strong attraction between the surfaces exists, the particle will simply fall into the surface and the force cannot be measured. This limits applications of TIRM to cases where a sufficient electrostatic or steric repulsion exists between the sample and particle; forces cannot be measured in vacuum or air. Finally, if the assumption that the decay of the scattered evanescent wave is directly proportional to the decay of the evanescent wave is correct, the absolute separation between the particle and surface can be measured (chapter 2 gives experimental evidence that an exponential profile for a scattering particles is not always the case at all separations). This is a large advantage compared to AFM measurements, which does not have an explicit measure of separation. Measurement of the separation through equation 1.22 also requires that θ_I, η_1, η_2, and the wavelength of light remain constant and known during an experiment. This may not always be the case.

1.3.4 Conclusions on SFA, AFM, and TIRM

Using these three instruments it is possible to perform force measurements that are at times accessible to all three instruments, and at other times, unique situations dictate the use of one instrument over another. It is with this overall limitation in mind that a new instrument was designed in our lab to combine advantages of each instrument into one instrument. This new instrument has been termed an Evanescent Wave Atomic Force Microscope[13] and can be used to measure the absolute separation between colloidal surfaces for both attractive and repulsive regimes, with simultaneous measurement of the refractive index between the two surfaces.

1.3.5 Evanescent Wave Atomic Force Microscope

The following is a description of the EW-AFM[13] used during the experiments presented in the following chapters. Variations of the instrument for each particular experiment will be discussed where needed.

Figure 1.6 is a schematic of the apparatus. The evanescent wave atomic force microscope consists of a Zeiss Axiovert 200 inverted light microscope (Carl Zeiss, Thornwood, NY), a MFP-3D Asylum AFM (Asylum Research, Santa Barbara, CA), and a 532 nm solid state laser (GCL-50-L CrystaLaser, Reno, NV). Additional lasers used include a 405 nm diode laser (Oxiuss, France), and a 532 nm diode laser (TECGL-10, World Star Tech, Toronto Canada). Borosilicate or fused silica prisms (Knight Optical, U.K.) are used as the internal reflection element. A smooth borosilicate glass slide, which serves as the sample surface, is coupled to the prism using an index matching fluid.

The AFM, light source, and internal reflection element sit on a microscope translation stage which allows lateral translation (x and y directions) of the AFM cantilever and evanescent wave in the viewing axis of the microscope. A second lateral translation stage is used to translate the evanescent wave in relation to the AFM cantilever. This allows alignment of the cantilever and maximum intensity of the evanescent wave. The piezo electric crystal of the AFM is used to translate the cantilever/probe in the direction normal to the interface of total internal reflection, and the distance moved is measured by a linear variable displacement transducer (LVDT). When an AFM cantilever tip or colloidal probe is translated

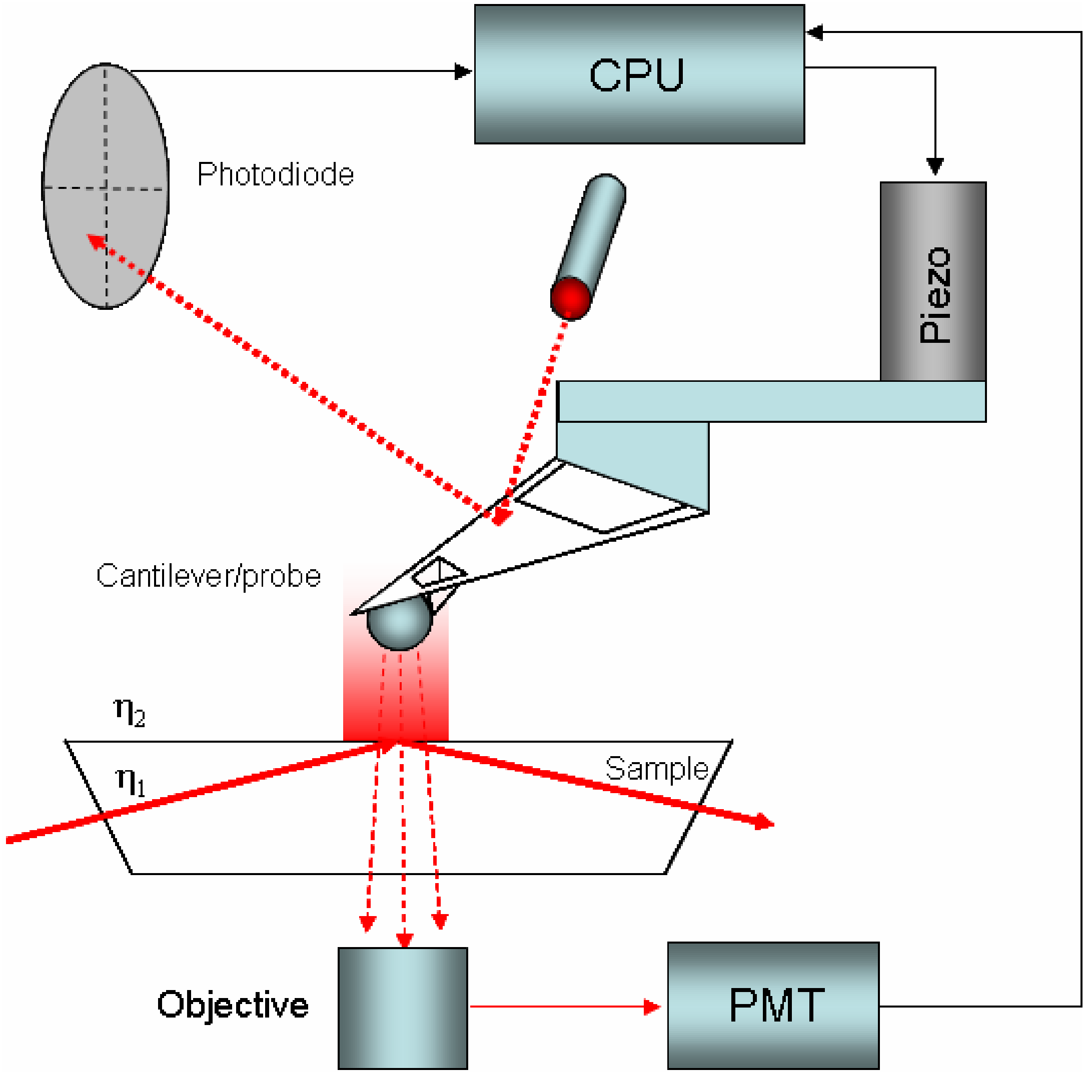

Figure 1.6. Schematic of an Evanescent Wave Atomic Force Microscope. The AFM is used to position and translate a particle over an evanescent wave generated at a glass prism-solution interface. The scattering signal that is transmitted back through the prism is collected by an objective in an inverted light microscope, and is then sent to a photomultiplier tube. The voltage output from the PMT is sent to the CPU controlling the motion of the piezo electric crystal of the AFM.

in the evanescent wave, it scatters light. The light that is transmitted back through the prism interface is collected with a 50 times objective, and is sent to a photomultiplier tube (H5784-20, Hamatsu). The entire experimental apparatus is isolated from external vibrations through a simple bungee arrangement or through an active vibration isolation unit (TS-150, Herzan, Laguna Hills, CA).

1.3.5.1 Measurement of Separation

Using an evanescent wave atomic force microscope, it is possible to simultaneously measure the separation by traditional AFM techniques described in section 1.3.2.1, and through monitoring the scattering from the cantilever tip or colloid probe described in section 1.3.3.1. Because the AFM does not directly measure the separation and can only be used to measure the *absolute* separation between rigid samples, the scattering signal greatly enhances the functionality of the AFM. This is because the scattering signal is absolute and does not depend on the rigidity of the samples (assuming a surface force does not deform the scattering object). It was initially assumed and verified[13] that the scattering profile from a colloidal particle attached to a cantilever, scattered an evanescent wave as an exponential function of distance as described by Chew[80] (this has since been studied in greater detail). The advantage of the EW-AFM over TIRM is that by attaching the colloid particle to an AFM cantilever, both attractive and repulsive regimes can be studied, with a measure of absolute separation.

1.3.5.2 Measurement of Force

The force measured by EW-AFM can be done by two distinct methods. The first was described previously in section 1.3.2.2. The second method uses the scattering profile of the evanescent wave by a particle[13]. As stated above, if the scattering profile of the wave is an exponential function of separation, then the separation can by determined by collecting the scattered light during an approach of a particle towards a surface. If there is no deflection of the cantilever, then a plot of the separation determined from equation 1.22, versus the amount of movement by the piezo electric crystal would be linear at all separations down to zero separation. If however, the scattering particle deflects away from the sample as the separation decreases, then a plot of scattering separation vs. piezo position will no longer be linear, and the difference between the linear fit and the actual data is the deflection of the cantilever. This is analogous to the SFA analysis of deflection discussed in section 1.3.1.1. Once the deflection of the cantilever is determined, the force is determined through Hooke's law. This analysis will be demonstrated graphically in chapter 3.

1.3.5.3 Measurement of the Refractive Index

Using an EW-AFM it is possible to monitor the refractive index between a scattering object and sample as a function of separation[82]. This is because the decay of the evanescent wave depends of the refractive index of the transmission medium. Equations 1.20 and 1.21 have been rewritten to show this.

$$\eta_2 = \sqrt{\eta_1^2 \sin^2 \theta_i - \left(\frac{\lambda}{4\pi\delta_{measured}} \right)^2} \tag{1.23}$$

Where $\delta_{measured}$ is the experimentally measured decay length over some finite distance. Applications of this will be demonstrated in chapter 4.

1.4 Cited Literature

1. LeNeveu, D. M.; Rand, R. P.; Parsegian, V. A., Measurement of forces between lecithin bilayers. *Nature (London, United Kingdom)* **1976,** 259, (5544), 601-3.
2. Parsegian, V. A.; Rand, R. P.; Fuller, N. L.; Rau, D. C., Osmotic stress for the direct measurement of intermolecular forces. *Methods in Enzymology* **1986,** 127, (Biomembranes, Pt. O), 400-16.
3. Barclay, L. M.; Ottewill, R. H., Measurement of forces between colloidal particles. *Special Discussions of the Faraday Society* **1970,** 1, 138-47.
4. Israelachvili, J. N.; Adams, G., Measurement of Forces between Two Mica Surfaces in Aqueous Electrolyte Solutions in the Range 0-100 nm. *J. Chem. Soc., Faraday Trans 1* **1978,** 74, 975-1001.
5. Kolarov, T.; Cohen, R.; Exerowa, D., Direct measurement of disjoining pressure in black foam films. II. Films from nonionic surfactants. *Colloids and Surfaces* **1989,** 42, (1-2), 49-57.
6. Bergeron, V.; Radke, C. J., Equilibrium measurements of oscillatory disjoining pressures in aqueous foam films. *Langmuir* **1992,** 8, (12), 3020-6.
7. Manev, E. D.; Pugh, R. J., Diffuse layer electrostatic potential and stability of thin aqueous films containing a nonionic surfactant. *Langmuir* **1991,** 7, (10), 2253-60.
8. Derjaguin, B. V.; Rabinovich, Y. I.; Churaev, N. V., Direct measurement of molecular forces. *Nature (London, United Kingdom)* **1978,** 272, (5651), 313-18.
9. Binnig, G.; Quate, C. F.; Gerber, C., Atomic Force Microscope. *Phys. Rev. Lett.* **1986,** 56, 930-933.
10. Ducker, W. A.; Senden, T. J.; Pashley, R. M., Direct Measurement of Colloidal Forces Using an Atomic Force Microscope. *Nature* **1991,** 353, (6341), 239-241.
11. Prieve, D. C.; Frej, N. A., Total Internal-Relfection Microscopy - A Quantitative Tool for the Measurment of Colloidal Forces. *Langmuir* **1990,** 6, (2), 396-403.
12. Prieve, D. C., Measurement of Colloidal Forces with TIRM. *Adv. Colloid Interface Sci.* **1999,** 82, 93-125.
13. Clark, S. P.; Walz, J. Y.; Ducker, W. A., AFM Colloid-Probe Measurements with Explicit Measurement of Particle-Solid Separation. *Langmuir* **2004,** 20, 7616-7622.
14. Derjaguin, B. V., Friction and Adhesion. IV. The Theory of Adhesion of Small Particles. *Kolloid Z.* **1934,** 69, 155-164.
15. Derjaguin, B. V.; Landau, E. M., Theory of the Stability of Strongly Charged Lyophobic Sols and of the Adhesion of Strongly Charged Particles in Solutions of Electrolytes. *Acta Physicochim* **1941,** 14, 633-662.
16. E.J.W., V.; Overbeek, J. T. G., Theory of the Stability of Lyophobic Colloids. *Elsevier* **1948**, 216.

17. Israelachvili, J.; Pashley, R. M., Measurement of the Hydrophobic Interaction between Two Hydrophobic Surfaces in Aqueous Electroltye Solution. *Journal of Colloid and Interface Science* **1984,** 98, 500-514.
18. Pashley, R. M.; McGuiggan, P. M.; Ninham, B. W.; Evans, D. F., Attractive Forces Between Uncharged Hydrophobic Surfaces: Direct Measurements in Aqueous Solution. *Science* **1985,** 229, 1088-1089.
19. Vigil, G.; Xu, Z.; Steinberg, S.; Israelachvili, J., Interactions of silica surfaces. *Journal of Colloid and Interface Science* **1994,** 165, (2), 367-85.
20. Chapel, J. P., Electrolyte Species Dependent Hydration Forces between Silica Surfaces. *Langmuir* **1994,** 10, (11), 4237-43.
21. Pashley, R. M., Hydration Forces between Mica Surfaces in Aqueous Electrolyte Solutions. *J Colloid Interface Sci* **1981,** 80, (1), 153.
22. Hodges, C. S., Measuring forces with the AFM: polymeric surfaces in liquids. *Advances in Colloid and Interface Science* **2002,** 99, 13-75.
23. Tulpar, A.; Henderson, D. B.; Mao, M.; Caba, B.; Davis, R. M.; van Cott, K. E.; Ducker, W. A., Unnatural Proteins for the Control of Surface Forces. *Langmuir* **2005,** 21, 1497-1506.
24. Evans, D. F.; Wennerström, H. K., *The Colloidal Domain*. 2nd ed.; Wiley: New York, 1999; 'Vol.' Chapter 5.1, p.
25. Ninham, B. W.; Parsegian, V. A., *J Theor Biol* **1971,** 31, (31), 405.
26. Hamaker, H. C., The London-van der Waals Attraction Between Spherical Particles. *Physica* **1937,** 4, 1058-1072.
27. Dzyaloshinskii, I. E.; Lifshitz, E. M.; Pitaevskii, L. P., General Theory of the van der Waal's Forces. *Uspekhi Fiz. Nauk* **1961,** 73, 381-422.
28. Hough, D. B.; White, L. R., The Calculation of Hamaker Constants from Lifshitz Theory with Applications to Wetting Phenomena. *Advances in Colloid and Interface Science* **1980,** 14, 3-41.
29. Israelachvili, J.; Pashley, R., The hydrophobic interaction is long range, decaying exponentially with distance. *Nature* **1982,** 300, (5890), 341-2.
30. Evans, D. F.; Wennerström, H. K., *The Colloidal Domain*. 2nd ed.; Wiley: New York, 1999, Chapter 5; 'Vol.' p 221.
31. Christenson, H. K.; Claesson, P. M., *Science* **1988,** 239, 390.
32. Rabinovich, Y. I.; Deryaguin, B. V., *Colloids Surfaces* **1988,** 30, 243.
33. Attard, P., Thermodynamic Analysis of Bridging Bubbles and a Quantitative Comparison with the Measured Hydrophobic Attraction. *Langmuir* **2000,** 16, (10), 4455-4466.
34. Carambassis, A.; Jonker, L. C.; Attard, P.; Rutland, M. W., Forces measured between hydrophobic surfaces due to a submicroscopic bridging bubble. *Physical Review Letters* **1998,** 80, (24), 5357-5360.
35. Parker, J. L.; Claesson, P. M.; Attard, P., Bubbles, Cavities, and the Long-Ranged Attraction between Hydrophobic Surfaces. *J. Phys. Chem.* **1994,** 98, 8468-8480.
36. Wood, J.; Sharma, R., How Long Is the Long-Range Hydrophobic Interaction? *Langmuir* **1995,** 11, 4797-4802.
37. Tyrrell, J. W. G.; Attard, P., Atomic force microscope images of nanobubbles on a hydrophobic surface and corresponding force-separation data. *Langmuir* **2002,** 18, (1), 160-167.

38. Tyrrell, J. W. G.; Attard, P., Images of nanobubbles on hydrophobic surfaces and their interactions. *Physical Review Letters* **2001,** 8717, (17).
39. Craig, V. S. J.; Ninham, B. W.; Pashley, R. M., Direct Measurement of Hydrophobic Forces: A Study of Dissolved Gas, Approach Rate, and Neutron Irradiation. *Langmuir* **1999,** 15, (4), 1562-1569.
40. Claesson, P. M.; Blom, C. E.; Herder, P. C.; Ninham, B. W., Interactions between water-stable hydrophobic Langmuir-Blodgett monolayers on mica. *Journal of Colloid and Interface Science* **1986,** 114, (1), 234-42.
41. Evans, D. R.; Craig, V. S. J.; Senden, T. J., The hydropobic force: nanobubbles or polymeric contaminant? *Physica A* **2004,** 339, 101-105.
42. Zhang, J.; Yoon, R. H.; Mao, M.; Ducker, W. A., Effect of dissolved gas on the force between silica and glass in aqueous ocyadecyltrimetylammonium chloride solutions. *Publications of the Australasian Institute of Mining and Metallurgy* **2005,** 5/2005, (Centenary of Flotation Symposium, 2005), 659-664.
43. Mao, M.; Zhang, J.; Yoon, R.-H.; Ducker, W. A., Is There a Thin Film of Air at the Interface between Water and Smooth Hydrophobic Solids? *Langmuir* **2004,** 20, (5), 1843-1849.
44. Takata, Y.; Cho, J. H. J.; Law, B. M.; Aratono, M., Ellipsometric Search for Vapor Layers at Liquid-hydrophobic Solid Surfaces. *Langmuir* **2006,** 22, (4), 1715-1721.
45. Eriksson, J. C.; Ljunggren, S.; Claesson, P. M., A phenomenological theory of long-range hydrophobic attraction forces based on a square-gradient variational approach. *Journal of the Chemical Society, Faraday Transactions 2: Molecular and Chemical Physics* **1989,** 85, (3), 163-76.
46. Yaminsky, V. V.; Ninham, B. W., Hydrophobic force: lateral enhancement of subcritical fluctuations. *Langmuir* **1993,** 9, (12), 3618-24.
47. Tsao, Y. H.; Evans, D. F.; Wennerstrom, H., Long-Range Attractive Force between Hydrophobic Surfaces Observed by Atomic-Force Microscopy. *Science* **1993,** 262, (5133), 547-550.
48. Belloni, L.; Spalla, O., Attraction of Electrostatic Origin Between Colloids. *J. Chem. Phys.* **1997,** 107, 465-480.
49. Evans, D. F.; Wennerstrom, H., The Colloidal Domain. In 2nd ed.; Wiley: New York, 1999; 'Vol.' Chapter 5, p^pp 260.
50. McLean, S. C.; Lioe, H.; Meagher, L.; Craig, V. S. J.; Gee, M. L., Atomic Force Microscopy Study of the Interaction between Adsorbed Poly(ethylene oxide) Layers: Effects of Surface Modification and Approach Velocity. *Langmuir* **2005,** 21, (6), 2199-2208.
51. Kelley, T. W.; Schorr, P. A.; Johnson, K. D.; Tirrell, M.; Frisbie, C. D., Direct Force Measurements at Polymer Brush Surfaces by Atomic Force Microscopy. *Macromolecules* **1998,** 31, (13), 4297-4300.
52. Pasche, S.; Textor, M.; Meagher, L.; Spencer, N. D.; Griesser, H. J., Relationship between Interfacial Forces Measured by Colloid-Probe Atomic Force Microscopy and Protein Resistance of Poly(ethylene glycol)-Grafted Poly(L-lysine) Adlayers on Niobia Surfaces. *Langmuir* **2005,** 21, (14), 6508-6520.

53. Klein, J.; Luckham, P., Forces between two adsorbed poly(ethylene oxide) layers immersed in a good aqueous solvent. *Nature (London, United Kingdom)* **1982,** 300, (5891), 429-31.
54. Vincent, B., Dispersion stabilization and destabilization by polymers. *Special Publication - Royal Society of Chemistry* **1999,** 227, (Food Emulsions and Foams), 19-28.
55. Derjaguin, B. V.; Churaev, N. V., Structural Component of Disjoining Pressure. *Journal of Colloid and Interface Science* **1974,** 49, (2), 249-255.
56. Drost-Hansen, W., Effects of vicinal water on colloidal stability and sedimentation processes. *Journal of Colloid and Interface Science* **1977,** 58, (2), 251-62.
57. LeNeveu, D. M.; Rand, R. P.; Parsegian, V. A.; Gingell, D., Measurement and modification of forces between lecithin bilayers. *Biophysical Journal* **1977,** 18, (2), 209-30.
58. Evans, D. F.; Wennerström, H. K., In *The Colloidal Domain*, 2nd ed.; 'Ed.'^'Eds.' Wiley: New York, 1999; 'Vol.' p^pp 108-110.
59. Healy, T. W.; Homola, A.; James, R. O.; Hunter, R. J., *Faraday Discussions* **1978,** 65, 156.
60. Franks, G. V.; Johnson, S. B.; Scales, P. J.; Boger, D. V.; Healy, T. W., Ion-Specific Strength of Attractive Particle Networks. *Langmuir* **1999,** 15, (13), 4411-4420.
61. Franks, G. V., Zeta potentials and yield stresses of silica suspensions in concentrated monovalent electrolytes: Isoelectric point shift and additional attraction. *Journal of Colloid and Interface Science* **2002,** 249, (1), 44-51.
62. Donose, B. C.; Vakarelski, I. U.; Higashitani, K., Silica Surfaces Lubrication by Hydrated Cations Adsorption from Electrolyte Solutions. *Langmuir* **2005,** 21, (5), 1834-1839.
63. Higashitani, K.; Ishimura, K., Evaluation of interaction forces between surfaces in electrolyte solutions by atomic force microscope. *Journal of Chemical Engineering of Japan* **1997,** 30, (1), 52-58.
64. Yotsumoto, H.; Yoon, R. H., Application of extended DLVO theory. II. Stability of silica suspensions. *Journal of Colloid and Interface Science* **1993,** 157, (2), 434-41.
65. Yotsumoto, H.; Yoon, R. H., Application of extended DLVO Theory. I. Stability of rutile suspensions. *Journal of Colloid and Interface Science* **1993,** 157, (2), 426-33.
66. Paunov, V. N.; Kaler, E. W.; Sandler, S. I.; Petsev, D. N., A Model for Hydration Interactions between Apoferritin Molecules in Solution. *Journal of Colloid and Interface Science* **2001,** 240, (2), 640-643.
67. Manciu, M.; Ruckenstein, E., Oscillatory and Monotonic Polarization. The Polarization Contribution to the Hydration Force. *Langmuir* **2001,** 17, (24), 7582-7592.
68. Manciu, M.; Ruckenstein, E., Role of the Hydration Force in the Stability of Colloids at High Ionic Strengths. *Langmuir* **2001,** 17, (22), 7061-7070.
69. Ruckenstein, E.; Manciu, M., The Coupling between the Hydration and Double Layer Interactions. *Langmuir* **2002,** 18, (20), 7584-7593.

70. Attard, P.; Batchelor, M. T., A mechanism for the hydration force demonstrated in a model system. *Chemical Physics Letters* **1988,** 149, (2), 206-11.
71. Basu, S.; Sharma, M. M., Effect of dielectric saturation on disjoining pressure in thin films of aqueous electrolytes. *Journal of Colloid and Interface Science* **1994,** 165, (2), 355-66.
72. Valle-Delgado, J. J.; Molina-Bolivar, J. A.; Galisteo-Gonzalez, F.; Galvez-Ruiz, M. J.; Feiler, A.; Rutland, M. W., Hydration forces between silica surfaces: Experimental data and predictions from different theories. *Journal of Chemical Physics* **2005,** 123, (3), 034708/1-034708/12.
73. Israelachvili, J. N.; Adams, G. E., *Nature* **1976,** 262, 774.
74. Tabor, D.; Winterton, R., Direct Measurement of Normal and Retarded Van Der Waals Forces. *Proceedings of the Royal Society of London Series a-Mathematical and Physical Sciences* **1969,** 312, (1511), 435.
75. Tabor, D.; Winterton, R. H. S., *Nature* **1968,** 219, 1120.
76. Horn, R. G.; Smith, D. T.; Haller, W., Surface Forces aand Viscosity of Water Measured Between Silica Sheets. *Chemical Physics Letters* **1989,** 162, 404-408.
77. Horn, R. G.; Clarke, D. R.; Clarkeson, M. T., Direct Measurement fo Surface Forces between Sapphire Crystals in Aqueous Solutions. *J. Mater. Res.* **1988,** 3, 413-416.
78. Clasohm, L. Y.; Connor, J. N.; Vinogradova, O. I.; Horn, R. G., The "Wimple": Rippled Deformation of a Fluid Drop Caused by Hydrodynamic and Surface Forces during Thin Film Drainage. *Langmuir* **2005,** 21, (18), 8243-8249.
79. Tolansky, S., *Multiple-Beam Interferometry of Srufaces and Thin Films*. ed.; Oxford University Press: London, 1948; 'Vol.' p.
80. Chew, H. D.; Wang, D.-S.; Kerker, M., Elastic Scattering of Evanescent Electromagnetic Waves. *Applied Optics* **1979,** 18, 2679-2687.
81. Prieve, D. C.; Walz, J. Y., Scattering of an Evanescent Surface Wave by a Microscopic Dielectric Sphere. *Applied Optics* **1993,** 32, (9), 1629-1641.
82. McKee, C. T.; Ducker, W. A., Refractive Index of Thin, Aqueous Films between Hydrophobic Surfaces Studied Using Evanescent Wave Atomic Force Microscopy. *Langmuir* **2005,** 21, (26), 12153-12159.

Chapter 2

Scattered Intensity vs. Separation for Particles in an Evanescent Field

2.1 Introduction

When a colloidal particle sits in an evanescent field, it will scatter light, and detection of this light can be used to determine the separation between a particle and an interface. In particular, TIRM has been used to measure a variety of colloid energy separation profiles.[1, 2] In TIRM it is usually assumed that the intensity of scattered light captured by the detector is proportional to the evanescent wave, i.e. $I_h \propto \exp(-h/\delta)$, where h is the separation between the particle and the interface where the evanescent wave is generated. Experimental evidence for this proportionality was performed by Prieve and Walz[3] using MgF_2-coated glass slides for the case when the incident angle was close to the critical angle (within 2°). They found that the scattering did decay exponentially with h, but the variability in the measurement was large (the scattering intensity for a set of nominally identical particles at a given separation varied by a factor of 7.5).

The ability of AFM techniques to accurately position a particle near an interface of total internal reflection allows a more accurate test of the relationship between the scattered intensity and the evanescent wave intensity. The following describes EW-AFM measurements of the scattering profile for a range of particles and AFM tips. I can confirm that the scattering profile is exponential at large separations ($I_h \propto \exp(-h/\delta)$ when $h > 3\delta$), but that there are significant deviations at smaller separations for colloidal particles.

2.2 Materials and Methods

2.2.1 Experimental Method

The evanescent wave is generated at an interface between a borosilicate glass prism (η = 1.515) and water (η = 1.333) by a 532 nm solid-state laser (CrystaLaser GCL-50-L, Reno, NV). The laser light source, glass prism, and AFM (MFP-1D-plus Asylum, Santa Barbara, CA), sit on a microscope translation stage mounted to an inverted light microscope (Zeiss Axiovert 200, Carl Zeiss, Thornwood, NY).

The translation stage allows alignment of both the evanescent wave and AFM relative to the viewing axis of the optical microscope. The piezoelectric crystal of the AFM controls translation of the scattering particle in the evanescent wave normal to the reflection interface. With this apparatus I can simultaneously measure the deflection of an AFM cantilever and the scattered light as the colloid probe or cantilever tip interacts with the evanescent wave.

The AFM obscures the light that is scattered upward, into the region above the cantilever. Therefore the majority of these results arise from experiments in which the scattering object is attached to, or directly part of an AFM cantilever. The captured scattered light is that fraction of light that passes back through the sample prism underneath the AFM cantilever, and into a microscope objective lens. The fraction of scattered light that is collected is defined by the numerical aperture of the objective lens (Zeiss Epiplan 50x/0.50). The intensity of the scattered light is transferred to and monitored via a photomultiplier tube (PMT; HC120-01 Hamamatsu) with two 12 V gel-type batteries as a power source. The PMT signal is synchronized with the position and deflection information from the AFM. Plots of the scattering signal as a function of separation calculated by traditional AFM analysis, can then be produced.[4]

Recent advances in Asylum AFM design have allowed an end user to view the cantilever from above, using a 10 x objective. This new design was used to collect transmitted scattered evanescent light, with a CCD camera from above the cantilever. Using this setup, the scattering profile was measured simultaneously from above and below the scattering object.

2.2.2 Experimental Materials

Unless stated otherwise, all experiments reported in this section were performed in 0.1M NaCl solutions. Concentrated salt solutions will decrease the electrostatic force between two surfaces. Because an AFM cantilever is used to detect the force and determine the separation between surfaces, increasing the salt concentration keeps the correction for cantilever deflection to a minimum. Sodium chloride was obtained from Aldrich and roasted at ~ 500°C for ~ 12 h. Water was purified in an in-house reverse osmosis system and then filtered using a

Barnstead EasyPure UV system (Dubuque, IA). Borosilicate (Duke Scientific, part #'s, 9002, 9005, and 9020, Palo Alto, CA), fluorescent (Duke Scientific 36-2), and nickel spheres (Duke Scientific 136) were glued to tipless silicon AFM cantilevers (Veeco, ULCT-NTNM, Santa Barbara, CA) using epikote 1004 or two-part epoxy. Epikote glue is often used for making colloid probes because the glue quickly dissolves in chloroform. However, when surface preparations require the use of chloroform, this glue cannot be used. I find that two-part epoxy does not rapidly dissolve in chloroform. In addition to colloidal probes, silicon nitride and silicon AFM tips were used (Veeco, NP and Asylum AC240TS respectively). The silicon nitride cantilevers have 15 nm of chromium and 60 nm of gold deposited on the side facing away from the sample.

2.3 Results

2.3.1 Scattering from AFM Tips

To determine the functional form of the scattering profile from AFM tips or colloid probes, traditional AFM analysis was used to determine the separation between the scattering object and the surface.

Most commercial atomic force microscope cantilevers have a sharp tip incorporated at their free end to enable high-resolution imaging. I have studied the scattering profile generated from silicon nitride and silicon cantilevers, each with unique tip geometry. The silicon nitride cantilevers have a square pyramid tip that is 4 microns in height. The pyramid is hollow with no base. The silicon cantilever tips have a roughly pyramidal shape, are 15-20 microns high, solid throughout, and have a much higher aspect ratio compared to the silicon nitride pyramid. Scanning electron microscope images of these tips are shown in Figure 2.1.

Figure 2.2 shows the simultaneous measurement of the scattering intensity from a silicon nitride tip and deflection of the cantilever as a function of piezo displacement. The raw output from the silicon tip is visually similar on a linear scale and so not shown. The PMT voltage (figure 2.2A) is proportional to that part of the signal that is captured by the microscope lens that is immediately underneath the sample and prism. This voltage is recorded as a function of the displacement of the cantilever in relation to the sample surface as measured by the linear variable displacement transducer (LVDT) on the AFM piezo. At large separations, the PMT voltage is a constant and defined by I_∞. This background signal, which is not sensitive to the separation, is subtracted from the relative intensity at all separations. The background signal is a sum of the electrical background, stray light from the room, and imperfections or particles at the solid liquid interface that scatter light. We use the symbol I_h to define the intensity of

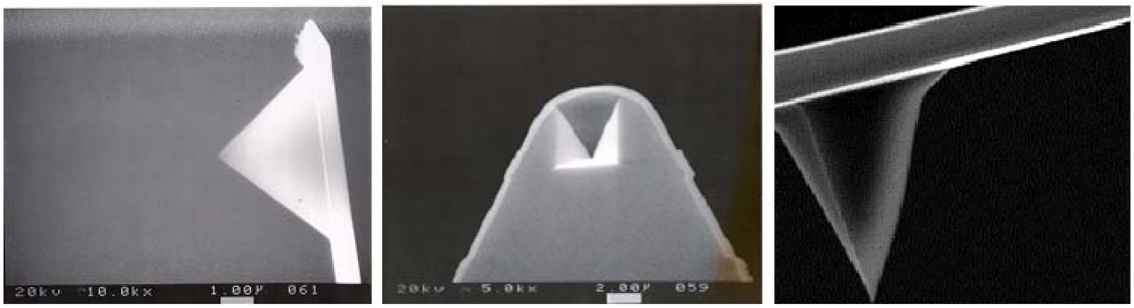

Figure 2.1. From left to right. A silicon nitride tip, side on view. Top down view of the hollow in these silicon nitride tips. A silicon tip.

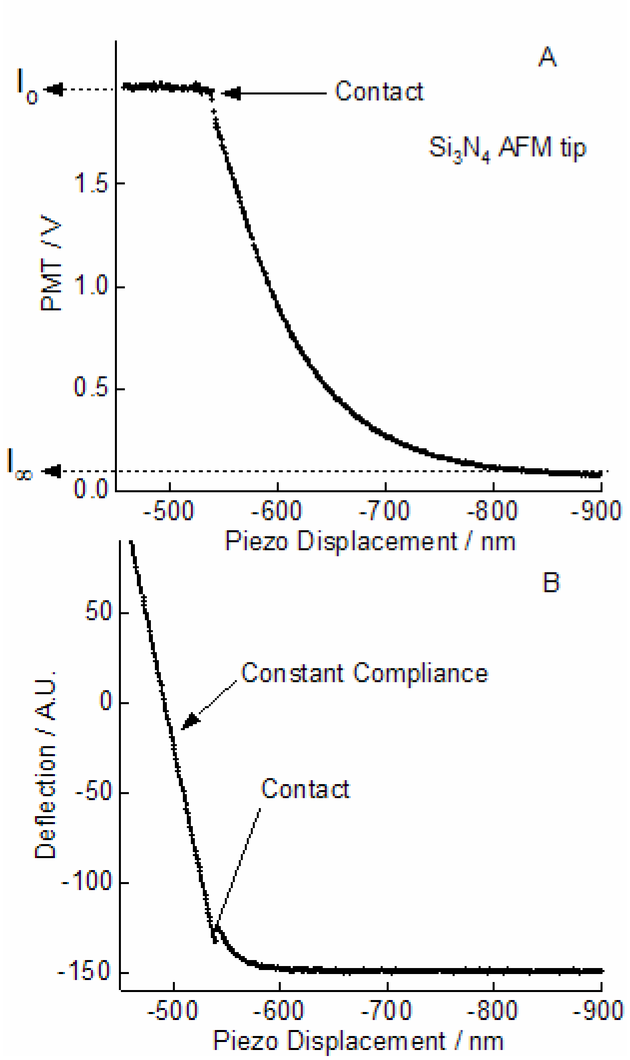

Figure 2.2. (A) Scattering of light from a square pyramid Si_3N_4 AFM tip in an evanescent field. The raw data shows the voltage output from the photomultiplier tube as a function of displacement of the piezoelectric transducer that drives the AFM cantilever. I_o and I_∞ are the voltages in contact and at infinite separations, respectively. (B) Cantilever deflection vs. piezo displacement measured simultaneously to scattering data in A. The point of contact in deflection data is mirrored in scattering I_o.

scattered light as a function of separation h. After contact, the scattering intensity as a function of piezo displacement is approximately constant and is defined by I_o.

As discussed in the introduction, the relative separation is normalized by the region of contact to obtain the absolute separation. In traditional AFM analysis the point of contact is defined when there is a steep, and constant gradient in the cantilever deflection vs. piezo displacement curve[4]. The onset of this region occurs at the same position of constant scattering, as shown in figure 2.2B, and remains constant as the piezo continues to push the cantilever towards the surface. Thus when using AFM cantilever tips and rigid samples, the scattering intensity could be used to define the zero of separation. This would be particularly useful when a large repulsive force is required to displace a material from between a tip and surface, which would confuse the region of constant compliance.

In figure 2.3 the raw scattering and deflection has been transformed to show the decay of the scattered light as a function of separation (determined by traditional AFM analysis) for the silicon nitride and silicon cantilevers. The scattering is plotted on a natural log scale vs. separation. Part A shows that the scattering from a silicon nitride tip, $\ln (I_h/I_o)$, is proportional to the separation. For comparison, a straight line has been added, with a slope of $-\delta$, where $\delta = 70.0$ nm. This experimental value is similar to the theoretical value of $\delta = 70.1$ nm calculated with equation 1.22 at all separations. Part B shows that the scattering from a silicon tip is proportional to the separation, but that a straight line fit to the data using $\delta = 70.0$ nm does not agree with the experimental results at all separations. Deviation from the linear fit occurs for $h > 150$ nm. This is better illustrated in part C and D, which shows the difference between the experimental data and the linear fit. The linear fit is extremely good for the Si_3N_4 tip for $h <$ 300nm. The silicon tip shows deviations for $h < 150$ nm.

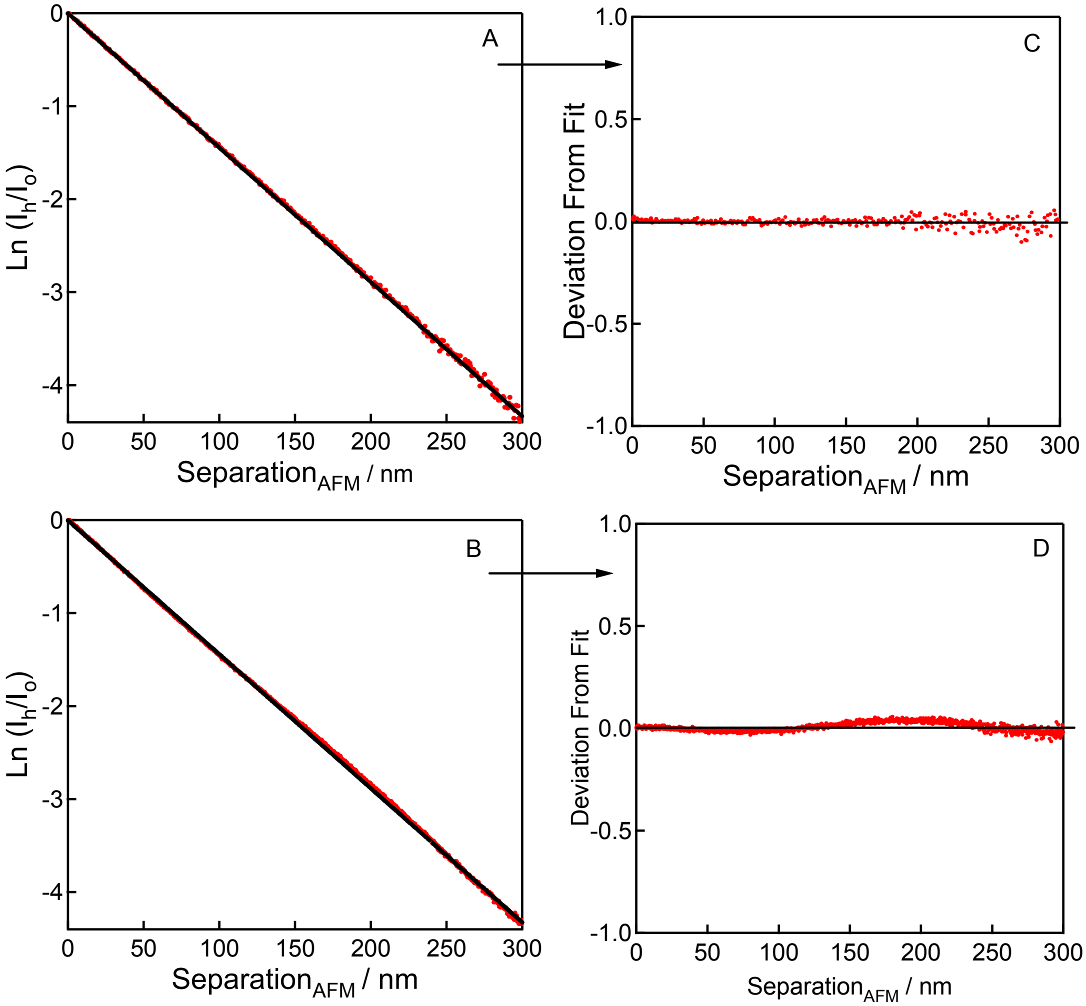

Figure 2.3 (A) data from figure 1 replotted to reveal the exponential decay of the silicon nitride tip. (B) same as (A) except for a silicon tip. The piezo displacement has been converted to separation by accounting for deflections of the cantilever. The background intensity I_∞ has been subtracted from the intensity to give I_h and I_o, and the data is plotted on a log scale. The solid lines are fits ($-h/\delta_{meas}$) to the experimentally measured decay using, where $\delta_{meas} = 70.0$ nm. (C) and (D) are the difference between the experiment result and the linear fit to better demonstrate deviations from an exponential decay.

The exponential decay of the scattering from a silicon nitride tip, plus the agreement between the theoretical decay length of the evanescent wave and the measured decay length, shows that the scattering from a silicon nitride tip is proportional to the intensity of the evanescent wave reaching the tip at all separations. The simple form of the scattering plus the large signal to noise ratio shows that monitoring the scattered intensity from a silicon nitride tip could be used to measure the separation between the tip and a flat plate. Importantly, not all small particles produce this simple scattering profile.

2.3.2 Scattering from Glass Particles

In the following sections, the scattering profile has been studied for larger radius glass particles, 1 μm < R < 11 μm, which were glued onto the end of AFM cantilevers. These cantilevers are coated on the opposite side with 3 nm of titanium, and have no tips. This was done to avoid possible complications of scattering from the tip. I have also done experiments with cantilevers that did include an integrated tip, but found no significant difference in the general features of the scattering profiles.

Figure 2.4 shows the scattering from a glass particle, R = 11.4 μm. Part A is the raw data; Part B shows the scattering decays exponentially with distance at large separation ($h > 3\delta$). Note that the decay length of the scattering is consistent with the decay of the evanescent wave in the absence of the particle. If the exponential region is extrapolated to smaller separations, it is found that the measured intensity is always less than the extrapolated intensity. For clarity, I_o' is defined to be the value of the intensity obtained by extrapolating the data at large separations to zero separation on a natural log plot. In contrast, I_o is the actual measured scattering in contact.

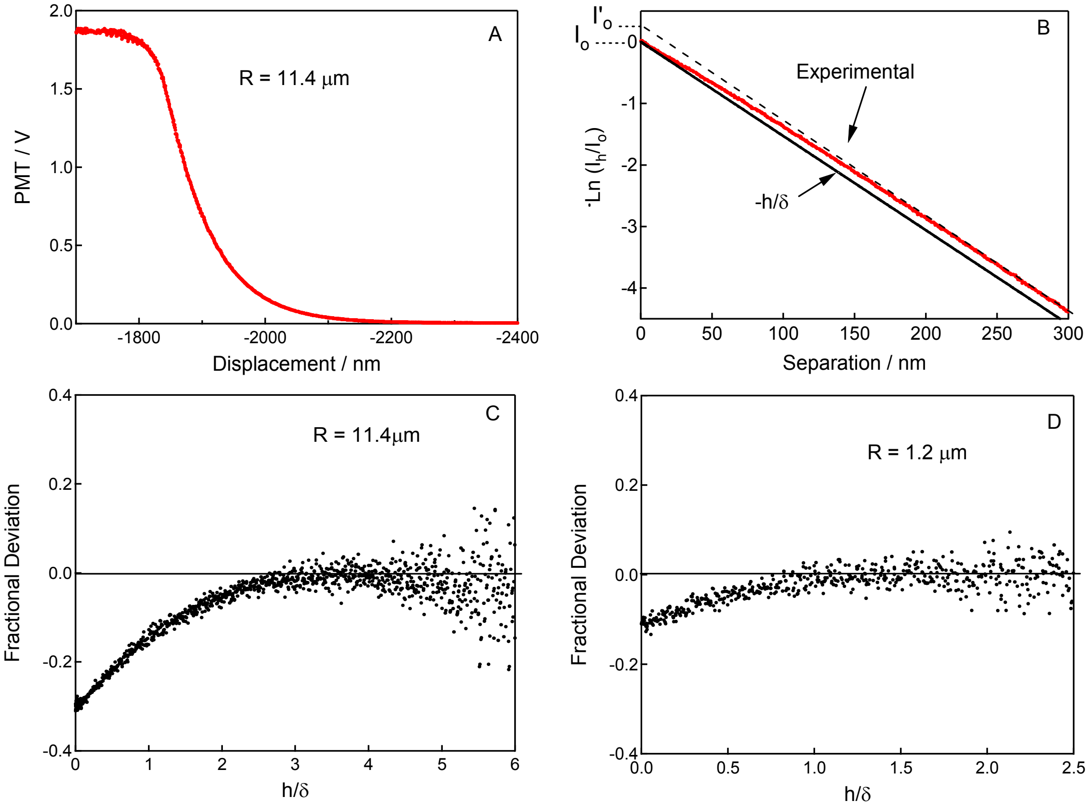

Figure 2.4. (A) PMT voltage corresponding to particle scattering as a function of AFM separation for a 11.4 μm glass sphere. (B) Data from (A) replotted to show natural log of intensity as a function of the separation between the particle and the plate. The solid line is $-h/\delta_{meas}$, using the δ_{meas} at large separations. I_o' is the extrapolation of exponential region of the experimental curve. (C) Data replotted to more clearly show the difference between experimental measurements I_h and purely exponential decay as a function of separation normalized by the decay length δ. (D) Same as (C), but for a 1.2 μm radius sphere.

The range and magnitude of deviation from linearity is hard to see in part B, so the data has been replotted to focus on the deviation only. We define ΔI as the absolute deviation of the intensity from the purely exponential decay:

$$\Delta I = I_h - I_o^{'} \exp(-h/\delta) \qquad (2.1)$$

To express the deviation as a fraction of the exponential signal, equation (2.1) is divided by $I_o^{'} \exp(-h/\delta)$, giving:

$$\text{Fractional Deviation} = \frac{I_h}{I_o^{'}\exp(-h/\delta)} - 1 \tag{2.2}$$

Figure 2.4 C shows that for an 11.4 μm radius particle, the measured scattering intensity starts to deviate from a purely exponential decay at approximately 200 nm separation, or about 3δ, and the deviation at $h = 0$ is about 30%. In contrast, part D shows that the deviation for a smaller particle, R = 1.2 μm occurs at a smaller separation, and is only about 10% in contact. These magnitudes are typical for a sample of glass particle of R = 1.2 and 11.4 μm. If the silicon nitride tip is treated as a particle, the deviation at contact increases from zero when R < 60 nm (radius of curvature of Si_3N_4 tip) to about 30% when R = 2.5 μm. A difference could not be resolved in the fractional deviation at contact as the radius was varied from 2.5 to 11.4 μm.

If the scattering-separation profile is repeated with the same particle on the same position on the sample prism, the results are almost identical. However, when the prism is moved to a new position (total internal reflection at a new interface) the scattering-separation profile can change. This suggests that the scattering profile is influenced to some degree by the prism/surface quality in the vicinity of the sphere.

Figure 2.5 shows that the plot of *ln (ΔI)* versus separation is linear, which suggests that the scattering can be approximated as a sum of two exponentials:

$$I_h = I_o^{'}\exp(-h/\delta) - I_o^{''}\exp(-h/\delta^{''}) \tag{2.3}$$

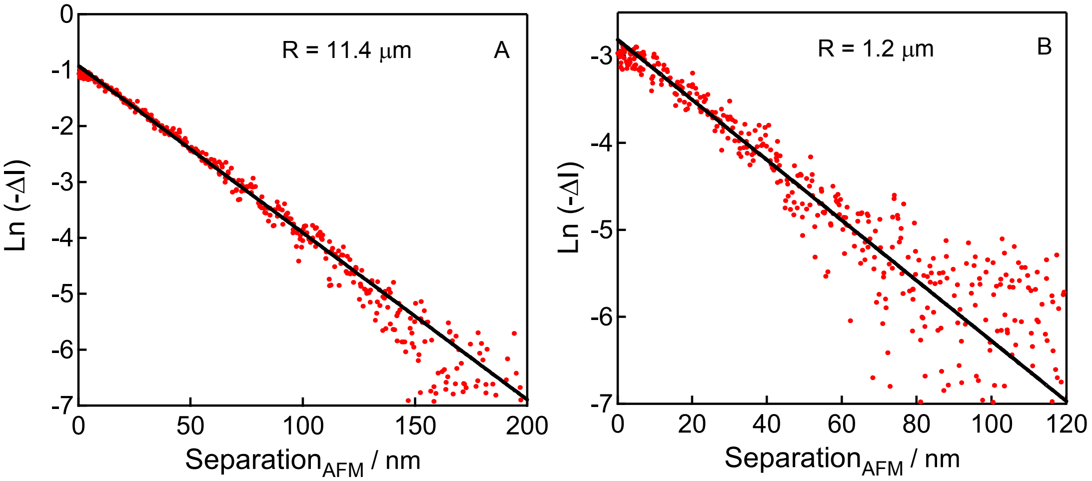

Figure 2.5. The difference between experimental I_h and I_o'exp(-h/δ) plotted on a natural log scale. Solid line is exponential fit of the deviation I_o''exp(-h/δ''). Decay lengths for the 11.4 and 1.2 μm radius spheres are 37 and 24 nm, respectively.

This result is useful for calibrating the separation-scattering profile and can be used to quantify the range of the deviation through the parameter δ''. δ'' = 37 nm (0.56δ) for the 11.4 μm particle and 24 nm (0.37δ) for the 1.2 μm particle; the range of deviation is greater for the larger particle.

2.3.3 Scattering from Metal Particles

The signal that is collected at our detector for glass spheres is composed of light that has scattered directly from the glass particle-solution interface (front reflection), and light that has transmitted into the glass sphere, undergone multiple internal reflections, and is then retransmitted to the surrounding solution. This light can leave over a 360-degree angle and therefore the total collected signal is also potentially composed of light that has reflected from the cantilever back to the detector. To determine the affects of this scattered cantilever light, the scattering

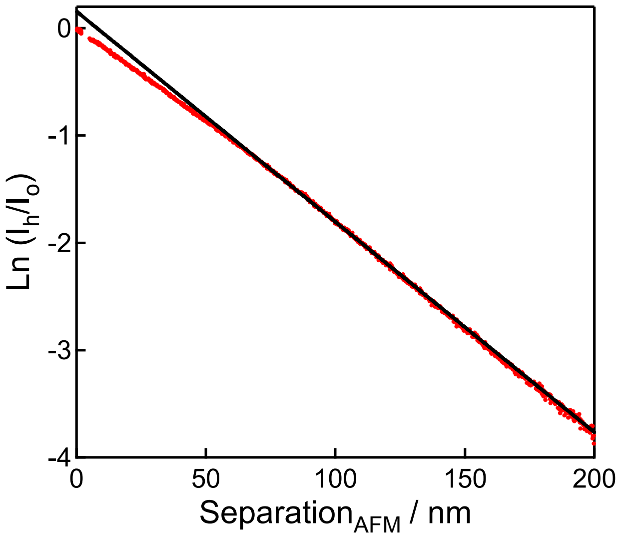

Figure 2.6. Scattering from a nickel sphere attached to a tipless silicon cantilever. The non-exponential features of the scattering profile from a metal sphere are the same as for the glass spheres.

profile was measured from a solid nickel sphere. Using a metal sphere minimizes the signal that is frustrated through the sphere to the cantilever and back to the detector. Figure 2.6 shows the scattering profile from a metal sphere on a natural log scale. As can be seen, the general features of the deviation measured for a glass sphere are also observed for metal spheres.

2.3.4 Effect of Direction of Laser Propagation

The cantilever is asymmetric, so one might expect that reflections from the cantilever would depend on the angle between the axis of the cantilever and the plane containing the incident and reflected light. Depending on the direction of propagation, the cantilever presents a different profile as a reflecting surface. Experiments were conducted at 0^o and 90^o with the sphere mounted at the furthest

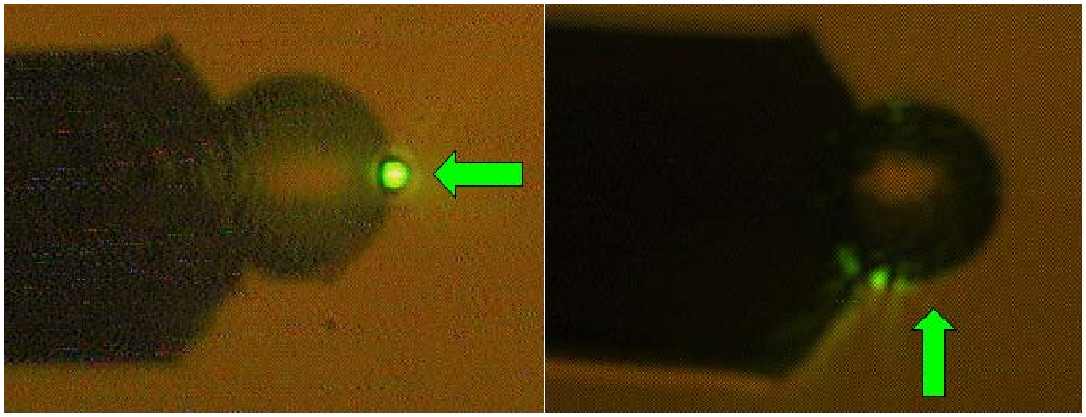

Figure 2.7. Scattering pattern observed when light is incident at 0^o (left) and 90^o (right), for a glass particle that is mounted at the furthermost end of the cantilever. Green arrows indicate the direction of light propagation

most position on the cantilever. There is no significant difference between the scattering profile measured at 0^o and 90^o. Figure 2.7 shows the scattering pattern observed by eye when light is striking at 0^o and 90^o. The scattering pattern observed at 0^o is consistent with those observed for free floating particles in an evanescent field. The scattering pattern observed at 90^o is more complex which suggests the light is interacting with asperities on the surface of the sphere, the glue binding the sphere to the cantilever, or the cantilever itself. Repeats of this experiment did not always show a single scattering point when the light propagation was 0^o to the colloidal probe.

The scattering profile for both the 0^o and 90^o directions of laser light propagation, demonstrate a non-exponential dependence on the separation between the probe and sample, which suggests that the cantilever is not the cause of the non-exponential scattering profile measured from larger spherical particles.

2.3.5 Scattering Profile for Transmitted Light

The following experiments were conducted to deal directly with differences in experimental conditions used in TIRM measurements[3] and the EW-AFM measurements of scattering intensity versus separation for spherical particles. The physical arrangement in a typical TIRM experiment is different to that used in EW-AFM. In my experiments, the signal arises from light that passes back through the sample surface and prism, whereas is conventional TIRM the signal arises from light that travels in the opposite direction (i.e. light transmitted away from the prism). The incident angle in previously discussed results is also further from the critical angle than is typical for TIRM; the incidence angle may also affect the scattering profile.

Original design issues with our first Asylum AFM prevented the viewing of the scattering particle from above. Subsequent design changes in the Asylum AFM (manufacturer changes) have allowed a user to view and capture light from above the cantilever with a 10x objective. Using this new feature and a commercial CCD camera, the scattering profile was measured simultaneously from above and below the scattering object. This is demonstrated schematically in figure 2.8. This experiment was conducted using a particle glued to the end of a tipless cantilever, similar to that shown in (figure 2.7). This was done to minimize the effects of the cantilever contribution to the scattering signal measured both from above and below the scattering particle. Figure 2.9A shows the raw signal generated by a scattering particle as a function of time, captured both by the PMT

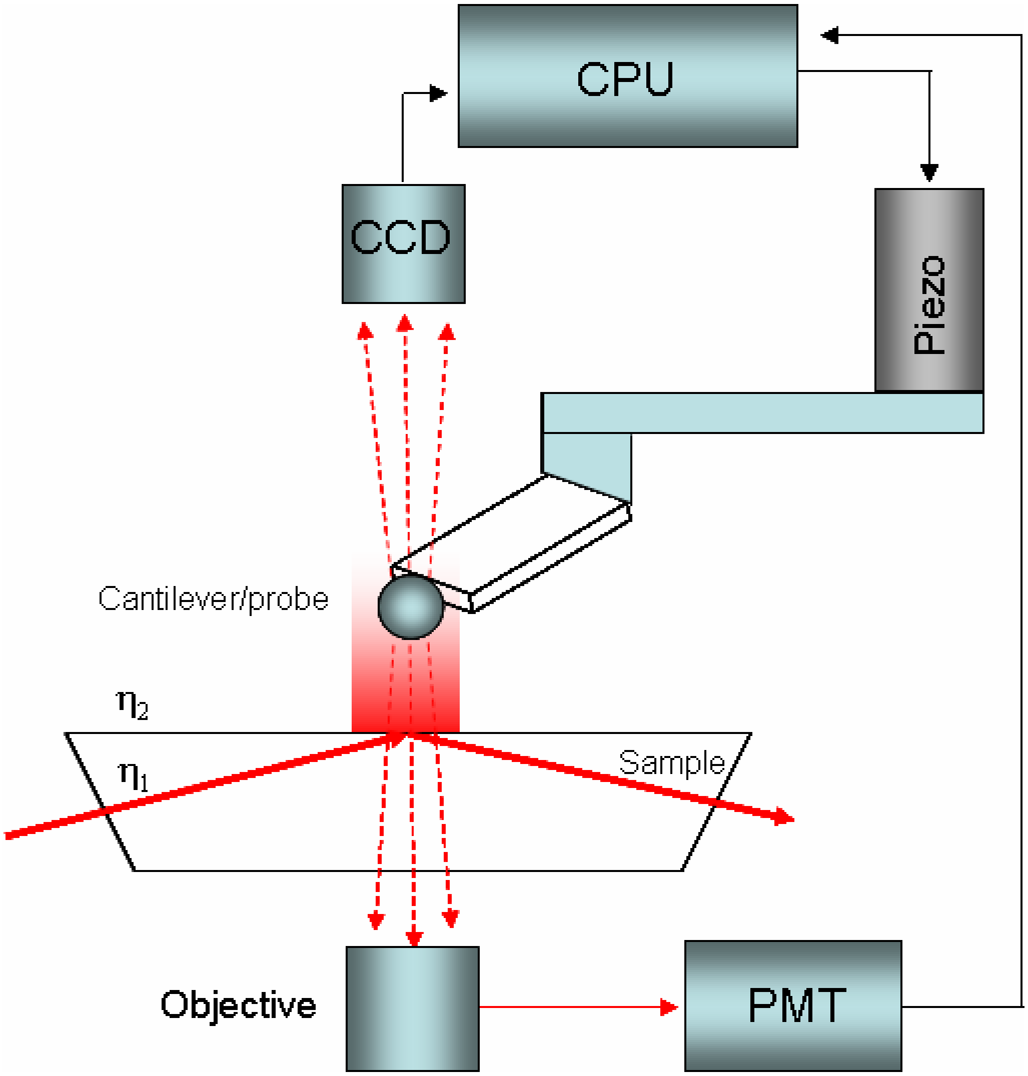

Figure 2.8. Schematic of alteration to EW-AFM to collect light that is scattering from both above and below the scattering object

(below) and CCD (above). The data acquisition rate of the PMT far exceeds that of the CCD, and because of the light amplification systems in the PMT, the signal to noise ratio from the PMT is also much larger than for the CCD. Analysis of this experiment was complicated because the CCD signal is not in sync with the piezo position, and is not collected at the same data acquisition rate. Therefore the

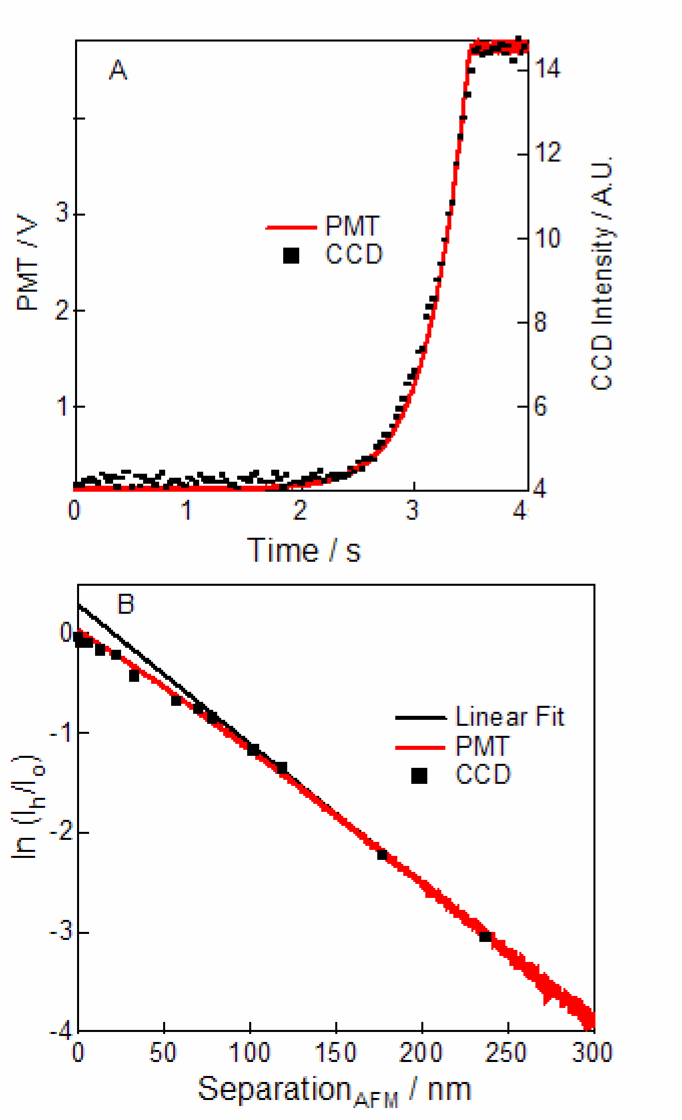

Figure 2.9. (A) Raw scattering signal as a function of time as measured by the CCD (black line) and PMT (red line). The signal from the CCD has a much lower signal to noise ratio due to the sensitivity of the CCD. (B) is the detected signal plotted on a natural log scale as a function of separation.

CCD signal was superimposed on the PMT signal as a function of time, for only a significant enough number of points to determine the scattering profile. This is shown in figure 2.9B. Within the noise limits, there is no difference in the scattering profile measured from above and below.

2.3.6 Effect of the Angle of Incidence

It was difficult to study the effects of the angle of incidence on the resulting scattering profile, because the prism used in these experiments is a trapezoid cut at an angle of 78°. With this prism, it is difficult to create laser reflections with angles of incidence lower than ~ 73 degrees. The critical angle at the glass water interface is ~ 61°, which is much to low an angle to access. Therefore, chloroform was used as the transmission medium to increase the critical angle to an accessible angle. Chloroform has a refractive index of 1.444 and the borosilicate glass prism has a refractive index of 1.515, which produce a critical angle of 72.38°. The minimum incident angle in these experiments was 73.7° or approximately 1.5 degrees from the critical angle. The incident angle, θ_I, was determined by measuring the decay length of the scattering signal at large separations through

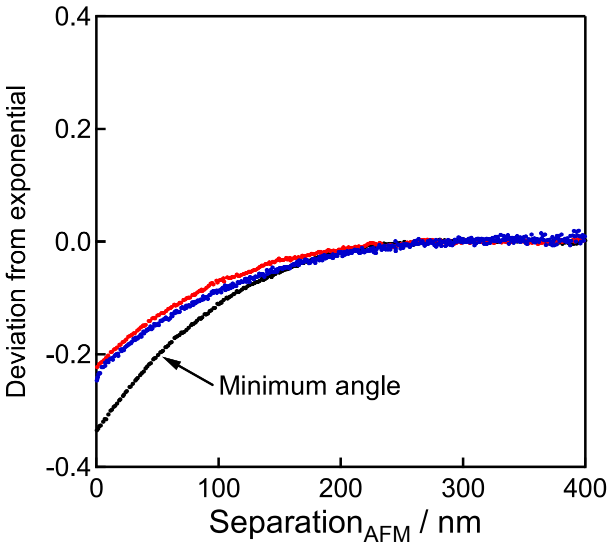

Figure 2.10. $(-h/\delta_{meas}) - \ln(I_h/I_o)$ versus separation as a function of angle of incidence. The deviation from an exponential fit is a maximum at approximately 73.7° (black) and is approximately constant as the incident angle is increased first to 74.4° (red) and then to 77.4° (blue). The critical angle for the chloroform glass interface is 72.4°.

equation 2.4. The decay length depends on the wavelength of light λ, and the refractive index of the reflection, η_1, and transmission medium η_2.

$$\delta = \frac{\lambda}{4\pi\eta_2\left((\eta_1/\eta_2)^2 \sin^2\theta_i - 1\right)^{1/2}} \tag{2.4}$$

Figure 2.10 shows that the magnitude of the deviation from an exponential fit decreases as incident angle is changed from 1.5° to 2.1° from the critical angle and remains constant when we change from 2.1° up to 5°. Even close to the critical angle the deviation from exponential is still prominent, and in fact, these results show that the magnitude of that deviation increases, not decreases as the critical angle is approached.

Finally, it should be emphasized, that regardless of the experiments conducted, the particle scattering results are still obtained in the presence of a cantilever. It is therefore difficult to make a general statement about the nature of the scattering-separation relationship in TIRM solely on the basis of the results from these experiments.

2.4 Discussion

2.4.1 Use of Scattering to Measure Separation

Clearly the scattering of an evanescent wave by a particle is a strong function of separation, so scattering provides a useful method for measuring separation. For a small object such as the silicon nitride AFM tip, the decay has a simple exponential form, but for silicon tips and larger particles, the profile is more complex. If an independent method for measuring the separation is available (as in EW−AFM), one can measure the entire scattering-separation profile and thereby obtain a calibration curve for future measurements of separation from scattering experiments.

Figure 2.11 shows an example of what would happen if one assumed that the scattering profile was purely exponential at all separations for large particles, when in fact it is not. The solid red circles show the experimental points at large separation, where the profile is exponential. The solid line is given by ($-h/\delta_{meas}$) where δ_{meas} is the measured decay length at large separation. In a TIRM experiment, the approach commonly used for obtaining absolute separation distances is to bring the test particle into contact by the addition of salt, measure I_o, and obtain δ from theory (by knowing λ, θ, and the refractive indices). Because of the difference between I_o and I_o', at large separations, there is a

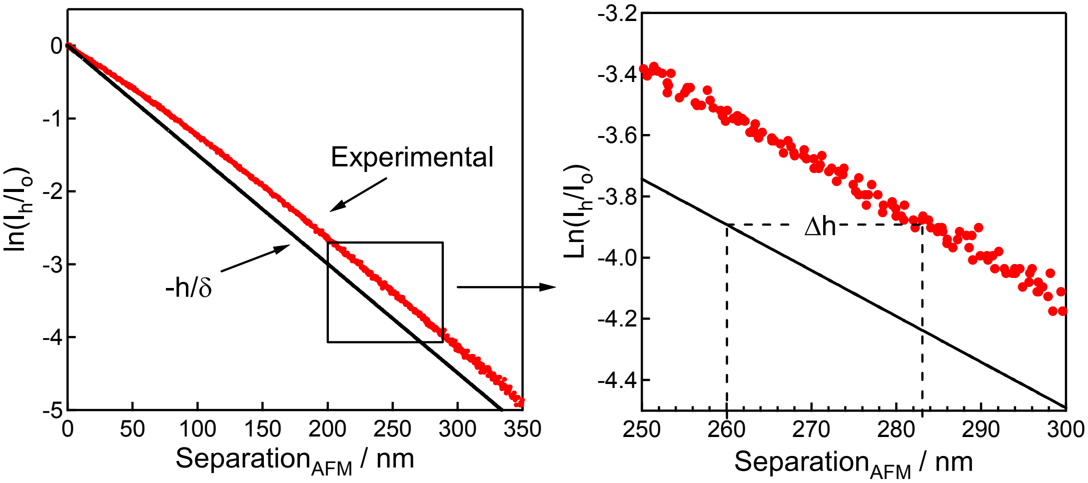

Figure 2.11. Error in separation, Δh, assuming a purely exponential decay from I_o. $\Delta h = (\ln(I_h/I_o) - (-h/\delta)) \times \delta$. The average deviation for an 11.4 μm radius sphere is 23 ± 1 nm. For a 1.2 μm radius sphere, 9 ± 1 nm.

constant error in the separation obtained by mistakenly assuming a simple exponential profile. For example in Figure 2.11 (R = 11.4 μm particle), the actual separation is 23 ± 1 nm greater at large separations. For a 1.2μm particle, the error is 9 ± 1 nm at large separations. The error in assuming that the scattering decay is exponential into contact is not even constant in the important region when the separation is less than 3δ.

These glass particles are glued to an AFM cantilever, and both the silicon and silicon nitride tips are fabricated as a single piece with the cantilever. It is natural to wonder to what extent the physical coupling of the cantilever affects the scattering that is measured. This is particularly relevant to researchers who may wish to apply these findings to applications using free particles e.g. TIRM. First, it is clear from the scattering signal produced by the integrated silicon nitride tip cantilever, that the cantilever itself is not responsible for the deviation of the scattering from an exponential profile. This still leaves open the possibility that the deviations result from light that is collected by the particle and reflected into the detector by the cantilever. The ideal experiment would of course measure the scattering profile from a free sphere while determining the separation by a method other than by the AFM. In the absence of a method to perform this ideal experiment, I have investigated the effect of the angle of incidence, direction of laser propagation, the position where the particle is mounted on the cantilever, and position of light collection, and found that under all these conditions the scattering profile is still non-exponential.

Without the development of a more complex model for the scattering profile, it may still be possible to use simple mathematical fits to certain regions of the scattering profile to obtain the separation. For example, the scattering signal from the silicon tip is approximately linear for h < 150 nm. This is well within range of most electrostatic repulsions and short range repulsions. The separation could be determined for this region assuming a purely exponential behavior, and the remaining long range scattering can be discarded. The error in separation assuming a purely exponential profile for h < 100 nm is shown in figure 2.12. The y-axis is a plot of the actual separation measured by traditional AFM analysis

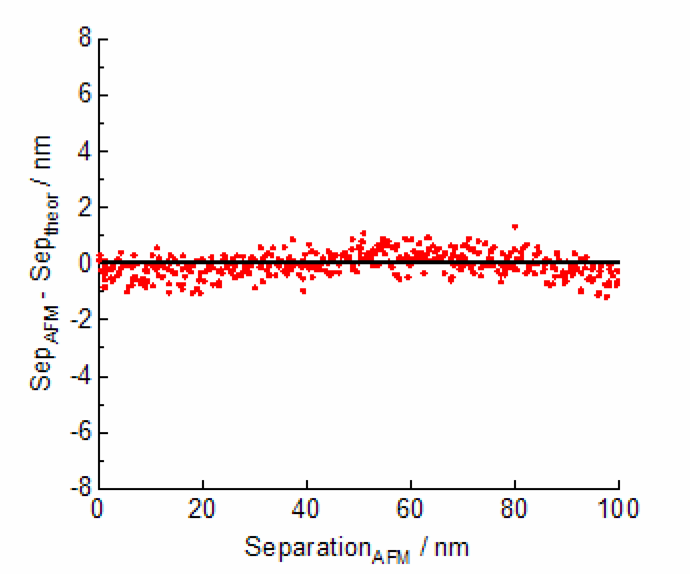

Figure 2.12. A plot of the difference between the separation determined by tradition AFM analysis (Sep_{AFM}), and the separation determined from the silicon scattering data (Sep_{theor}, figure 2.3), as a function of the actual separation. The theoretical separation was determined assuming a purely exponential scattering profile in the region of 0 to 100 nm and a decay length of 68.5 nm.

minus a calculated separation assuming an exponential decay between 0 and 100 nm with a decay length of 68.5 nm. The standard deviation of the assumed separation from the actual separation is 0.43 nm.

2.4.2 Origin of the Deviation from Exponential Decay of Scattering

Court and von Willisen[5] showed that the transmitted intensity of an evanescent wave across a thin ($d < \lambda$) film sandwiched between two flat planar sheets is approximately exponential for $d > 3\delta$ and smaller than exponential for thinner films, i.e. the same trend as in these experiments for large glass particles. The amount of deviation from exponential is much larger in magnitude for two flat sheets. It has been stated that the deviation from exponential for the *flat* sheets is due to the interference of multiply reflected beams[3]. Note, this is consistent with our metal particle results, in which the scattering signal that is collected is primarily from front reflections off the particle, i.e. the most likely to be involved in multiple reflections between the particle and surface. Finally, experimental results suggest that the observed deviations are increasingly dependent on an increasing particle radius. The results presented in this chapter demonstrate a progression in the magnitude of deviation as we progress from a silicon nitride tip ($R < 60$ nm) to the case of two flat sheets. This indicates that as the particle radius increases, it begins to approximate a flat sheet.

2.5 Conclusions

The scattering of an evanescent wave by a silicon nitride AFM tip is large and decays exponentially with separation from a refractive index boundary. Scattering is thus a useful method for measuring the separation between a Si_3N_4 AFM tip and sample. The scattering profile for silicon tips is not exponential over all separations, but can still be used to determine the separation at short range separations (h < 150nm) where the scattering profile is approximately linear. The scattering profile for colloidal particles attached to AFM cantilevers is exponential at large separations (h > 200 nm for visible light) and deviates from exponential at smaller separations. The non-exponential profile does not depend on the position of light collection (above or below), and is still observed when the proximity of the cantilever is minimized. A non-exponential profile was observed when the overall effect of the cantilever was minimized by using a metal particle. For borosilicate glass particles and $\theta_i = \sim 75^o$, the smallest deviation from exponential are found for a small radius (R ≈ 1 μm).

Because the particles were attached to cantilevers in all these experiments, it is not certain whether deviations from exponential decay would also occur for free particles (e.g. in TIRM measurements). However these results suggest that it would be wise to perform an independent check of the separation-dependence of scattering in TIRM measurements, particularly for larger particles and smaller separations.

2.6 Cited Literature

1. Prieve, D. C.; Frej, N. A., Total Internal Reflection Microscopy - A Quantitative Tool for the Measurment of Colloidal Forces. *Langmuir* **1990,** 6, (2), 396-403.
2. Prieve, D. C., Measurement of Colloidal Forces with TIRM. *Adv. Colloid Interface Sci.* **1999,** 82, 93-125.
3. Prieve, D. C.; Walz, J. Y., Scattering of an Evanescent Surface Wave by a Microscopic Dielectric Sphere. *Applied Optics* **1993,** 32, (9), 1629-1641.
4. Ducker, W. A.; Senden, T. J.; Pashley, R. M., Direct Measurement of Colloidal Forces Using an Atomic Force Microscope. *Nature* **1991,** 353, (6341), 239-241.
5. Court, N.; von Willisen, F. K., Furstrated Total Internal Reflection and Application of its Principle to Laser Cavity Design. *Appl. Opt.* **1964,** 3, 719726.

Chapter 3

Measurement of the Absolute Separation between Surfaces

3.1 Introduction

As demonstrated in Chapter 2, the scattering of an evanescent wave by a silicon nitride tip uniquely depends on the tip-sample separation, and importantly the experimentally measured scattering profile is consistent with the theory of scattered evanescent waves. This means the refractive index of the medium between the tip and sample can be accounted for[1]. The simple functional form for the scattering profile means the separation between a tip and sample can be obtained with great precision. The following chapter examines force-separation profiles obtained between a scattering Si_3N_4 tip and a glass substrate (knowing the functional form is exponential) when there is an additional thin film, with a refractive index gradient to the bulk fluid, between the tip and sample.

Atomic force microscopes are widely used to determine the force between polymer-coated solids.[2-5] A fundamental limitation of an AFM surface force measurement is that the separation between the solids is not measured explicitly; the separation is inferred from the force measurement[6]. In conventional AFM measurements the *relative* separation is obtained by adding the deflection of the cantilever to the displacement of the piezoelectric translation stage. The *absolute* separation is obtained by locating the point of zero separation from interpretation of the force-distance profile. Usually one defines zero separation to be where

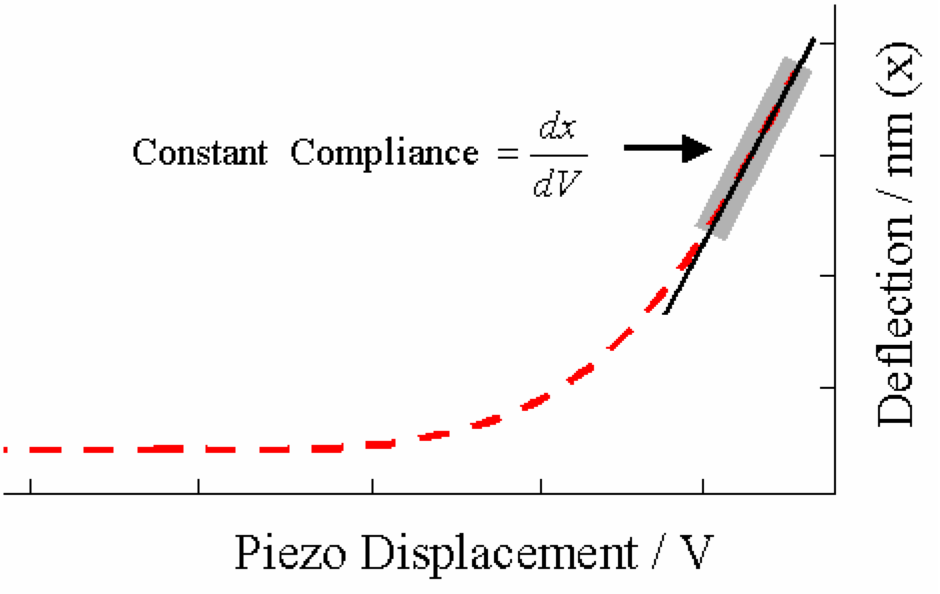

Figure 3.1. Graphical representation of the deflection of an AFM cantilever as it approaches a surface (left to right). The cantilever experiences a repulsive force until it makes hard contact, which is defined by a steep gradient in the deflection vs. piezo displacement, and is linear.

there is a very steep gradient in the surface force (this is demonstrated graphically in figure 3.1). This procedure is acceptable when the solids are incompressible and the adsorbed material can be displaced at an accessible force.[7, 8] However, when the solids are compressible or the attached films cannot be displaced at an accessible force, problems arise in determining the cantilever deflection contribution to both the relative and absolute separation.

The relative separation can be obtained through a calibration step. For example, when measuring the forces between rigid solids coated with a physisorbed polymer layer, one usually measures the cantilever deflection at contact prior to adsorption. In this step, the cantilever deflection slope (deflection vs. piezo displacement) can be calibrated by pushing against the rigid solid, so the relative separation and force can be measured in the presence of the physisorbed polymer. The problem arises when determining the absolute separation in the presence of the polymer. The cantilever often cannot generate enough pressure to displace the polymer, so the tip cannot reach zero separation. There may also be a very steep gradient in the force when there is a significant thickness of the polymer film between the solids, thereby confusing the signature of zero separation.

A low cantilever spring constant is desirable for high resolution of weak forces in thin films, but a weak spring makes it difficult to distinguish between the stiffness of the solid and the composite solid plus film. In practice one must compare the deflection of the slope of the spring during calibration against a hard surface to the very similar deflection slope during compression of the polymer. This comparison must be made over a large range of spring deflection to achieve displacement of the film, which may not occur. Also the stiffness of the polymer layer usually increases as the film thickness decreases, which results in a deflection slope that asymptotes to value that cannot be distinguished from the rigid solid. The consequence is that the absolute position of zero separation cannot be reliably determined by traditional AFM analysis. At best, the force profiles are represented as a force vs. an *apparent* separation.

In principle the absolute separation could be determined in the presence of a polymer film simply by measuring both the piezo displacement and deflection of the spring in the range of zero separation when the solids are in contact without adsorbed polymer, and then re-measuring the piezo displacement and the deflection at all subsequent times in the presence of adsorbed polymer. The difference in the piezo displacement position at the onset of the region of constant compliance would give the absolute position of the tip after the adsorption of the polymer. Sadly this method is always defeated by small changes in the dimensions of the AFM caused by thermal drift.

A much better solution is to explicitly measure the separation between the solids. In the surface forces apparatus,[9] the separation is measured explicitly by interferometry. As discussed previously the scattering of an evanescent wave can be used to measure the absolute separation between a tip and a sample or a colloidal probe and a sample.[10] The scattering from a silicon nitride AFM tip varies exponentially with separation, so it is simple to obtain the separation from scattering. Importantly, changes in the dimensions of the AFM due to thermal fluctuations do not affect this relationship. For a colloidal probe, the scattering is non-exponential so a calibration curve or a more complex theory is required.

In this chapter focus is placed on silicon nitride AFM tips, because the scattering is proportional to the evanescent wave in the absence of the tip, and therefore the refractive index of the film can be quantitatively accounted for. Explicit measurements of the refractive index of thin films will be presented in chapter 4.

As discussed in the introduction, the evanescent wave in the absence of the tip is an exponential function with distance away from the point of total internal reflection. The decay of the wave depends on the wavelength of light λ, the refractive index of the incident and transmission medium η_1 and η_2, and the incident angle θ_i. By experiment, it is found that the scattering intensity I_h, from a silicon nitride tip measured below the sample is proportional to the intensity of the evanescent wave, so:

$$I_h = I_o \exp(-h/\delta) \tag{3.1}$$

$$\delta = \frac{\lambda}{4\pi\eta_2\beta} \tag{3.2}$$

$$\beta = \sqrt{\left(\eta_1 / \eta_2\right)^2 \sin^2\theta_i - 1} \tag{3.3}$$

Again the separation between the tip and sample is defined as h and the decay δ, depends on the refractive index of the incident and transmission medium η_1 and η_2. Clearly the separation h can be obtained from equation 3.1 by measuring I_h and I_o.

3.2 Materials and Methods

3.2.1 Experimental Method

The evanescent wave atomic force microscope, which was described earlier, was used with the following modifications. The evanescent wave was created, either by a 405 nm (405-50-COL-004, Oxiuss, France) or a 532 nm diode laser (TECGL-20, World Star Tech, Toronto, Canada), at the interface between a borosilicate glass plate (12-544-12 Fischer Scientific) and an aqueous solution. The borosilicate glass plate was separated from a borosilicate reflection prism by index matching fluid. For the 532 nm laser, the incident angle was approx 75^o, so the decay length was 70 nm. For the 405 nm laser the corresponding values were 76^o and 52 nm. The scattering signal was collected by a Nikon LU Plan 50x/0.55NA objective and transferred to a Hamamatsu photomultiplier tube (H5784-20).

Fluid exchange during experiments was achieved by altering the Asylum cantilever mount to hold 2 lengths of PEEK tubing (Valco Instruments, Houston, Texas) in close proximity to the cantilever. This enabled fluid exchange in a capillary of liquid formed between the cantilever head and sample, without the danger of “bumping” the AFM head (importance discussed in section 3.3.2).

3.2.2 Experimental Materials

The silicon nitride tips (NP, Veeco, Santa Barbara, California) used in this work were cleaned under ultraviolet light prior to use. All solutions were prepared in water purified in an EasyPure UV system (Barnstead, Dubuque, Indiana); the water had a resistivity of 18.2 MΩ-cm and surface tension of 72.3 mN/m. The borosilicate glass slides have an RMS roughness of 0.26 nm over an area of 5 square microns. The glass slides were used immediately after they were cleaned in oxygen plasma for 45 seconds at 250 Torr, using a Plasma Prep II (SPI Supplies, West Chester, PA).

Dr. Greg Qiao and Dr. Tiziana Russo, of the University of Melbourne, kindly provided the zwitterionic polymer used in these experiments. It is a polysulfobetaine[11-13] synthesized by the polymerization of N,N-dimethyl-N-[2-[(2-methyl-1-oxo-2-propenyl)oxy]ethyl]-3-sulfoethanaminium. These polymers are insoluble in de-ionized water, so all experiments were performed in solutions containing 100 mM NaCl. The sodium chloride (Aldrich 99.99%) was roasted for six hours at 560^{o}C. Didodecyldimethylammonium bromide (DDAB) (Fluka, ≥ 98%) was used as supplied.

3.3 Results

The results section is organized as a progression of experiments that are of increasing difficulty to analyze. First are the measurements where there is only salt solution between the tip and sample, followed by measurements where there is a thin organic film that can easily be displaced by the AFM tip. The final results describe when the film cannot be displaced.

3.3.1 Salt and Surfactant Solutions

Figure 3.2 shows the concordance between conventional AFM analysis of separation and the separation measured from evanescent wave scattering, in the

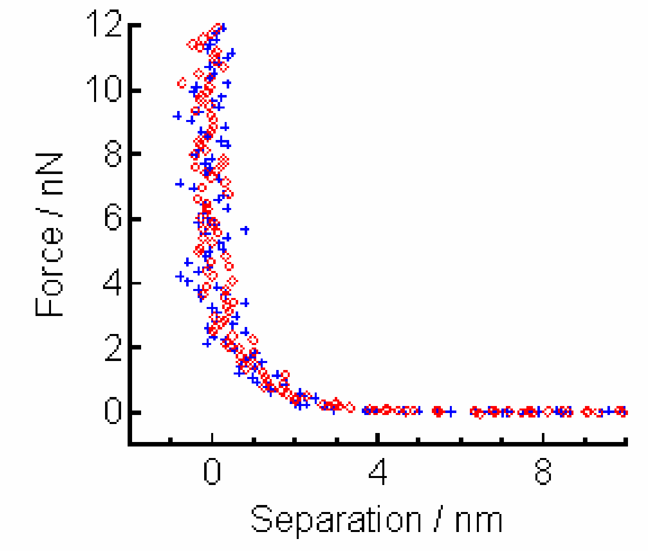

Figure 3.2. The force-separation profile measured between a hydrophilic Si_3N_4 tip (k = 0.12 N/m) and a hydrophilic glass surface in 100mM NaCl. The separation between the surfaces was determined by conventional AFM techniques (blue crosses), and by using equations 3.1-3.3, to determine the separation from the scattering of the AFM tip (red circles). Scattering and deflection data are collected simultaneously.

presence of 100 mM NaCl. The force-separation profile was measured between a hydrophilic tip and a hydrophilic glass plate and is purely repulsive on approach and withdrawal (for clarity only the approach data is plotted). Because the salt is easily displaced from between the tip and surface, the force determined from traditional AFM analysis was used for the scattering analysis of separation.

Figure 3.3 shows the concordance between conventional AFM separation and scattering measurements in the presence of a thin film of low molecular weight surfactant, which is easily displaced from between the AFM tip and sample. In this case, the thin film was prepared by the adsorption of didodecyldimethylammonium bromide (DDAB) in equilibrium with a 0.5 mM solution in bulk. This concentration is just above literature reported results for the

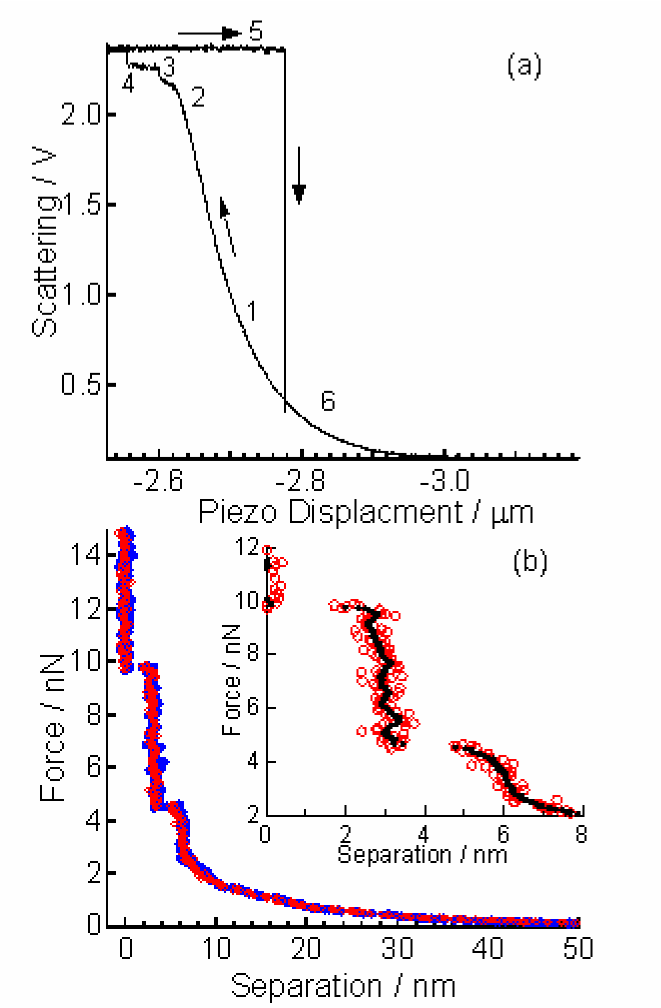

Figure 3.3. Profiles measured for a Si_3N_4 tip (k= 0.58N/m) and a glass solid in 0.5 mM DDAB. (a) Scattering Intensity as a function of piezo displacement. The profile shows hysteresis due to the adhesion of the tip to the glass. (b) Force as a function of separation measured by conventional AFM analysis (blue circles) and EW-AFM (red circles). The inset shows scattering data only on an expanded scale. The black line is running average of 10 points.

CMC of DDAB.[14] DDAB forms flat bilayers and the glass water interface. The scattering data in this case is more complex because of the more complex force profile. Figure 3.3A shows the raw data of the scattering intensity vs. piezo displacement. In region 1, the force is negligible so the scattering is an exponential function of piezo displacement. As the separation between the two surfaces decreases, an electrostatic repulsion between the head groups of opposing adsorbed bilayers, causes the AFM cantilever to deflect. The deflection of the cantilever results in a deviation from the exponential scattering in the raw signal (region 2). When surfactant bilayers from opposing surfaces begin to interact, the rate at which the AFM tip approaches the sample surface begins to dramatically decrease, and the scattering intensity levels off. The two outermost surfactant layers from opposite surfaces are pushed out from between the tip and sample, resulting in a rapid decrease in the separation and a step in the scattering data (region 3). In region 4 the two primary surfactant layers are expelled, the tip and sample make hard contact, and the scattering intensity remains constant as the piezoelectric translation stage continues to drive the cantilever chip towards the surface. As the piezo begins to retract, the tip and surface remain in contact until the force of the spring exceeds the force of adhesion (region 5). The surfaces then separate suddenly, and the scattering intensity jumps to the value measured on approach (region 6).

Figure 3.3B compares the force-separation profile determined from the scattering intensity and by conventional AFM analysis. In both cases the amount of the cantilever deflection, used to determine the force, was measured by traditional AFM analysis. Both methods produce the same force-separation profile. The separation for the scattering experiments was calculated using equation 3.1, and the experimentally measured decay length at large separations.

The force-separation profiles are concordant despite the fact that the decay length in the surfactant film is longer due to the increased refractive index of the film.

The inset in figure 3.3B shows detail of the region of surfactant exclusion as measured by scattered separation only (red circles). This figure can be used to demonstrate the resolution of the evanescent wave AFM. The surfactant is displaced from the thin film in two discrete steps from 5 to 3 nm, and ~2.5 to 0 nm. The data was collected at 0.44 Hz at 2000 points per second. If we take a running average of 10 points in the data, so that the data acquisition rate is effectively 200 points per second (black line), we can clearly resolve the slope of the force separation profile for the ~3 nm film. The stiffness of the film is 3.2 N/m, and the standard deviation of the averaged points from a straight line is 0.13 nm.

The force-separation profile shows the layering of the surfactant in the thin film between the tip and sample. The all trans (maximum length) conformation of DDAB has a length of about 1.9 nm, but neutron-reflectivity measurements[15] are consistent with a thinner layer of about 1.1 nm. Our data shows that the force gradient increases more rapidly starting at about 10 nm. Then there is a steep rise in the force at ~ 6 nm corresponding to direct interaction between charged head groups from opposing bilayers. This gives a measurement of approximately 1.5 nm per surfactant layer. When these bilayers are compressed to about 5 nm they yield, and a new structure is formed with a thickness of 3 nm, again approximately

1.5 nm per surfactant layer. This very stiff layer is then compressed to about 2.7 nm before it yields and the surfactant is displaced from between the tip and sample.

3.3.2 Polymer Solution

Often an AFM cantilever cannot apply enough force to displace an adsorbed polymer from between a tip and sample. In this case, it is necessary to have the correct value of I_o prior to the adsorption of the polymer in order to measure the absolute separation by the scattering method. Two different methods (*reference* and *contact*) have been used to obtain a value of I_o prior to polymer film formation. The *reference* method involves measuring the value of I_o in the solvent prior to the addition of polymer. This value of I_o (to be used for all subsequent measurements) is used to determine the separation between the two surfaces after the polymer solution is added and adsorbed to the surface. This method suffers from the assumption that the adsorbed film does not change the magnitude of the scattering when the tip is in contact with the sample, and that there are no changes in the intensity of the laser/scattering or alignment of the laser as a function of time. The *contact* method involves adding the polymer solution while the tip remains in contact with underlying sample. I_o is measured immediately before the tip is withdrawn from the surface and is then used to determine the separation between surfaces with adsorbed polymer.

Both methods require a constant value of I_o. In practice, I_o can change due to the appearance of other scattering particles in the field of view, or by a change in the intensity or position of the evanescent zone. To reduce the error associated with the latter, the asylum cantilever mount was modified to allow two tubes in close proximity to the cantilever. This helped to exchange fluids between the tip and sample without disturbing the position of the AFM tip in the viewing field of the PMT, or in the ellipse of total internal reflection.

The results for both the *reference* and *contact* procedures are shown in figure 3.4. Figure 3.4A shows the scattering output from the Si_3N_4 tip (k = 0.58 N/m) which is initially in contact with the glass surface while a 1 mg/ml polymer-salt solution was added. After an adsorption time of 5 minutes, the tip was withdrawn (W) and then brought back to the surface (A). The piezo was run at a rate of 200 nm/s over a scan range of 4.2 μm; with a 10 second dwell away from the surface. While the tip was away from the surface (~1 minute), polymer adsorption occurred in the space previously occupied by the tip. When the tip was brought back towards the surface, the newly formed polymer layer kept the tip from contacting the glass surface (this is shown schematically in figure 3.5). Because the tip cannot displace the polymer, the measured scattering intensity at the point of closest approach, is less than the intensity measured when the tip was in direct contact with the glass surface. Clearly the tip is not in contact with the glass when it has returned to rest on the polymer coated surface.

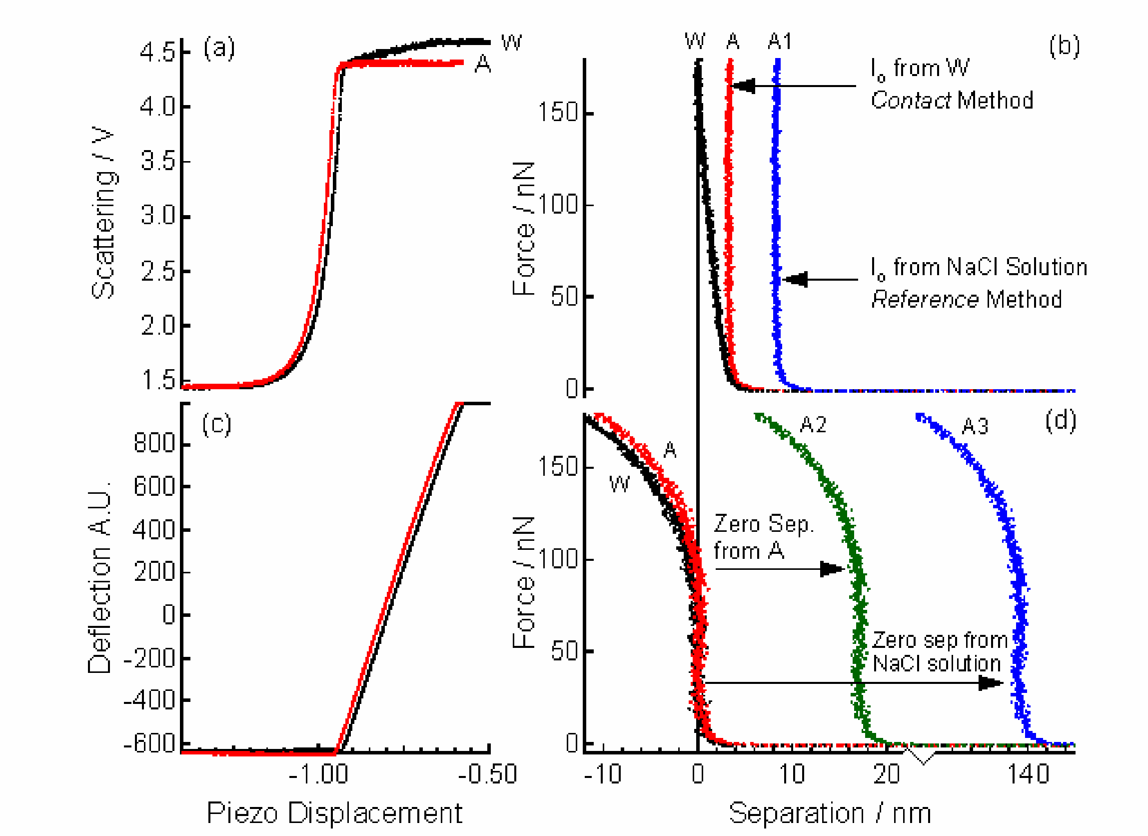

Figure 3.4. (a) Raw scattering intensity. The intensity is greater at the start of the withdrawal because the tip is in contact with glass on withdrawal. (b) Force-separation profile measured using equation 4 for the separation. The red curve (A) is the film thickness using the contact method to determine the tip position on approach. The blue curve (A1) would be the separation if the reference method is used to determine separation. (c) AFM tip deflection captured simultaneously to scattering data in (a). (d) The force-separation profile determined using the AFM deflection data. The withdrawal (W) and approach (A) are coincident using conventional AFM analysis. The green curve (A2) would be the apparent film thickness if we assumed the displacement between approach and withdrawal runs is due to the thickness of the film. The blue curve (A3) would be film thickness if the piezo position prior to the addition of polymer was used to determine the tip position on approach.

Figure 3.4B is the force-separation profile obtained by using the scattering intensity to measure the separation. When I_o, measured before the withdrawal, is used to determine the separation (*contact* method), the surfaces begin to interact on approach (A) at a separation of ~7nm, and the film cannot be compressed to less than ~3 nm. The *contact* method also ensures that the maximum measured

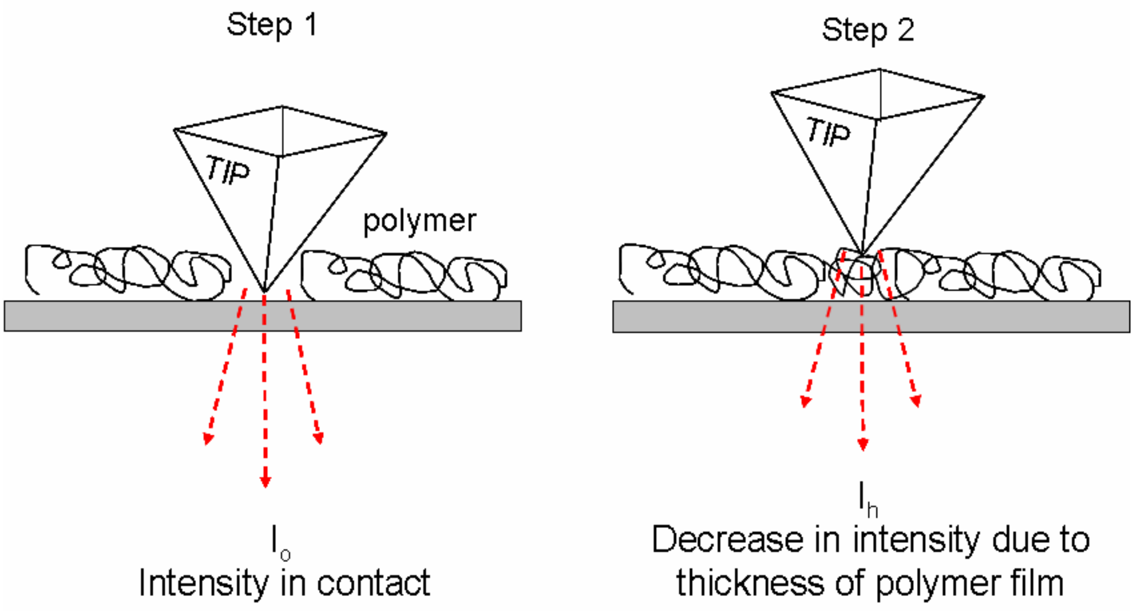

Figure 3.5. Schematic of experiment. In step 1, the polymer is added while the tip is in contact with the bare substrate. After equilibration, the scattering intensity is measured and used as Io. In step 2, the tip is removed from surface, polymer adsorbs in the space left behind from the tip, and when the tip returns it cannot displace the polymer. The measured intensity in "contact" has decreased due to the thickness of the polymer film.

intensity during withdrawal (W) corresponds to zero separation. If the *reference* method is used to determine the separation between these surfaces (I_o measured prior to addition of polymer), we get a different answer for both the onset of interaction and the minimum film thickness (~ 12 and 8 respectively, A1). The *reference* method also shifts the withdrawal curve (not shown) ~ 5nm off the surface (this is clearly not rational, as the tip was left in contact prior to the force run). Again, the force was determined by using the deflection calibration obtained by traditional AFM analysis.

Experimentally, small increases and decreases are observed in I_o during the adsorption of the polymer layer. These small changes make it difficult to use I_o

measured before the addition of polymer (*reference* method) to determine separation. Because these changes in intensity are random, they may be corrected for with a more rigid optical setup. It will therefore be assumed that the *contact* method is the correct way to determine the separation between surfaces after the adsorption of polymer in these experiments. For the remainder of this chapter, only results for the contact method will be used because only this method produces consistent results that are physically reasonable.

Figure 3.4C is the deflection of the cantilever measured during the same experiment as 3.4A. If conventional AFM analysis is used to analyze this data, zero separation is defined by the region with a steep and constant slope of cantilever deflection vs. piezo displacement (region of constant compliance). Differences in the slope between constant compliance regions on approach and withdrawal cannot be distinguished, so they are both assigned to zero separation (figure 3.4D). Alternatively, it is noted that the approach and withdrawal curves are displaced by 18nm in figure 3.4C; and it could therefore be assumed that the film is 18 nm thick (3.4D, A2). Clearly this is an error: the actual displacement varies between 3 and 7 nm. This discrepancy is due to unmeasured changes in the dimensions of the AFM, which vary depending on the experimental conditions and time during the measurement.

The deflection data in figure 3.4C could also be analyzed by a ‘reference’ method. In this case the deflection and position of piezo displacement in contact prior to the addition of polymer is used as a reference position after the addition of polymer. In this case the polymer film would have a measured thickness of 140 nm (figure 3.4D, A3). Clearly the drift in the AFM dimensions (140nm) is much worse than the "drift" introduced from the I_o reference method (~ 5 nm), making the deflection reference method totally impractical.

All three methods that can be used to determine the separation in the conventional AFM method give an incorrect offset to the force-separation curves. Note that the traditional analysis also gives the incorrect *shape* to the withdrawing force curve. The withdrawal of the tip through the polymer film can be observed in by scattering analysis (compare 3.4B (W) to 3.4D (W)).

The scattering method has an additional advantage over the deflection method for determining zero separation. Note that at forces > 100 nN, the deflection data indicates that the sample stiffness is decreasing at an accelerating rate. This unphysical situation is usually blamed on non-linearity of the cantilever diode response, and this region of data is discarded. In contrast, reliable separations can be measured by the scattering analysis in this force range.

3.3.3 Polymer Response to Applied Loads

The ability to determine zero separation enables EW-AFM to perform new measurements. To demonstrate this, I have measured the time-response of the polymer to applied loads. Figure 3.6 shows how the adsorbed polymer film

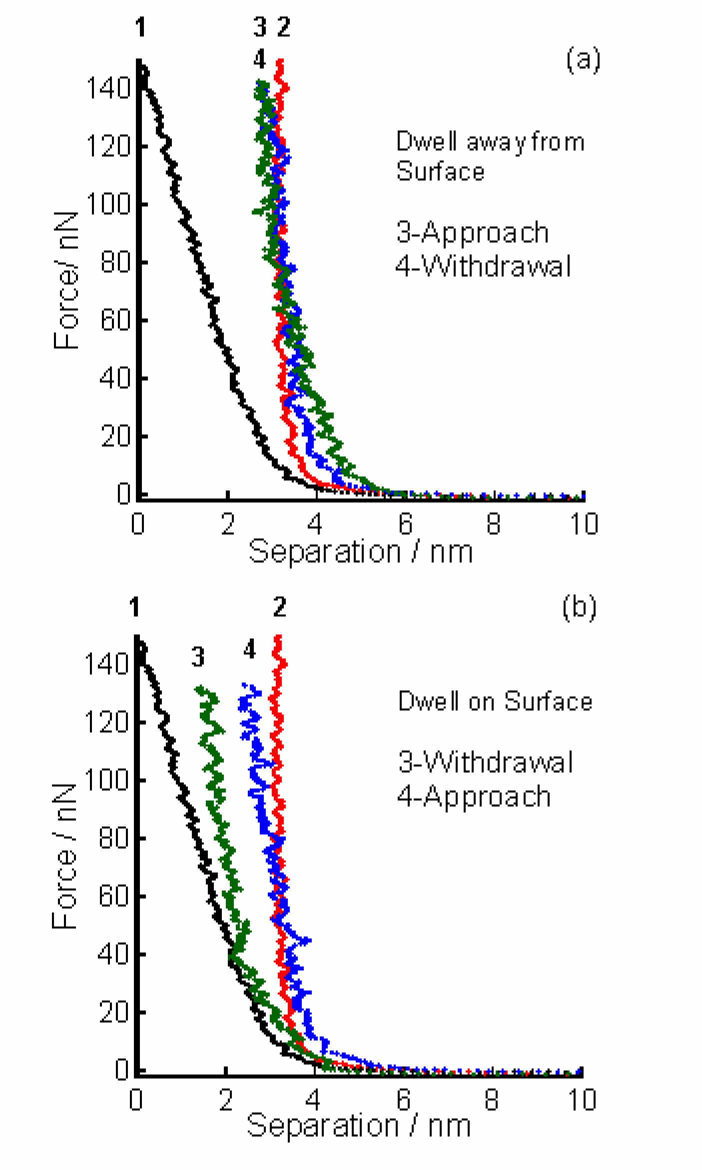

Figure 3.6. Force-Separation profiles determined using equation 4 in polymer-salt solution. The first withdrawal (1) and approach (2) are re-plotted from Fig. 3 (a) approach-withdrawal collected after a 10-minute equilibration time with the tip away from the surface. (b) The tip was left in contact with the polymer surface for 1 minute, withdrawn (3), and then immediately brought back into contact (4). All data shown is the average of 10 measured points.

relaxes after compression. The data has been averaged over an interval of 10 points to clarify the separation values. Curve 1 and 2 show the force on withdrawal and approach re-plotted from figure 3.4B. After the primary withdrawal-approach curve, the tip was left away from the surface for 10 minutes (assumed adsorption equilibrium), and then an approach 3, - withdrawal 4 curve was run (figure 3.6A). The separation was determined using the maximum I_o measured in curve 1. In figure 3.6B the tip was left in contact with the polymer film for 1 minute, then withdrawn (3), and brought back to the surface (4). This data shows that, (a) 10 minutes is enough time for the film to reach its equilibrium thickness and (b) the film thins with time under an applied load.

The latter was also observed by monitoring the scattering intensity in contact with time. Figure 3.7 shows how the intensity in contact changes as a function time (polymer compression) between a withdrawal and subsequent approach curve. The starting point for this experiment is for a tip that has been

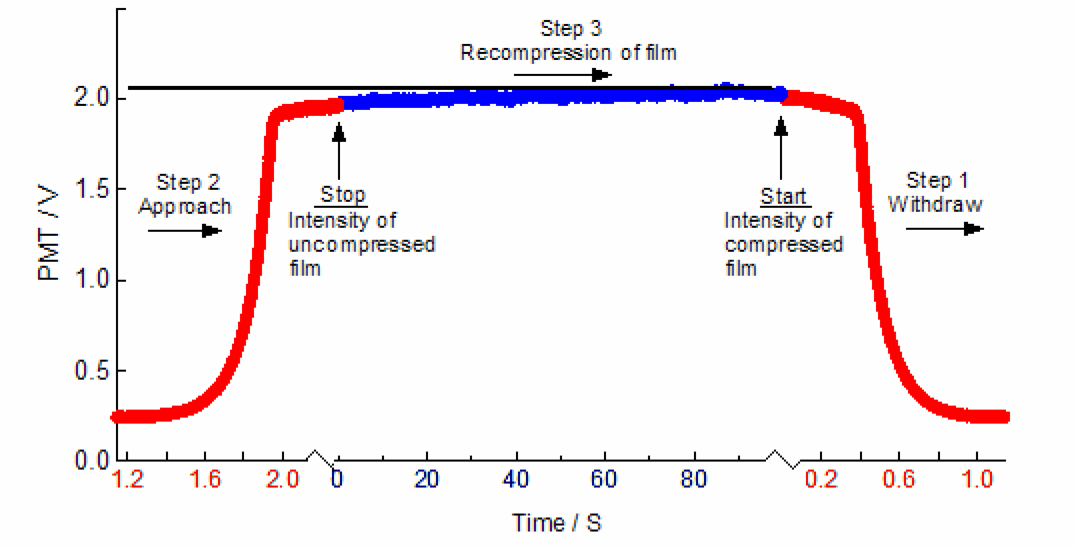

Figure 3.7. Step 1- the tip is initially in contact, and has compressed the film. The tip withdraws (red) and then approaches, Step 2. The maximum intensity on approach is less than the withdrawal (film is thicker). Step 3 – Scattering intensity measured in contact for 100 seconds immediately after approach curve stops (blue). The intensity increases back to the original withdrawal indicating a compression of the film under load.

left in contact with the polymer film for a significant enough time to compress the polymer film to it's minimum (starting point is on right hand side of graph indicated by arrow, red line). In step 1, the tip is withdrawn (moving to the right), and then is brought back to the surface in step 2 (left hand side of graph, moving left to right, red line). I have purposefully split the withdrawal and approach scattering intensity apart. The scattering intensity in contact at the end of step 2 is less than it was at the start of the withdrawal (step 1), i.e. a thicker film. Immediately after contact in step 2, a scattering curve was collected over a piezo travel distance of 1nm (step 3, blue line), for a duration of 100 seconds. During this time, the intensity slowly increases back to the intensity measured immediately before the start of step 1, i.e. the film is compressing. This is a real-time measurement of a tip approaching the underlying substrate, by compressing a physisorbed polymer layer.

3.4 Discussion

3.4.1 Effect of a Thin Organic Film on the Scattering Profile

The deflection-scattering-displacement measurements in surfactant solution (figure 3.3) provide an interesting opportunity to investigate the effect of a thin organic film on the scattering from the AFM tip. The solid surface is very stiff, so reliable measurements of cantilever deflection can be obtained. The stiff solid and the ability to displace the surfactant under high loads allow unambiguous measurement of the absolute separation from conventional AFM analysis. Thus a plot of scattering as a function of film thickness determined by traditional AFM analysis can be obtained. It is found that the scattering profile agrees well with the intensity profile of the evanescent wave in the absence of the thin film. This is clearly shown by the concordance between the two data sets in figure 3.3B. Thus the separation can be measured (by scattering) in the presence of a very thin film, even without knowing the thickness or refractive index of the film (or indeed without knowing whether the film exists at all).

Can the presence of all film types be ignored? It should be noted that the surfactant film is special in so far as surfactant molecules tend to pack into certain preferred geometries, and DDAB in particular packs into flat bimolecular sheets. It is therefore expected that a broad capillary of surfactant will not form between the surfaces; instead a film that remains as a flat sheet is expected. The important point is that when a sharp tip contacts the surface only a small fraction of the AFM tip will penetrate into the film.

To try and account for the film, a simple model has been employed to consider the effect of a thin film on the scattering by an AFM tip. It is assumed that the scattering that is measured is proportional to the intensity of the wave in the absence of the tip. The intensity of the evanescent wave will be determined by adding an additional exponential to account for the thin film. This is in keeping with success of the same model in the absence of the thin film.

When an evanescent wave passes through a series of slabs of different refractive index, the decay in each slab is given by equation 3.2 and 3.3, using the refractive index for the particular slab. Thus for a single film, the intensity of the evanescent wave at distances greater than the film thickness is given by:

$$I_h = I_o \exp\left(\frac{-t}{\delta_{film}}\right)\exp\left(\frac{-(h-t)}{\delta_{bulk}}\right) \tag{3.4}$$

Where t is the thickness of the film, δ_{film}, is the decay length in the film and δ_{bulk} is the decay length in the bulk solution. The only h dependence is in the last term, so the scattering decay length at tip separations greater than the film thickness is given by the properties of the bulk. This explains why relative displacements are accurate in the presence of the film: the presence of the film changes the intensity of the evanescent wave outside the film, but not the decay length outside the film.

The situation is more complex when the end of the tip is partially immersed in the film. As the tip approaches the solid, some parts of the tip displace the film, and some parts displace the bulk liquid. The exact dimensions of these sections are unknown but are definitely smaller than both the decay length and the wavelength of light. The fact that the separation derived from the scattering data analyzed with the bulk refractive index gives the same separation as the conventional AFM analysis suggests that only a small amount of the scattering portion of the tip is immersed in the film. This is reasonable for a sharp tip in an evanescent wave with a decay length of 70 nm and a film thickness of only 6 nm: most of the scattering regions of the tip stay in the bulk liquid environment. It is reasonable to assume that the intensity of the light that reaches sections of the tip outside the film is affected by the presence of the film, but because we have measured I_o in the presence of the film, this effect is rolled into the value of I_o. Thus, sections of the tip that never enter the film produce scattering that is consistent with equation 3.1 (simple exponential). In the reference method, the addition of the film after the reference is measured will affect the scattering intensity from all parts of the tip.

In general, if you wish to have a scattering signal that is independent of film properties (e.g. when the film properties are unknown and unwanted), you should aim to have a long evanescent decay length and a sharp probe so that much of the scattering tip moves only through the 'bulk' solution above the film. Clearly, if you want to sense the refractive index of the adsorbed film, you need a blunter probe and a shorter decay length.

3.4.2 Using the Scattering Profile to Obtain Cantilever Deflection

When determining the force between the surfaces in all the above experiments, the amount of cantilever deflection was determined using the slope of the cantilever deflection vs. piezo displacement curve. In the water and surfactant solutions, this is quite reasonable as direct contact between the tip and solid substrate is easily achieved because both the salt and surfactant are easily displaced from between the tip and surface. This is obviously not the case for the polymer, which could not be excluded from between the tip and surface during force runs. It is therefore necessary to determine the amount of error in the force

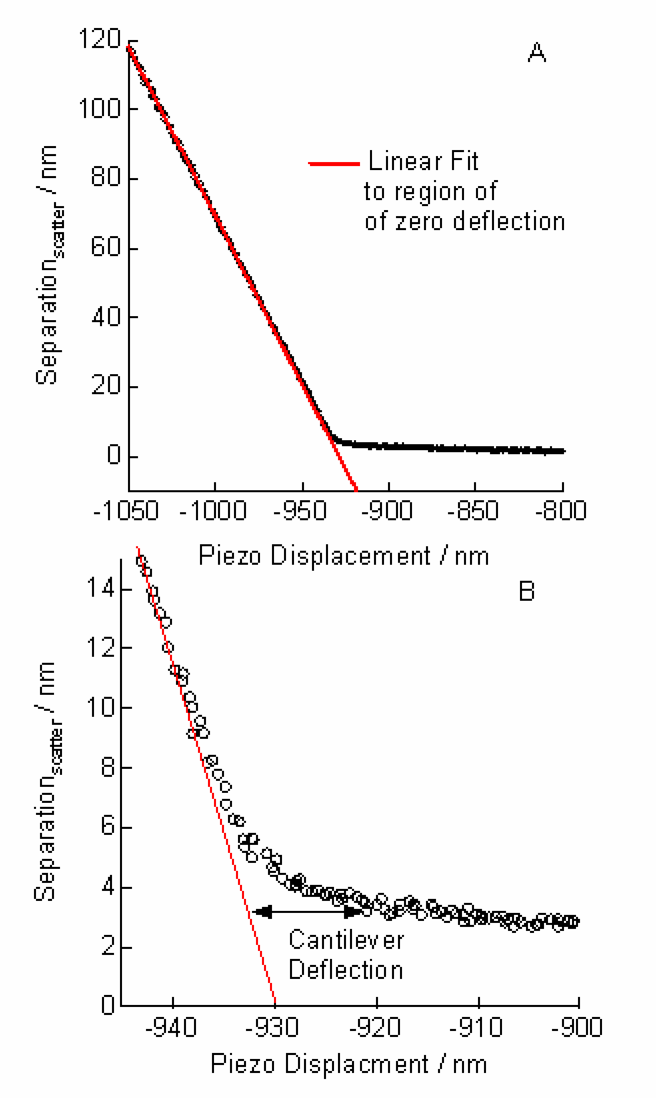

Figure 3.8. (A)-Separation determined from the scattering from a silicon nitride tip vs. piezo displacement. At separations greater than ~20 nm the plot is linear. If the linear region of the plot is extrapolated forward (red line), the deflection of the cantilever can be determined. (B)-Increased resolution of (A). The amount of cantilever deflection is the difference between the experimental data (black) and the forward extrapolation (red) of the expected curve if no deflections occurred.

when it was determined by the ratio of deflection distance to piezo movement in the presence of the polymer film. To due this, the scattering intensity and piezo displacement *only*, will be used to determine the amount of cantilever deflection[16], and separation.

As has been previously demonstrated, the scattering from the silicon nitride tip is purely exponential as a function of distance. Deviations from this simple profile (during a force run) can be ascribed to deflections of the cantilever. In theory, if no deflection of the cantilever occurred, a plot of the separation (determined by the scattering, equation 3.1) vs. the piezo displacement should be linear. Figure 3.8A is a plot of scattering separation vs. piezo displacement during withdrawal in the presence of adsorbed polymer (same data used in figure 3.4A). Moving from left to right, the tip is far away from the surface in a region of zero force, and so the plot is linear. As the tip gets closer to the surface, interactions between opposing polymer layers force the tip to deflect away from the surface causing a deviation from linearity. When the surfaces contact and the polymer can no longer be compressed, the separation between the tip and sample stops decreasing, and the plot is again linear with a slope of zero. The red line is an extrapolation of the linear region (if no deflection occurred). The difference between the linear extrapolation and the experimental data is the amount of deflection experienced by the cantilever. This is shown in greater magnification in figure 3.8B.

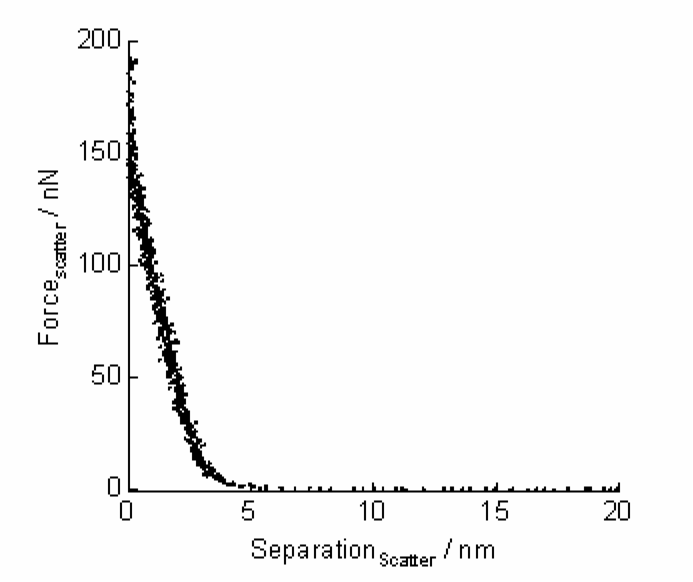

Figure 3.9. Withdrawing force vs. separation as determined by the scattering data only. There is no appreciable difference to the data presented in figure 4.3B when the force was determined from conventional AFM analysis.

Figure 3.9 is a plot of withdrawing force vs. separation (same experiment as figure 3.4 B), when both the force and separation are determined solely by the scattering data. There is no appreciable difference when this is compared to the force (AFM) vs. separation (scattering) curve of figure 3.4B.

This demonstrates that the compressed polymer film behaves as a rigid solid, indifferent from the glass substrate underlying the polymer. An unavoidable consequence of this is that traditional AFM analysis would lead the researcher to believe that the tip and underlying solid had made direct contact, when we know from the scattering data that contact between the underlying substrate and tip definitely did not occur. In this specific case, the relative position of the tip prior to contact is correct regardless of analysis technique, but the absolution separation is incorrect by traditional AFM analysis.

3.5 Conclusions

A new method has been demonstrated to measure the absolute separation between a tip and sample. By measuring the scattering of an evanescent wave by a silicon nitride AFM tip in contact with a solid before the adsorption of a film, it is possible to later measure the thickness of a film and a complete force-separation profile without again contacting the tip to the sample. This allows an accurate measure of the force-separation profile in the presence of strongly adsorbing polymers. Further, the force can be measured without the need to ever make contact between two physisorbed layers, provided a value of scattering intensity in contact with the underlying substrate has been made, prior to adsorption. New measurements that are not possible by traditional AFM analysis have been conducted to study the time response of a polymer layer under applied loads.

3.6 Cited Literature

1. McKee, C. T.; Ducker, W. A., Refractive Index of Thin, Aqueous Films between Hydrophobic Surfaces Studied Using Evanescent Wave Atomic Force Microscopy. *Langmuir* **2005,** 21, (26), 12153-12159.
2. Hodges, C. S., Measuring forces with the AFM: polymeric surfaces in liquids. *Advances in Colloid and Interface Science* **2002,** 99, 13-75.
3. McLean, S. C.; Lioe, H.; Meagher, L.; Craig, V. S. J.; Gee, M. L., Atomic Force Microscopy Study of the Interaction between Adsorbed Poly(ethylene oxide) Layers: Effects of Surface Modification and Approach Velocity. *Langmuir* **2005,** 21, (6), 2199-2208.
4. Kelley, T. W.; Schorr, P. A.; Johnson, K. D.; Tirrell, M.; Frisbie, C. D., Direct Force Measurements at Polymer Brush Surfaces by Atomic Force Microscopy. *Macromolecules* **1998,** 31, (13), 4297-4300.
5. Pasche, S.; Textor, M.; Meagher, L.; Spencer, N. D.; Griesser, H. J., Relationship between Interfacial Forces Measured by Colloid-Probe Atomic Force Microscopy

and Protein Resistance of Poly(ethylene glycol)-Grafted Poly(L-lysine) Adlayers on Niobia Surfaces. *Langmuir* **2005,** 21, (14), 6508-6520.

6. Ducker, W. A.; Senden, T. J.; Pashley, R. M., Direct Measurement of Colloidal Forces Using an Atomic Force Microscope. *Nature* **1991,** 353, (6341), 239-241.
7. Subramanian, V.; Ducker, W., Proximal adsorption of cationic surfactant on silica at equilibrium. *Journal of Physical Chemistry B* **2001,** 105, (7), 1389-1402.
8. Lokar, W. J.; Ducker, W. A., Forces between glass surfaces in mixed cationic-zwitterionic surfactant systems. *Langmuir* **2004,** 20, (11), 4553-4558.
9. Israelachvili, J. N.; Adams, G., Measurement of Forces between Two Mica Surfaces in Aqueous Electrolyte Solutions in the Range 0-100 nm. *J. Chem. Soc., Faraday Trans 1* **1978,** 74, 975-1001.
10. McKee, C. T.; Clark, S. C.; Walz, J. Y.; Ducker, W. A., Relationship between Scattered Intensity and Separation for Particles in an Evanescent Field. *Langmuir* **2005,** 21, (13), 5783-5789.
11. Kato, T.; Kawaguchi, M.; Takahashi, A.; Onabe, T.; Tanaka, H., Adsorption of sulfobetaine polyampholyte on silica surfaces from aqueous salt solutions. *Langmuir* **1999,** 15, (12), 4302-4305.
12. Lowe, A. B.; McCormick, C. L., Synthesis and Solution Properties of Zwitterionic Polymers. *Chemical Reviews (Washington, DC, United States)* **2002,** 102, (11), 4177-4189.
13. Gauthier, M.; Carrozzella, T.; Penlidis, A., Sulfobetaine zwitterionomers based on n-butyl acrylate and 2-ethoxyethyl acrylate: monomer synthesis and copolymerization behavior. *Journal of Polymer Science, Part A: Polymer Chemistry* **2002,** 40, (4), 511-523.
14. Esumi, K.; Matoba, M.; Yamanaka, Y., Characterization of Adsorption of Quaternary Ammonium Cationic Surfactants and Their Adsolubilization Behaviors on Silica. *Langmuir* **1996,** 12, (9), 2130-5.
15. Eastoe, J.; Hetherington, K. J.; Dalton, J. S.; Sharpe, D.; Lu, J. R.; Heenan, R. K., Microemulsions with didodecyldimethylammonium bromide studied by neutron contrast variation. *Journal of Colloid and Interface Science* **1997,** 190, (2), 449-455.
16. Clark, S. P.; Walz, J. Y.; Ducker, W. A., AFM Colloid-Probe Measurements with Explicit Measurement of Particle-Solid Separation. *Langmuir* **2004,** 20, 7616-7622.

Chapter 4

Measuring the Refractive Index of Bulk Fluids and Thin Films

4.1 Introduction

Early studies on the rupture of thin films between air and methylated silica by Blake and Kitchener[1] and by Israelachvili and Pashley[2] on the forces between surfactant coated mica sheets in aqueous solutions, suggested that there is a long range attractive force between hydrophobic surfaces in excess of the predicted van der Waals force. This force has since been measured for a number of surfaces that exhibit a high contact angle for the air-water interface and so has been called the "hydrophobic force". Christenson and Claesson have reviewed results up to 2001[3] and Attard has reviewed results up to 2003[4]. The origins of the hydrophobic force are still highly debated. Mechanisms by which a long-range attractive force is manifested between hydrophobic surfaces include, electrostatic attraction[5-7], solvent ordering[8], and bridging of microscopic[9] and submicroscopic bubbles[10, 11].

The theory that microscopic and submicroscopic bubbles are the cause of the measured long-range attractions between hydrophobic surfaces, is gaining popularity. The bubble mechanism requires either a pre-existing bubble attached to one or both of the opposing surfaces, or a bubble formed as a result of the proximity of two surfaces. Both positive[11, 12] and negative[13, 14] results supporting the existence of pre-existing bubbles on smooth hydrophobic surfaces have been reported. The existence of a bubble either pre-existing or nucleated between two surfaces will produce a refractive index contrast that can be monitored optically. Christenson and Claesson[9] used fringes of equal chromatic order to measure the refractive index of the medium between two centimeter-sized hydrophobic surfaces in water and found that pockets of air formed between hydrocarbon surfaces ($\theta_a = 93$, $\theta_r = 60$) as they were separated, and similar pockets of air formed between fluorocarbon surfaces ($\theta_a = 113$, $\theta_r = 60$) when they came into contact. To the best of my knowledge, there have not been any observations of proximity induced bubble formation for colloidal sized particles. The aim of the work presented here is to search for such bubbles.

As demonstrated in the previous chapters, an evanescent wave is altered when an object with a refractive index contrast is introduced into a transmission medium that contains the evanescent wave. This can be used to determine the location of that object in the evanescent wave transmission medium. It was shown that silicon nitride AFM tips scatter evanescent light exponentially according to equation 4.1.

$$I_h = I_o \exp\left(\frac{-h}{\delta}\right) \tag{4.1}$$

The scattering profile from spheres attached to cantilevers is more complex. For spheres with a radius between 1 and 10 microns the scattering profile is exponential at large separations as predicted by Chew et al.,[15] but deviates from exponential as the film between the sphere and surface thins. Earlier results presented in chapter 2 show that the scattering from a colloidal probe is approximately the sum of two exponentials, the longer decay length is equal to decay length of the evanescent wave, and the shorter decay length depends on the radius of the sphere.

In the previous chapters, the problem of evanescent wave scattering was treated as a problem in which the refractive index was known, and so the scattering could be used to determine the separation, either via equation 4.1 or via a calibration curve. In this chapter, the opposite is done. It is assumed that the separation between the probe and the sample can be determined by traditional AFM analysis (because the tip and sample are rigid) and that the average refractive index of the medium between the probe and sample can be calculated from the scattering profile and the separation via the following equation.

$$\eta_2 = \sqrt{\eta_1^2 \sin^2 \theta_I - \left({}^{\lambda}\!/_{4\pi\delta_{meas}} \right)^2} \tag{4.2}$$

Where η_2 is the refractive index between the tip and sample, η_1 is the refractive index of the reflection prism, θ_I is the incident angle, and λ and δ_{meas} are the wavelength of light and measured decay length of the scattered evanescent wave respectively.

The application here is to find evidence for the formation of gas bubbles in a film between two hydrophobic surfaces. The analysis is more complicated by the fact that the formation of an air bubble may produce additional scattering at the air-water interface. Based on equation 4.1, figure 4.1 is an example of the expected scattering profile if an air bubble only, changes the refractive index of the medium between an AFM tip and sample. After the formation of a capillary of air or vapor

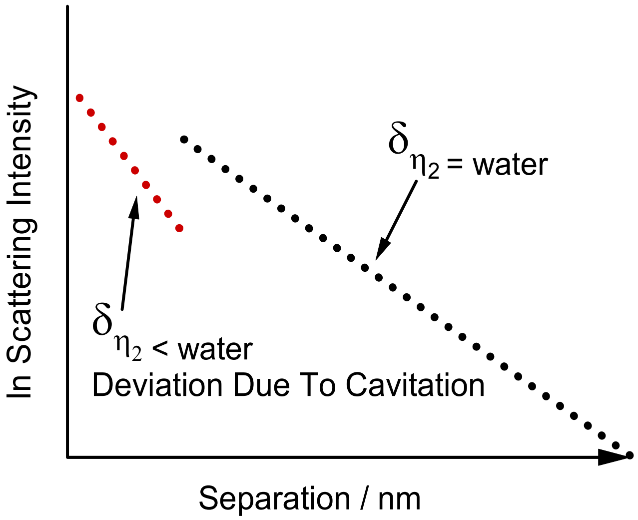

Figure 4.1. If cavitation occurs when a particle approaches a flat plate, we expect the refractive index to suddenly decrease below that of water, and the decay of the scattering will become steeper.

in the water, the decay length should decrease from that corresponding to the refractive index of water (1.33). If the air completely filled the evanescent zone near the tip, we would expect the decay length to correspond to the refractive index of air (1.00), but for a mixed film the decay length should correspond to a refractive index intermediate between that of the two phases.

4.2 Materials and Methods

4.2.1 Experimental Method

The setup for the evanescent wave atomic force microscope is similar to that described earlier. In this case the Asylum MFP-1Dplus AFM was mounted on a Zeiss Axiovert 200 inverted light microscope (Carl Zeiss, Thronwood, NY). The evanescent wave was generated at the interface between a flat borosilicate glass plate (Fisher Scientific) and an aqueous solution. The flat plates were used to ensure a smooth interface with few dust particles or scratches that can cause additional scattering. The evanescent wave was created by a 532 nm GCL-50-L (CrystaLaser Reno, NV) solid state laser. The laser is incident into a trapezoidal glass prism (Knight Optical, U.K.) which is coupled to the glass plate using index matching optical fluid (Nye Lubricants, Fairhaven, MA). In these experiments the entire apparatus was suspended on an optical table by bungee cords to minimize vibrations from the building.

The incident angle in these experiments is ~75.5^o, which produces and evanescent decay length δ of about 68 nm. The incident angle was constant during any individual experiment, but varied by ~0.5^o between experiments, producing decay lengths in the range of 67-69 nm. The scattering signal produced by particles interacting with the evanescent wave was collected by a microscope objective, Zeiss Epiplan 50x/0.50, below the prism and transferred to a photomultiplier tube (HC120-01, Hamamatsu). A short pass filter was used to block infrared radiation produced by the Asylum AFM used in measuring cantilever deflections. The data in figure 4.2 was collected with a slightly different experimental configuration. The evanescent wave was generated using a 532 nm diode laser (TECGL-10, World Star Tech, Canada). The scattered evanescent light was collected with a Nikon LU Plan 50x/0.55 objective and transferred to a photomultiplier tube (H5874-20, Hamamatsu).

4.2.2 Experimental Materials

The scattering objects used in these experiments are silicon nitride AFM tips (NP, Veeco, Santa Barbara, CA) and borosilicate glass spheres (9020, Duke Scientific, Palto Alto, CA). The AFM tips are the same used in previous chapters. The spheres had a root mean square roughness of ~0.3 nm over $(400\text{nm})^2$. The spheres were attached to rectangular tipless silicon cantilevers (NSC12 Silicon-MDT, Moscow, Russia) using two part epoxy and a hot stage. The epoxy was chosen because it was found that it could maintain adhesion during the later silination process. Water used in the experiments was prepared by an EasyPure UV system (D7401, Barnstead Thermolyne Co., Dubuque, IA) and had a measured conductivity of 18.3 MΩ/cm at room temperature and a surface tension of 72.3 mN/m at 22°C. The smooth borosilicate glass plates had an rms roughness of 0.26 nm over an area of 5 μm^2.

All surfaces (AFM cantilevers, spheres, and glass plates) were first cleaned by H_2O plasma for 45 seconds at 250 mTorr using a Plasma Prep II (SPI supplies, West Chester, PA) plasma cleaner. Immediately after cleaning, they were rendered hydrophobic by silination with n-octadecyltrichlorosilane (OTS, Aldrich 95%) in a solution-phase reaction as described in reference[13]. The measured advancing and receding contact angles on the flat borosilicate glass plates after silination were $\theta_A = 102^o$ and $\theta_R = 95^o$. Contact angles were measured using a FTA125 contact angle analyzer (First Ten Angstroms, Portsmouth, VA). The same procedure produced films that were 2.6 nm thick in water and had a refractive index of 1.55 on silicon wafers[13]. After surface preparation and reaction, the surfaces were immediately used for the experiments. All measurements were performed at room temperature (22 ± 2°C).

4.3 Results

4.3.1 Validation of the Refractive Index Measurement

To demonstrate the ability to resolve variations in the refractive index of a liquid between the AFM tip and sample, I have measured the scattering profile from a hydrophilic tip in a series of liquids: water, methanol, ethanol, and 1-butanol. All measurements were performed at 20.5 ± 1°C. The results are shown in Figure 4.2.

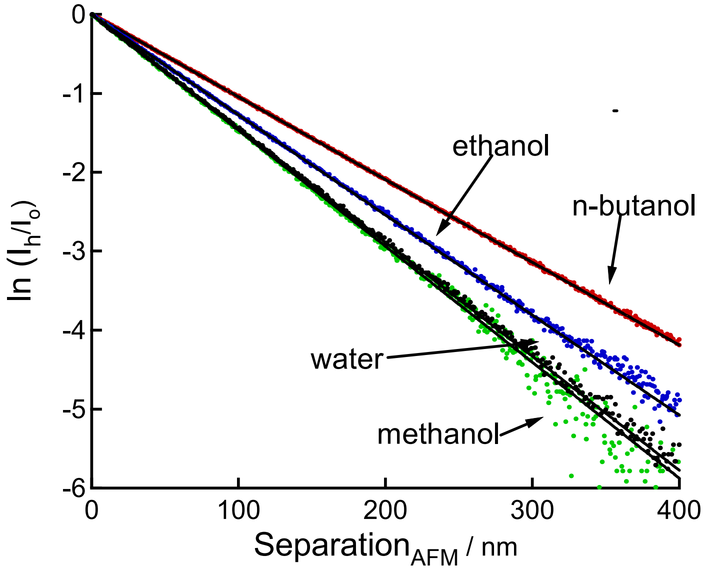

Figure 4.2. Scattering profile from a hydrophilic Si_3N_4 tip in a series of liquids: methanol (green), water (black), ethanol (blue), and n-butanol (red). The black lines are least squares fits to the ln (I_h/I_o) data. All measurements were performed at 20.5±1°C.

In all cases, the scattering profile is exponential, it is the same on approach and withdrawal, and the slope of $\ln(I_h/I_o)$ is constant. Here, we use I_o to represent the intensity of scattering at $h = 0$. Assuming the intensity of scattering is proportional to the intensity of the evanescent field in the absence of the probe, the slope of the experimental data yields:

$$\frac{d\ln\left({}^{I_h}\!/\!_{I_o}\right)}{dh} = -\frac{1}{\delta_{measured}} \tag{4.3}$$

The measured refractive index, η_2, can be calculated from equation 4.2. $\delta_{measured}$ is independent of h for the experiments in figure 4.2, but could in general depend on h. The approach of the tip could cause a change in the refractive index for all separations, so $\delta_{measured}$ could be a function h.

The values of $\delta_{measured}$ from figure 4.2 are shown in table 4.1, along with values of $\delta_{theoretical}$ and $\eta_{measured}$. The principle source of uncertainty arises from uncertainty in the angle of incidence, $75 \pm 1.5^{\circ}$, which produces a systematic error in $\eta_{measured}$. To remove the effects of this systematic error, the values of $\delta_{theoretical}$ have been calculated using the known refractive index and the scattering data from 1-butanol to calibrate the incidence angle (74.93°). Butanol produces the longest decay length, so $\delta_{butanol}$ is the most sensitive to the incidence angle.

The data in table 4.1 shows that the difference between the refractive index of water (1.3329) and methanol (1.3288) can be distinguished, so the resolution of refractive index is at least 0.004. The resolution in refractive index depends on the refractive index contrast between the solid and the liquid and also on the angle of incidence. The resolution increases for small index contrast between the prism and the liquid for angles approaching the critical angle (i.e. for large decay lengths).

Table 4.1 Comparison between the refractive index from the CRC Handbook of Chemistry and Physics and the measured refractive index[a]

Transmission medium	CRC η @ 20°C 589 nm	$\delta_{\mathrm{theoretical}}$	$\delta_{\mathrm{measured}}$	Measured η @ 20.5°C, 532 nm
Methanol	1.3288	67.92	67.9±0.1	1.3.28
Water	1.33299	68.91	69.4±0.2	1.335
Ethanol	1.3611	77.08	78.4±0.1	1.365
n-butanol	1.3993	95.58	95.5±0.1	1.399

[a] *The measured refractive index is calculated from $\delta_{measured}$ using equation 4.1*

4.3.2 Si_3N_4 AFM Tip Studies

4.3.2.1 Force Measurements

Figure 4.3 shows the force as a function of separation between a Si_3N_4 AFM cantilever (R < 60 nm, k = 0.58 N/m), and a flat borosilicate glass sample. Figure (4.3A) is the approach and withdrawal, for when the tip and sample are hydrophilic, which are purely repulsive at all separations. Figure 4.3 B and C, show the forces for the same materials made hydrophobic by reaction with OTS. The forces are similar to those measured previously by Attard and Tyrell[11], except that in our case we observed and jump into a "hard contact", between the tip and sample, whereas they observed a "soft contact". The approach curve (B) shows a repulsion, due to background charge on the tip and sample, followed by an instability at ~ 6 nm separation. The van der Waals force, was calculated using Derjaguin's approximation, a Hamaker constant of 2.07 x 10^{-20},[16] and a radius of

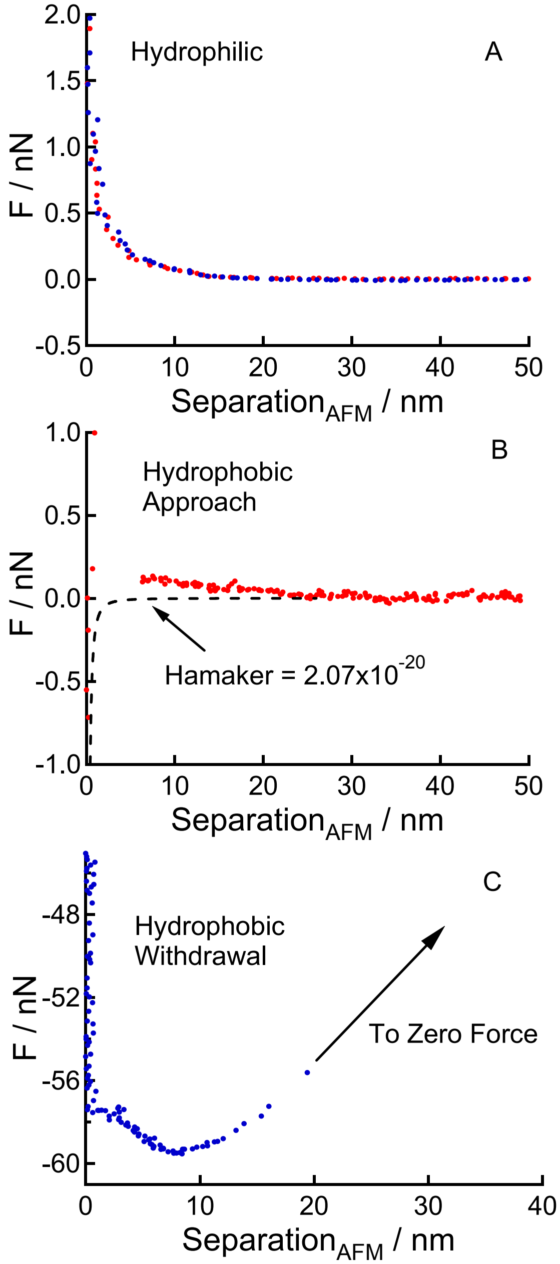

Figure 4.3. Force measured between Si_3N_4 tips (R<60 nm, k = 0.58 N/m) and a flat borosilicate plate. (A) Hydrophilic conditions. The force shows a repulsion during approach (red) and no adhesion on withdrawal (blue). (B) Force between the same materials after coating in OTS. The approach shows a repulsion followed by an instability at approximately 6 nm. Included is the predicted vdW's attraction as calculated by Derjaguin's approximation using a Hamaker constant of $2.07x10^{-20}$ using a radius of 60 nm. (C) On withdrawal there is a strong adhesion. The force remains large when the surfaces separate up to about 15nm.

60nm. A large and negative force is required to separate the surfaces and, in addition, this attractive force remains large at separations up to ~ 15 nm. This type of adhesion phenomenon has been observed by other researchers[11] and attributed to the bridging of a bubble between the surfaces.

4.3.2.2 Scattering Measurements

Figure 4.4 shows the scattering profiles that were captured simultaneously to the force curves presented in figure 4.3. The scattering data for the hydrophilic conditions is presented in figure 4.4A. The scattering profile is purely exponential down to contact with a measured decay length of $\delta_{measured}$ = 67.2 nm, which is in good agreement with the predicted value, $\delta_{theoretical}$ = 68.0 ± 1 nm. For repeat runs with the same cantilever, $\delta_{measured}$ = 67.7 ± 0.6 nm.

Figures 4.4 B and C are the scattering profiles for the approach and withdrawal for the surfaces that were coated in OTS. The scattering decay length on approach is $\delta_{measured}$ = 67.2 nm. For repeat runs with the same cantilever, $\delta_{measured}$ = 67.8 ± 0.6 nm. No deviations from exponential occur prior to the instability at ~ 6 nm. Because there are no data points in the unstable region, measurement of the decay length is not possible in that region. The intensity in contact is equal to the value that occurs by linear extrapolation of the data at larger values, so the average refractive index in the region around the tip has not changed after the tip has touched the plate. After decreasing the load in contact, the tip

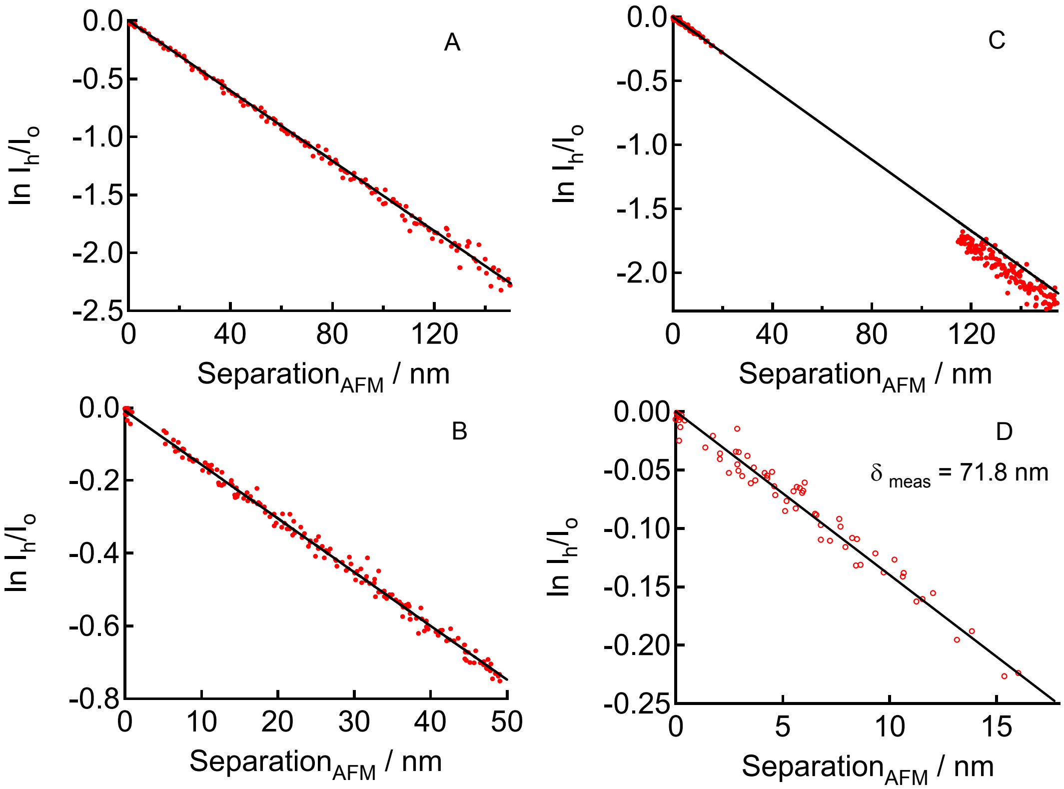

Figure 4.4. Scattering profiles corresponding to the force curves plotted in Figure 5.3. The lines are the linear fits (-h/δ_{meas}) based on experimentally obtained decay lengths. (A) The hydrophilic tip. The scattering is purely exponential down to contact with a decay length of 67.2 nm. (B) Hydrophobic tip on approach. The scattering profile is exponential down to contact with no measured deviation prior to the mechanical instability, with a measured decay length of 67.5 nm. (C) Hydrophobic tip on withdrawal. δ_{meas} = 71.8 nm for separation <20 nm, and δ_{meas} = 67.8 nm for separation >20 nm. (D) Detail from (C) to show region of fit.

separates from the glass plate. The decay in the short range region of increased attraction (figure (4.4D)) is $\delta_{measured}$ = 71.8 nm, with an average value for repeat runs at 71.1 ± 1.1 nm. In this region, a decay length that was less than the approach (67.5 nm) was never measured. After full release (next measure of separation ~ 120 nm), the scattering decay length returns to $\delta_{measured}$ = 67.8 nm. Changing the refractive index between the two surfaces from 1.33 (water) to 1.00 (air) would result in a decrease in the measured decay length. The measured increase in decay length during the short range pull off indicates a material with a refractive index greater than 1.33 between the two surfaces. Thus, the increase in refractive index is consistent with condensation of organic material such as OTS or organic impurities from the water, rather than condensation or bridging bubbles.

In the experiments described above, the cantilever was continually cycled towards and then away from the surface, so the time in contact was very short, and the force in contact was not constant ("short stay" experiment). Experiments were also conducted where the tip was first in contact with the surface, withdrawn, and then brought back into contact, where it remained until the next run, typically 10-20 seconds ("long stay" experiments). Compared to short-stay experiments, for long-stay experiments, the separation and attractive force were greater before the tip was fully released (~ 100 nm, figure 4.5A), and the decay length on withdrawal was even greater at small separations (< 50 nm). The decay length is 75.5 nm for the example shown in Figure 4.5B and 73.7 ± 1.3 nm on average for many runs. After full release for this run, the scattering decay length returns to 70.3 nm. Figure 4.5C is a plot of the calculated refractive index as a function of separation based on the measured decay length as the hydrophobic tip withdraws and the approaches for the long-stay experiment. The approach (red) shows the average value for the refractive index at 1.33. The withdrawal (blue) decays from a value of ~ 1.37 to 1.33 as the separation increases.

The "short-stay" and "long-stay" experiments are not consistent with the formation of an air bubble between the tip and the plate. The data are consistent

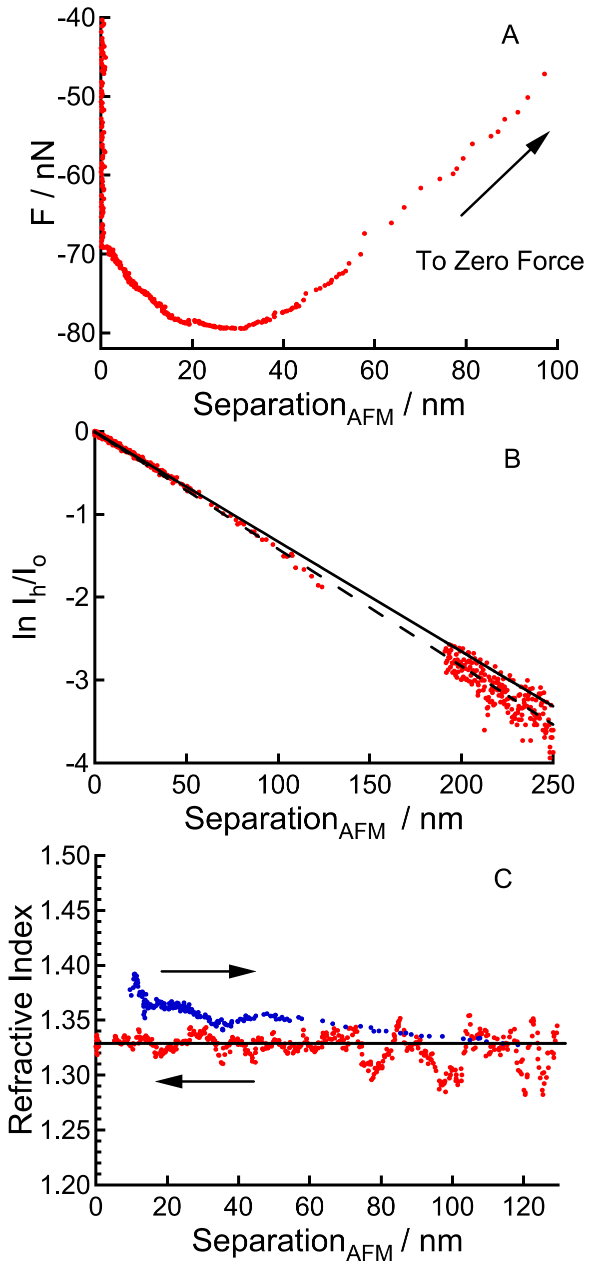

Figure 4.5. 'Long Stay' experiment. (A) Force vs. separation during withdrawal for a 'Long Stay". (B) The scattering profile during this pull off has a decay length of 75.5 nm (solid line). And after release is 70.3 nm (dashed line). The measured decay lengths during these 'long stay experiment' are always larger than during the 'short stays'. (C) Refractive index derived from equation 1 using experimentally measured values of the decay length (δ_{meas}) measured during approach (red) and withdrawal (blue) using an incident angle of 75° and a wavelength of 532 nm. The refractive index on approach is about 1.33; on withdrawal the refractive index decreases as the separation increases.

with the condensation of a material that has a refractive index greater than that of water. Possible explanations may include an increased density of water, or the presence of OTS or other organic condensation from solution. The longer the tip is left in contact with the sample, the greater the attractive force and the longer the decay length of scattering intensity. This is consistent with the accumulation of more organic material in the thin film. The further the tip moves away from the surface, the lower the mole fraction of organic material in the evanescent zone, and the average refractive index falls. It is noted that the condensation of organic material on the highly curved hydrophobic region around the tip is more favored than the formation of a gas bubble because the interfacial energy is low between the OTS-coated solid and organic liquids, and the organic-water interfacial energy is much less than the air-water interfacial energy.

4.3.3 Borosilicate Sphere Studies

4.3.3.1 Force Measurements

Figure 4.6 shows the force measured between a borosilicate sphere (R = 11.2 μm) attached to a rectangular, silicon, tipless cantilever (k = 14.4 N/m) and a flat borosilicate glass plate, without (A) and with (B) an OTS layer. For all experiments in which a comparison is made between hydrophilic and hydrophobic conditions, the same sphere/cantilever were used. Figure 4.6A shows the approach (red) and withdrawal (blue) of hydrophilic glass sphere to a hydrophilic glass plate. The force is purely repulsive at all separations during approach, and the withdrawal

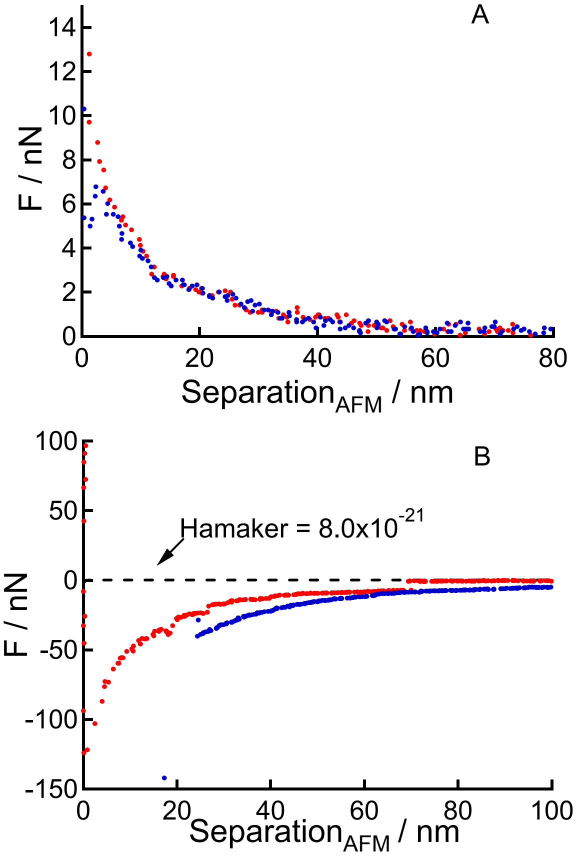

Figure 4.6. (A) Force between a hydrophilic borosilicate sphere (R = 11.2 um), and a hydrophilic borosilicate plate. The force shows a repulsion during approach (red). During withdrawal (blue) a small adhesion is measured before release, but the force is always repulsive. (B) Force between the same materials coated in OTS. The approach (red) shows an instability at approximately 70 nm, followed by a long-range attraction. The force during withdrawal (blue) has a measured attraction that is larger at all separations. Included is the predicted vdW's attraction as calculated by Derjaguin's approximation using a Hamaker constant of 8.0x10^{-21}.

shows a small adhesion before release. Figure 4.6B shows the force between the surfaces after silination with OTS. During approach an instability/step is measured at ~68 nm, followed by a long range-range attraction and additional steps down to contact. These instabilities and steps have been attributed to the formation of air/vapor bridges[11, 17]. The additional steps between 68 nm and contact are shown in greater detail if figure 4.7. During withdrawal there is a strong adhesion, then release, and the surfaces separate to ~ 20nm, where there is an attraction, which is much greater than the van der Waals force between silica surfaces (assuming a Hamaker constant of 8 x 10^{-20}).[18]

These sphere experiments, with their long-range attractions and data points collected in the region of attraction present an opportunity to study whether cavitation is the cause of long-range attractions during approach.

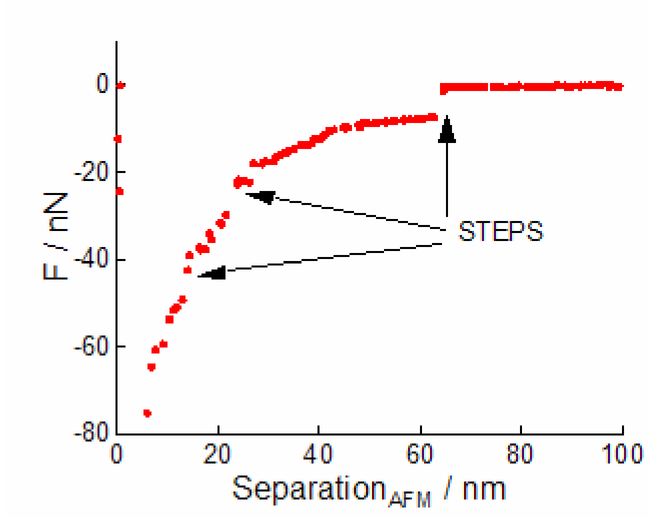

Figure 4.7. Figure 5.6 B replotted to more clearly show additional steps during approach of the two hydrophobic surfaces.

4.3.3.2 Scattering Measurements

As described in chapter 2, the scattering profile of a large particle attached to a cantilever is not purely exponential and that the scattering profile has to be calibrated.[19] For this reason the scattering profile was measured for the hydrophilic sphere/plate, and then re-measured after the surfaces were made hydrophobic by

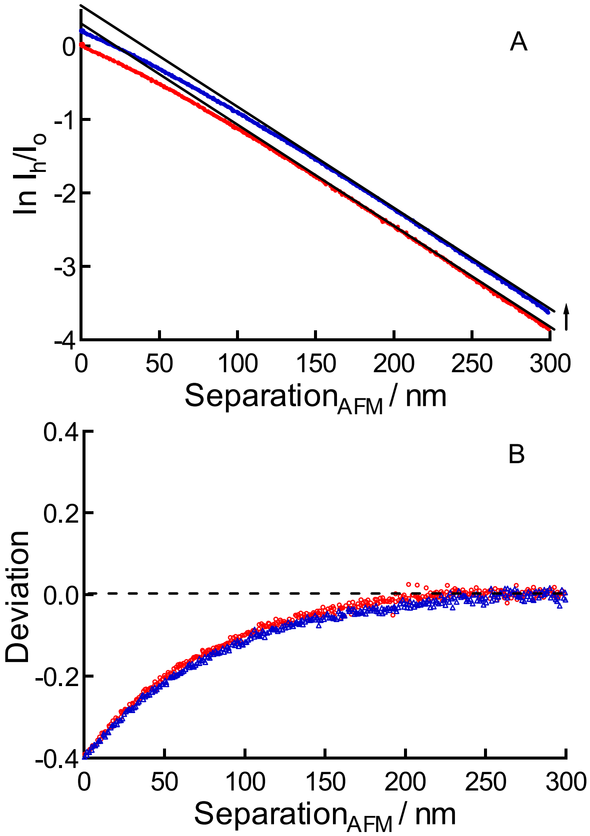

Figure 4.8. The same sphere-cantilever used in Figure 5.7 was made hydrophilic by plasma treatment and it's scattering as a function of separation was measured. This was done to observe whether or not there are differences in the scattering profile between the hydrophilic and hydrophobic conditions. (A) Scattering of the same 11.2 um radius sphere on a natural log scale. The hydrophilic plot (blue) has been offset is the positive direction for clarity. (B) Comparison between the hydrophilic and hydrophobic conditions as measured by the deviation from ($-h/\delta_{meas}$)*. The profiles show the same range and magnitude of deviation from exponential. If cavitation occurred, we would have expected a difference between the measured deviations from exponential between the hydrophilic and hydrophobic conditions.*

silinating with OTS. It is assumed that the medium between the hydrophilic materials is always water.

Figure 4.8 compares the scattering profile for the particle (same particle as figure 4.6) when it is hydrophilic to when it is hydrophobic. The effect of silinating the particle/plate did not produce a difference in the scattering profile; therefore, we could not detect a change in the refractive index of the medium when two hydrophobic surfaces are in close proximity. There is therefore no evidence for air bubble formation. Figure 4.9 shows the scattering profile and force for the hydrophobic conditions on the same plot. There is no change in the scattering intensity at the instability on approach, and the intensity is the same on approach and withdrawal (where it is measurable). Note that in the graph the withdrawal scattering data has been offset for clarity. Likewise, there is no difference in scattering profiles for hydrophilic and hydrophobic surfaces, despite the long range attractions. It is possible that there is a small capillary or bridge of either air or organic material that cannot be resolved. The contact area for a sphere (R ~ 11μm) is much larger than for a tip (R < 60 nm), so the ability to resolve the refractive index of a small bridge is reduced.

4.4 Discussion

4.4.1 Adsorbed Bubbles and the Hydrophobic Effect

In these experiments no evidence for the formation of an air bubble between a hydrophobic tip and hydrophobic plate is observed when they approach or withdrawal. In fact, the refractive between the surfaces actually increases upon separation. The attractive force together with the increase in refractive index on separation is consistent with an increase in the amount of organic material between the tip and surface after they have been brought into contact. This material could cause an attractive force by forming an organic capillary or bridging of individual molecules. These experiments do not shed light on the possibility of preexisting

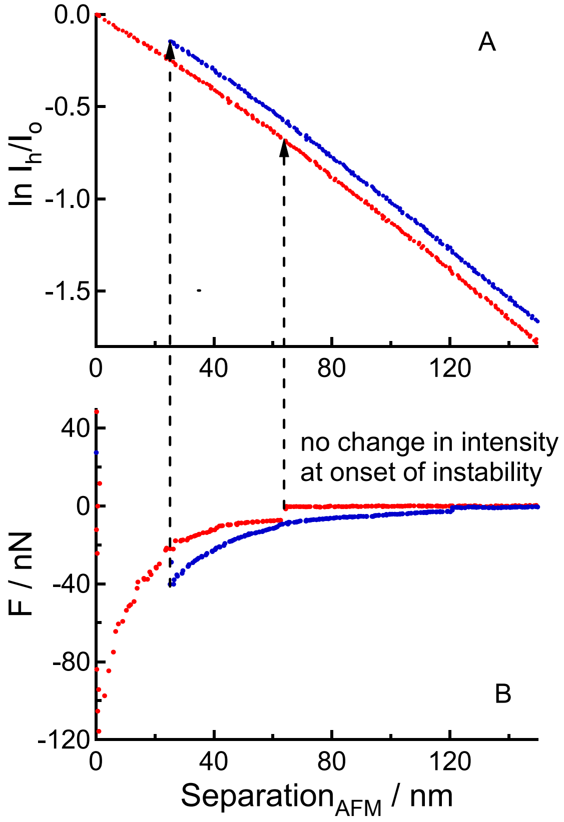

Figure 4.9. (A) The scattering-separation curve of an OTS coated borosilicate sphere (R = 11.2 um) on a natural log scale. The withdrawal data (blue) has been offset in the positive direction for clarity. (B) Concomitant force during approach and withdrawal. The scattering signal and profile does not change as a result of the instability and long-range attraction. Also the withdrawal (blue), which experiences a larger attraction at all separations, has a scattering profile and intensity that is identical to the approach.

bubbles between surfaces. A more extensive theoretical model would be needed to understand how the scattering profile of the tip would be affected as it approached a small bubble bound to the sample. It is expected that a discontinuity in the scattering profile would occur if a bubble bridged the two surfaces, but the cantilever instability has prevented studying this regime in these experiments.

4.4.2 Stability of an Air Capillary as a Function of Radius

Two recent articles[20, 21] discuss the energetic barrier to formation of an air bubble between two hydrophobic surfaces. At equilibrium, the barrier consists of a surface energy term for creating the new interfaces, a chemical term (for vaporizing the water or extracting dissolved gas from the liquid), and a pressure-volume term if the system is not at uniform pressure. In both of these analyses, the energetic cost of forming the liquid-vapor interface was ignored because flat or low-curvature solids (R >> separation) were considered. For a highly curved solid, such as an AFM tip, a formed bridging bubble (at the equilibrium contact angle) would have a much smaller lateral extent and volume. This decreases the magnitude of all energy terms, which would decrease the barrier to bubble formation, except that the liquid-vapor interfacial energy now becomes important. For example, for a cone ($\theta = 45^o$) in contact with a solid, both with contact angle $\theta = 90^o$, the area of the vapor-water interface is approximately equal to that of the solid-vapor interface ($A_{sv} \approx 1.2A_{sl}$). The energy penalty for creating liquid-vapor interface can no longer be ignored, because $\gamma_{lv} >> \gamma_{sv} - \gamma_{sl}$ and makes the formation of the bubble less favorable. This may be why evidence of air bubble formation between the tip and surface is not observed.

4.4.3 Limitations of Measurement of Refractive Index

The refractive index measurements presented here are derived from the decay length of tip scattering intensity. Unfortunately, because this entails measuring a slope, it decreases the signal to noise ratio. The exponential decrease in the signal with particle plate separation also makes the measurements noisier at larger separations, so the technique is best in thin films (100 nm and below). These limitations are not significant when measuring the refractive index of a bulk fluid, because the decay length can be accurately determined by measuring it over a large range of separation. Unfortunately, to resolve the dependence of the refractive index on distance, the scattering must be measured over small changes in separation and so noise in the scattering signal is amplified into the measured slope/refractive index. The ability to measure the refractive index in a thin film between a large particle and a plate is also hindered by the lack of knowledge of the optical scattering profile. At present a control experiment needs to be performed on the same particle with a film of known refractive index.

Despite all these limitations, I was clearly able to resolve changes in refractive index for very thin and narrow films, which are of interest to colloidal science.

4.5 Conclusions

A new method has been demonstrated for measuring the refractive index of bulk fluids and thin films that separate a small particle and plate. A refractive index difference of 0.004 for can easily be resolved in bulk fluids. Experiments reported here were conducted to determine whether a layer of air or vapor (e.g. a bubble) formed between a highly curved ($R < 60$ nm and $R \sim 10$ μm) hydrophobic solid approaching another hydrophobic solid. A change in scattering decay length that is consistent with the formation of a vapor layer that occupies a significant fraction of the region of the film between the tip and surface is not observed. For spherical particles R ~10 μm, there could still be small bubbles that occupy a small fraction of the interaction area. For AFM tips, the measured refractive index is always equal to or greater than for water, which is consistent with an increase in the concentration of the amount of organic material between the surfaces. This organic material could cause the observed attractive force by bridging between the surfaces or by the formation of a small capillary.

4.6 Cited Literature

1. Blake, T. D.; Kitchener, J. A., Stability of Aqueous Films on Hydrophobic Methylated Silica. *J. Chem. Soc Faraday Trans. I* **1972,** 68, 1435-1442.
2. Pashley, R. M.; McGuiggan, P. M.; Ninham, B. W.; Evans, D. F., Attractive Forces Between Uncharged Hydrophobic Surfaces: Direct Measurements in Aqueous Solution. *Science* **1985,** 229, 1088-1089.
3. Christenson, H. K.; Claesson, P. M., Direct measurements of the force between hydrophobic surfaces in water. *Advances in Colloid and Interface Science* **2001,** 91, (3), 391-436.
4. Attard, P., Nanobubbles and the hydrophobic attraction. *Advances in Colloid and Interface Science* **2003,** 104, 75-91.
5. Attard, P., Long-Range Attraction between Hydrophobic Surfaces. *J, Phys. Chem.* **1989,** 93, 6441-6444.
6. Podgornik, R., Electrostatic correlation forces between surfaces with surface specific ionic interactions. *Journal of Chemical Physics* **1989,** 91, (9), 5840-9.
7. Kekicheff, P.; Spalla, O., Long-Range Electrostatic Attraction between Similar, Charge-Neutral Walls. *Physical Review Letters* **1995,** 75, 1851-1854.
8. Eriksson, J. C.; Ljunggren, S.; Claesson, P. M., A phenomenological theory of long-range hydrophobic attraction forces based on a square-gradient variational approach. *Journal of the Chemical Society, Faraday Transactions 2: Molecular and Chemical Physics* **1989,** 85, (3), 163-76.
9. Christenson, H. K.; Claesson, P. M., *Science* **1988,** 239, 390.

10. Parker, J. L.; Claesson, P. M.; Attard, P., Bubbles, Cavities, and the Long-Ranged Attraction between Hydrophobic Surfaces. *J. Phys. Chem.* **1994,** 98, 8468-8480.
11. Tyrrell, J. W. G.; Attard, P., Atomic force microscope images of nanobubbles on a hydrophobic surface and corresponding force-separation data. *Langmuir* **2002,** 18, (1), 160-167.
12. Zhang, X.-H.; Li, G.; Wu, Z.-H.; Zhang, X.-D.; Hu, J., Effect of temperature on the morphology of nanobubbles at mica / water interface. *Chinese Physics (Beijing, China)* **2005,** 14, (9), 1774-1778.
13. Mao, M.; Zhang, J.; Yoon, R.-H.; Ducker, W. A., Is There a Thin Film of Air at the Interface between Water and Smooth Hydrophobic Solids? *Langmuir* **2004,** 20, (5), 1843-1849.
14. Takata, Y.; Cho, J. H. J.; Law, B. M.; Aratono, M., Ellipsometric search for vapor layers at liquid-hydrophobic solid surfaces. *Langmuir : the ACS journal of surfaces and colloids* **2006,** 22, (4), 1715-21.
15. Chew, H. D.; Wang, D.-S.; Kerker, M., Elastic Scattering of Evanescent Electromagnetic Waves. *Applied Optics* **1979,** 18, 2679-2687.
16. Bergstrom, L., Hamaker constants of inorganic materials. *Advances in Colloid and Interface Science* **1997,** 70, 125-169.
17. Carambassis, A.; Jonker, L. C.; Attard, P.; Rutland, M. W., Forces measured between hydrophobic surfaces due to a submicroscopic bridging bubble. *Physical Review Letters* **1998,** 80, (24), 5357-5360.
18. Evans, D. F.; Wennerström, H. K., *The Colloidal Domain*. 2nd ed.; Wiley: New York, 1999; 'Vol.' Chapter 5.1, p.
19. McKee, C. T.; Clark, S. C.; Walz, J. Y.; Ducker, W. A., Relationship between Scattered Intensity and Separation for Particles in an Evanescent Field. *Langmuir* **2005,** 21, (13), 5783-5789.
20. Wennerstrom, H., Influence of Dissovled Gas on the Interaction between Hydrophobic Surface in Water. *Journal of Physical Chemistry* **2003,** 107, 13772-13773.
21. Pashley, R. M.; Rzechowicz, M.; Pashley, L. R.; Francis, M. J., De-Gassed Water Is a Better Cleaning Agent. *Journal of Physical Chemistry B* **2005,** 109, (3), 1231-1238.

Chapter 5

Short Range Hydration Forces

5.1 Introduction

Studies of the forces between hydrophilic mica sheets in aqueous electrolyte solutions showed the existence of a short range repulsion that could not be described by DLVO theory[1, 2]. This force is large enough to overcome the vdW force and thus is important in determining the reversibility of colloid stability. Pashley and Israelachvili demonstrated that the force was an approximate double exponential, and was directly related to the hydrated radius of the ions in solution. The magnitude of the force decreased as the solution was exchanged from $Li^+ > Na^+ > K^+ > Cs^+$, i.e. decreased with decreasing hydrated radius, and no short range force was found in solutions containing no salt. It was suggested by the authors that the short range interaction was due to the force required to partially dehydrate the ion (secondary hydration, decay length ~ 1 nm). This partial dehydration allows the direct adsorption of the ion to the mica interface (no intervening water). The secondary hydration force is followed by the force required to disrupt and expel the water structure adjacent to the ionic surface (primary hydration, decay length ~ 0.17 - 0.3 nm). However, this mechanism was not found to be applicable to all surfaces. Chapel[3] studied the short range force between silica surfaces and found the opposite dependence on hydrated ion size. The force increased with decreasing hydrated radius; and the force had the longest range in a solution containing no salt. Chapel suggested that the adsorbed hydrated ions disrupts an ordered structure of water near the interface, and therefore the hydration force was due to the rupture of a hydrogen bonded network directly adjacent to each surface. Complicating the issue of the short range force between silica surfaces, are published reports suggesting the force is due to a steric interaction between polysilicic acid[4], formed at the solid liquid interface. Horn et al.,[5] showed that the force did not depend on the method of surface preparation of silica and concluded that the force was due to hydration of the ions adsorbed at the silica water interface. However the force was measured in the presence of NaCl at varying concentrations, and so the effect of ion radius was not examined. More recent measurement of the short range repulsion with the atomic force microscope have been reported by Higishitani[6]. These results are hard to interpret as the authors studied the force between a silica particle and a mica sheet. A short range repulsion was measured, and was consistent with SFA measurements between two mica sheets. The range of the force decreased with decreasing hydrated radius of the ion.

Several theories on the microscopic mechanism of the short range repulsion have been developed. These have been reviewed in a recent publication[7] and include: the overlap of layers of ordered water molecules next to a surface[8], interactions between surface dipoles[9-11], overlap of hydrated ions[12], polarization of water molecules by surface dipoles[13-15], and the formation and rupture of surface hydrogen bonds[16]. The authors of the review measured the short range repulsive force between two silica surfaces in the presence of 1 M NaCl (AFM) and compared this to the various theoretical models. The authors concluded, based on fits to the experimentally measured force, that the model of rupturing hydrogen bonds best describes the short range repulsive force. It is interesting that three of the five models predicted a longer range force than was measured experimentally. This suggests the possibility that there may be an error in the distances measured in AFM force measurements. Since it has been shown that EW-AFM can be used to directly measure the separation in AFM measurements, I have decided to re-examine hydration forces with improved distance measurements.

The purpose of the work presented in this chapter is to test the generality of the mechanism of the hydration force presented by Pashley. The test system is the forces measured between a silicon nitride tip and a glass substrate in solutions containing ions of Group I metals using EW-AFM.[17] Both the glass and silicon nitride have Si-OH groups at the solid liquid interface, and therefore present a more symmetric case for studying hydration forces than the mica/silica work of Higashitani.[6] In addition, the evanescent wave AFM is used to verify whether or not a layer of hydrated ions is actually displaced from between a tip and surface during a force run. The EW-AFM allows us to determine whether the AFM tip approaches to a smaller separation in the absence of metal ions (as on mica). This will be conducted using a solution containing no salt (HCl solution) as a control for the closest tip-sample separation. Subsequent scattering curves in the presence of hydrated cations will be compared to this HCl control. A strongly bound layer of cations would result in a scattering intensity in “contact” in the presence of salt with a smaller value than that measured in the HCl solution. The direct consequence of a salt layer which is not excluded between the tip and sample is a force-separation profile shifted to shorter separations. This would complicate comparison of experiment to theory.

Based on results presented in Chapter 3, I will assume that a refractive index change associated with a thin ordered layer of water or a layer of salt does not affect the scattering decay length of the evanescent wave, so the separation *h*, is simply

$$h = -\ln\left(\frac{I_h}{I_o}\right)\delta_{meas} \tag{5.1}$$

5.2 Materials and Methods

5.2.1 Experimental Method

The evanescent wave was created by a 405 nm (405-50-COL-004, Oxiuss, France) diode laser at the interface between a borosilicate glass plate (12-544-12 Fischer Scientific) and an aqueous solution. The borosilicate glass plate was separated from a borosilicate reflection prism by index matching fluid (Nye Optical, Fairhaven MA). The incident angle was approx 75°, so the decay length is approximately 53 nm. The scattering signal was collected by a Nikon LU Plan 50x/0.55NA objective and transferred to a Hamamatsu photomultiplier tube (H5784-20).

Fluid exchange during experiments was achieved by altering the Asylum cantilever mount to hold 2 lengths of PEEK tubing (Valco Instruments, Houston, Texas) in close proximity to the cantilever. This enables fluid exchange in a small capillary of liquid formed between the cantilever head and sample.

5.2.2 Experimental Materials

The silicon nitride tips (NP, Veeco, Santa Barbara, California) used in these experiments were cleaned under ultraviolet light (mercury lamp) prior to use. All solutions were prepared in water purified in an EasyPure UV system (Barnstead, Dubuque, Indiana); the water had a resistivity of 18.2 MΩ-cm and a surface tension of 72.3 mN/m. The borosilicate glass slides have an rms roughness of 0.26 nm over an area of 5 square microns. The glass slides were used immediately after they were cleaned in oxygen plasma for 45 seconds at 250 Torr, using a Plasma Prep II (SPI Supplies, West Chester, PA). Concentrated HCl was used as supplied (BDH, concentrated) to adjust the pH of solutions. All salts (LiCl, NaCl, KCl, and CsCl) were roasted at 500^{o}C for 6 hrs.

5.3 Results

5.3.1 Scattering and Force in HCl

Figure 5.1A shows the raw scattering signal captured from a silicon nitride tip approaching a glass surface in the presence of 1 mM HCl. At long range separations the scattering intensity is exponential with piezo displacement. When

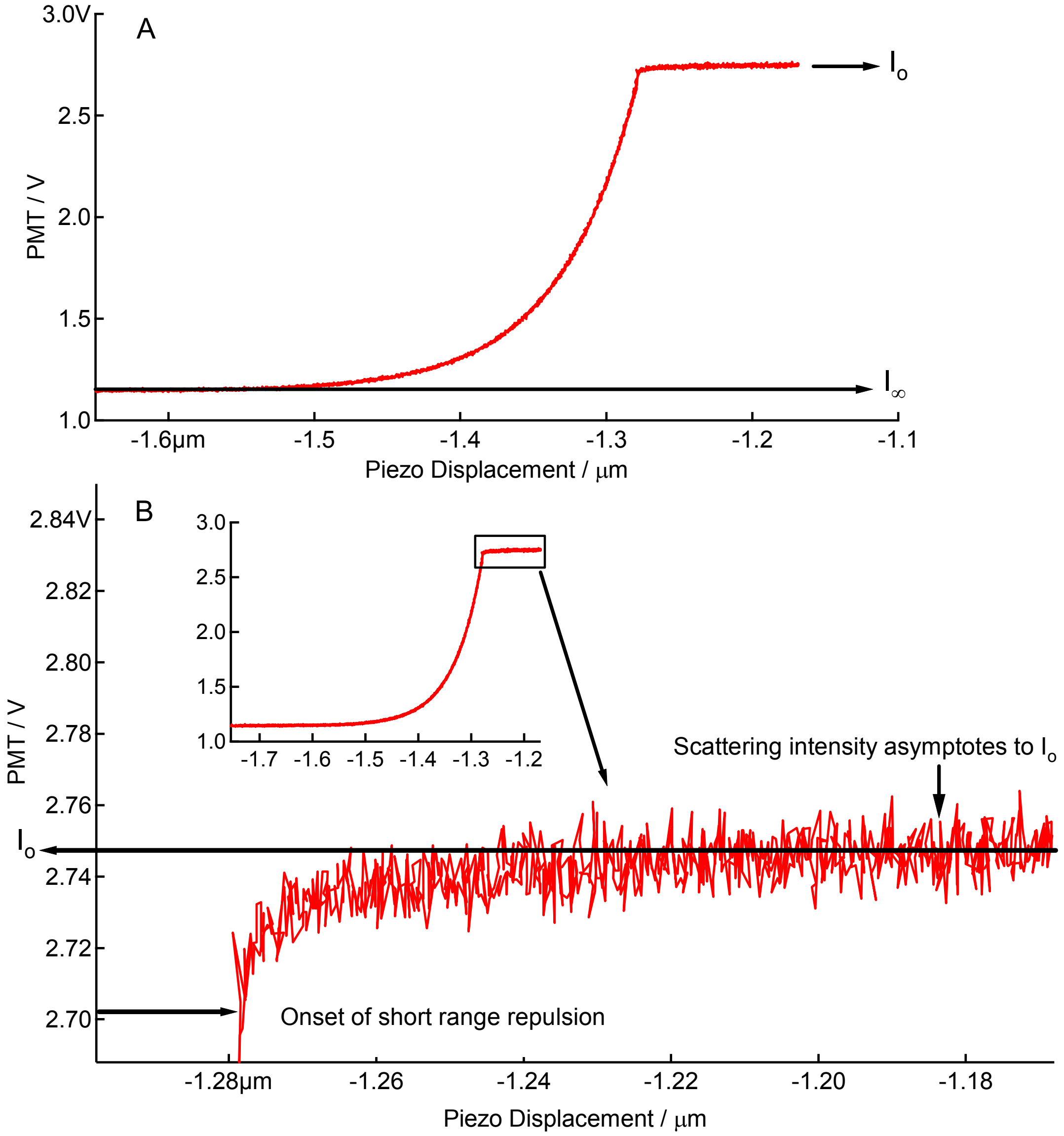

Figure 5.1. (A) Raw scattering from a Si_3N_4 tip in 1 mM HCl as a function of piezo displacement. (B) Scattering immediately before contact. The scattering intensity profile deviates from exponential as the short range force causes the tip to deflect away from surface. The scattering intensity then asymptotes to a constant value of I_o.

the tip is very close to the glass interface, the short range force causes the tip to deflect away from the surface, which results in a scattering intensity that is not exponential with piezo displacement. Figure 5.1B shows the short range scattering intensity asymptotes to an approximately constant value (this is used as the value of I_o for determining separation). After the tip and surface make hard contact the intensity should become constant. However, in some runs the scattering intensity has a very shallow gradient in intensity with piezo displacement, which confuses the true region of contact. One possible explanation of this effect is the movement of the tip across the glass plate into a region of different evanescent wave intensity, even while maintaining contact with the plate (the point of reflection where the evanescent wave is created has an intensity profile that reflects the laser source profile). Sliding or tilting is a necessity when a leaf spring of fixed length is pushed against a solid. The experiments reported in this chapter were conducted with a defocused beam to minimize this effect. Even after defocusing there were still gradients in the intensity in contact on some runs. In future work I will use less defocusing because defocusing reduces the intensity and therefore decreases signal to noise. It is noted that the slope is larger in some curves over others; it even varies on consecutive runs for the same experimental condition. Because of thermal drift, the tip contacts the sample at a slightly different position on each run and each position has a different roughness, so this suggests the intensity slope is due to compression of asperities on the sample under high load.

Figure 5.2 compares the force-separation profile determined by traditional AFM analysis and by scattering analysis of the forces between a hydrophilic glass and silicon nitride surface in 1mM HCl (same data as figure 5.1, the separation determined by scattering analysis has been averaged over ten points). The scattering analysis did not use the deflection data at all. The cantilever deflection used in the scattering curve was obtained from the difference between the piezo displacement and the tip translation (as measured by equation 5.1, demonstrated in chapter 3). This was done because forces are so large that (a) non-linear responses

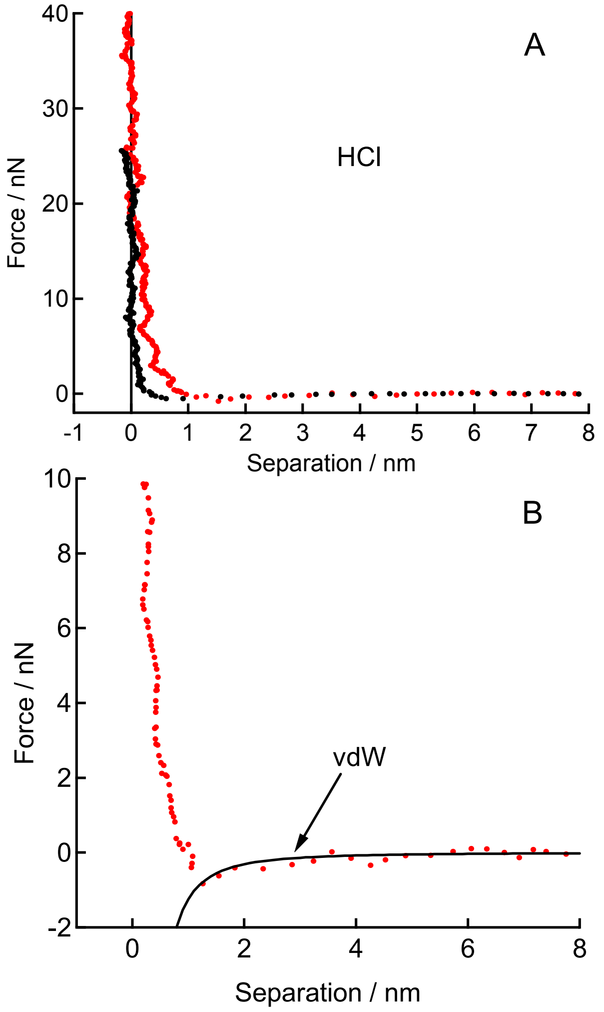

Figure 5.2. Force between a Si_3N_4 tip and a glass substrate in 1 mM HCl. (A) The separation was determined by traditional AFM analysis (black) and by scattering analysis (red). (B) The attractive vdW force has been fit to the data using a radius of 360 nm and the known Hamaker constant beteen silicon nitride and glass of 2.07×10^{-20}.

in the photodiode are common, and (b) the response of the photodiode to cantilever deflections can often go off scale. Scattering data is still being collected in regions where deflection output irregularities occur.

Both AFM analysis and scattering analysis show a force that is purely attractive at separations greater than 1 nm, and the force becomes repulsive at short range separations. The scattering analysis of separation (figure 5.2A, red) shows that at approximately 0.8-1 nm, the force becomes repulsive, and the magnitude of the repulsive force continues to increase as the separation between the tip and surface decreases. At a loading force of approximately 20 nN, the tip stops approaching the surface (scattering intensity vs. piezo displacement is approximately linear, with zero slope) and the separation remains constant as the cantilever chip continues to approach the surface. The withdrawal curve (not shown) overlays the approach curve at all separations. Figure 5.2B shows the attraction between the tip and surface, with a vdW's fit using a tip radius of 360 nm and Hamaker constant (*H*) of $2.07\text{x}10^{-20}$.[18]

$$F_{vdW} = -\frac{RH}{6h^2} \tag{5.2}$$

This is not a reasonable radius for these tips (R ~ 60nm). The fact that the attractive force is so large suggests the attraction may due to electrostatics. However, due to noise is the scattering signal, it is difficult to determine if the force is exponential with distance.

The scattering analysis of separation indicates that the short range repulsive force is slightly longer ranged than the separation obtained by traditional AFM analysis. The discrepancy between the two will be discussed in the next section.

5.3.2 Scattering and Force in Salts

We seek to answer three questions in this section. First, is there a thin layer of metal cations still bound between the AFM tip and surface at high loads? This is scientifically interesting, but also interesting from an instrument development perspective. Such a layer would not be detected by traditional AFM analysis because the region of constant compliance becomes the region of zero separation. This will be answered by comparing the zero of separation intensity without ions in solution, to solutions containing metal cations. Second, is the layer of ions very gradually pushed out and therefore traditional AFM analysis cannot be used to measure the stiffness of the layer? And finally, does the force depend on the type of metal cation?

It is assumed that the scattering intensity in contact in a solution of 1 mM HCl represents the closest possible tip sample separation. This does not necessarily mean that water has been completely excluded from between the tip and surface. I have measured the intensity in contact in HCl as a function of time. This measurement gives both the stability of the scattering signal, and the value of I_o to be used when a salt solution is present between the two surfaces (reference method). Figure 5.3 shows the average intensity of I_o measured over 100 seconds is 7.68 ± 0.016 V (black). Immediately after this measurement, the HCl was exchanged with 1 M KCl (the tip remains in contact during exchange). Once the KCl has been added, the tip is withdrawn and brought back to the surface. The raw scattering profile for this is shown in figure 5.3 (red curve). The scattering intensity in contact after the tip has re-approached the solid substrate is 7.69 ± 0.013 V, and thus the separation is the same as that measured in the presence of HCl (black). It can be concluded from this that a layer of adsorbed potassium ions, if present, is as easily desorbed as a layer of H_2O/H^+.

Figure 5.4 compares the force-separation profile as determined by traditional AFM analysis and scattering analysis in 1M KCl solution. The value of I_o measured in HCl solution was used to determine the separation by scattering

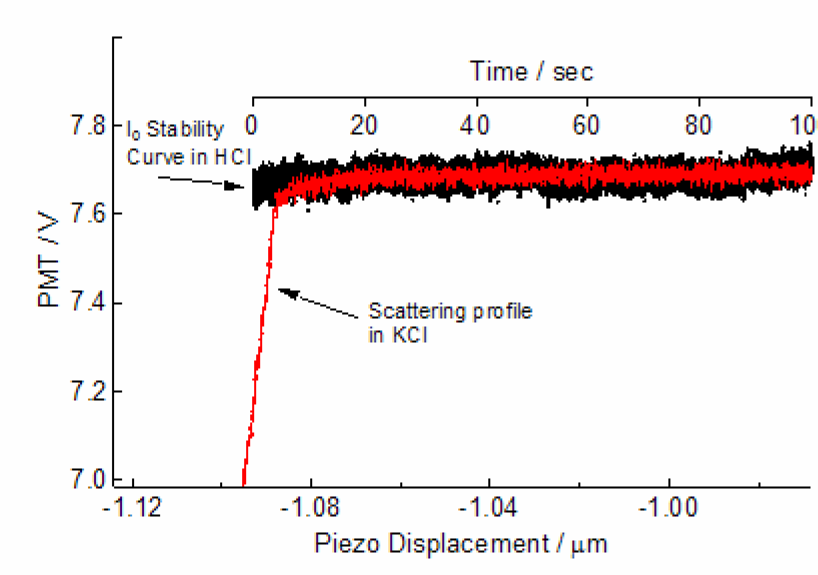

Figure 5.3. Raw scattering intensity vs. time for a tip left in contact for 100 seconds in HCl (black). Raw scattering intensity vs. piezo displacement in the presence of 1 M KCl (red). The salt curve (red) is run immediately after the HCl has been exchanged for the KCl. The scattering intensity in contact (red) is the same as the HCl curve (black). The salt has been completely excluded from between tip and surface.

analysis in the presence of KCl. The separation determined by scattering analysis is determined using equation 5.1 and a decay length measured at long range separations (between 20-100nm, $\delta_{measured}$ = 56.2nm) using the separation obtained by traditional AFM analysis. Again, the scattering analysis suggests that the short range repulsion is of a slightly longer range than by traditional AFM analysis.

For the force-separation profiles determined by traditional AFM analysis, I have chosen to assume that the scattering data is not available when determining the region of constant compliance. In figure 5.4 you will notice that the region of constant compliance I chose makes the average separation zero, in the range of 3-30 nN. At higher loads the separation is negative suggesting that the surface is deforming (the scattering data shows this is not the case). I have also reanalyzed the data using the deflection data from the time when the scattering intensity was

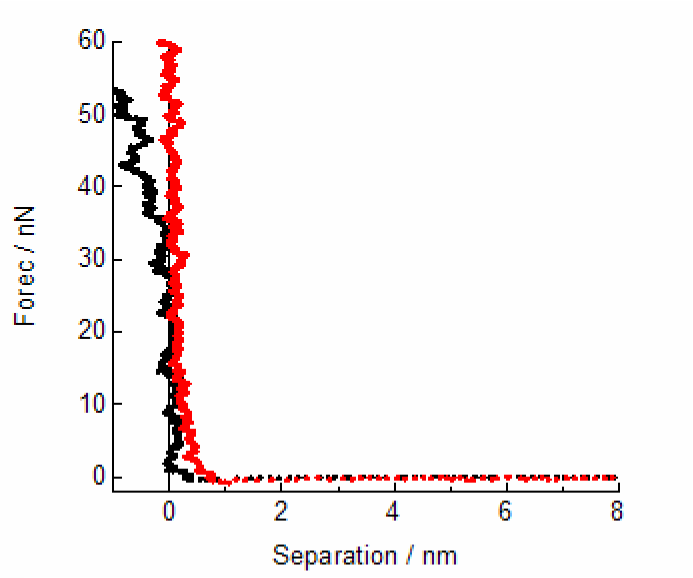

Figure 5.4. Force vs. Separation between a Si_3N_4 tip (k = 0.58 N/m) and glass substrate in the presence of 1 M KCl. The separation was determined by traditional AFM analysis (black) and scattering analysis (red).

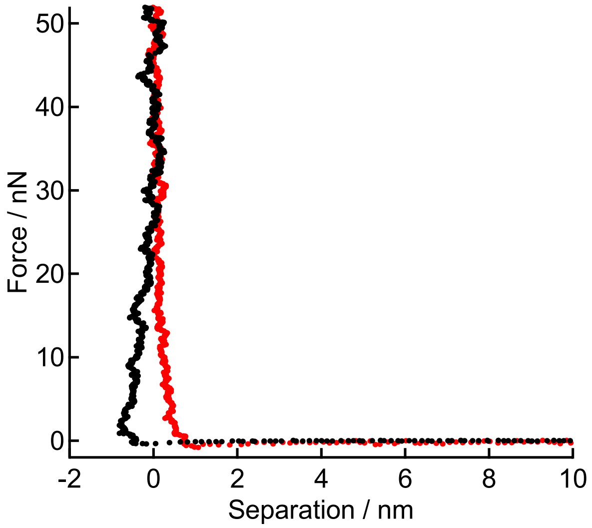

Figure 5.5. Data from figure 5.4 using the range of constant scattering intensity for the range of the region of constant compliance. The black line is the AFM data and the red is the scattering.

constant for my region of constant compliance. This is shown in figure 5.5. It is obvious from this figure, that my original determination of the region of constant compliance gives a more reasonable result. This result in figure 5.5 is unphysical because it does not give a unique value to the force at each separation. This error arises because of an uncalibrated non-linear response of the photodiode to cantilever deflection. Based on this result, I will from here on only present force-separation profiles determined from scattering analysis of separation.

The force measured in solutions of HCl, and salt solutions containing lithium, sodium, potassium, and cesium are shown in figure 5.6. The procedure for measuring the force in the salt solutions was conducted in the following manner. The starting solution between the tip and substrate was 1 mM HCl. The solution was exchanged for 1 M NaCl, and a force-separation profile was

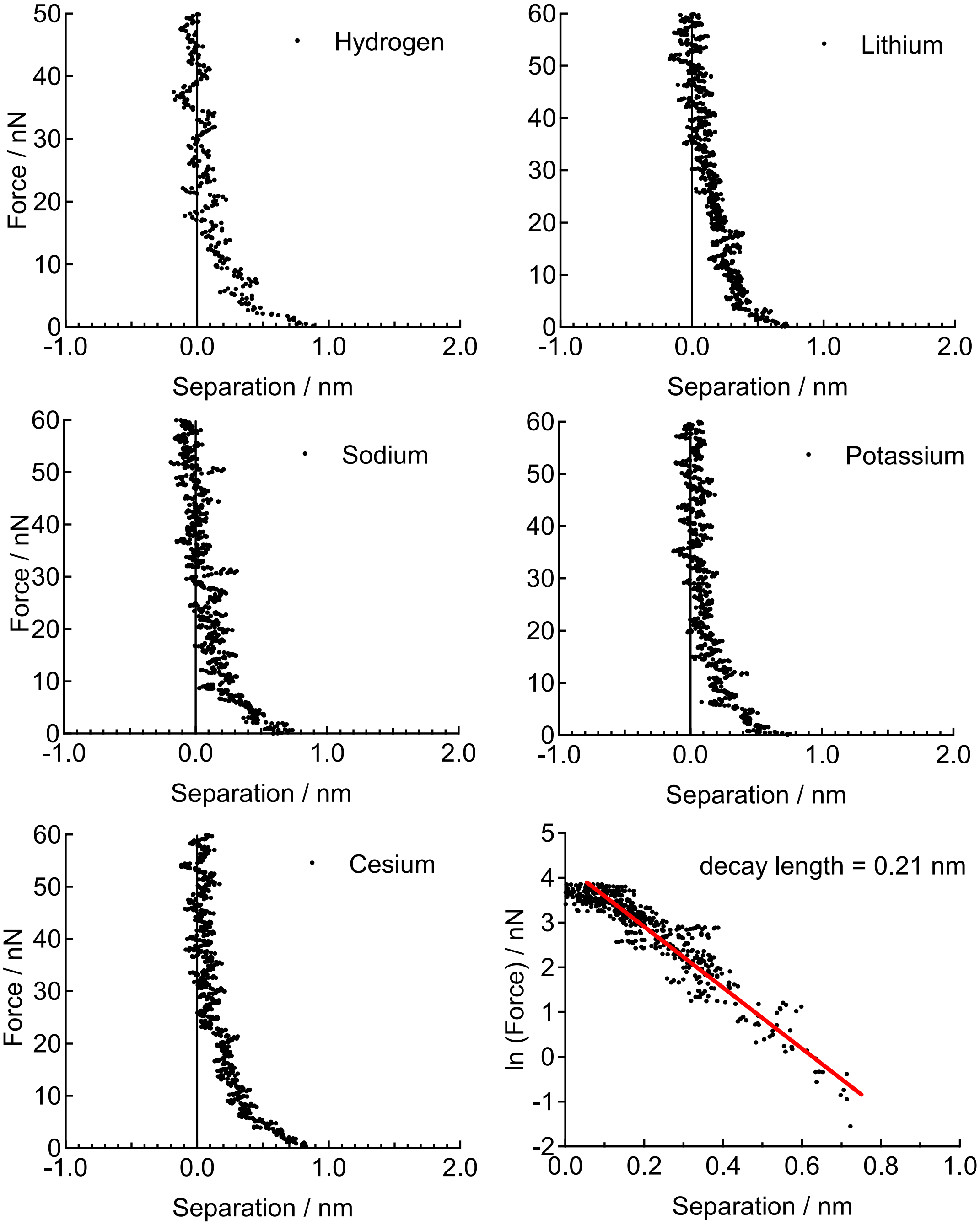

Figure 5.6. Forces measured between a Si_3N_4 tip (k = 0.58 N/m) and a glass substrate in metal chloride solutions. The last plot shows the force is approximately exponential, with a decay length of 0.21 nm.

measured. The solution was then exchanged with 1 M solutions of LiCl, KCl, and finally CsCl. At each exchange the force-separation profile is determined. The last part of figure 5.6 is the force between 0 and 0.8 nm in the presence of CsCl plotted on a natural log scale. The force is approximately exponential with a decay length of 0.21 nm.

Each salt shows a short range repulsion on approach. The force for each salt is similar. This is demonstrated in figure 5.7, which shows the short range repulsion with hydrogen, lithium and cesium superimposed. Figure 5.8 shows the withdrawing curve in the presence of LiCl and KCl, (forces in CsCl and NaCl are similar).

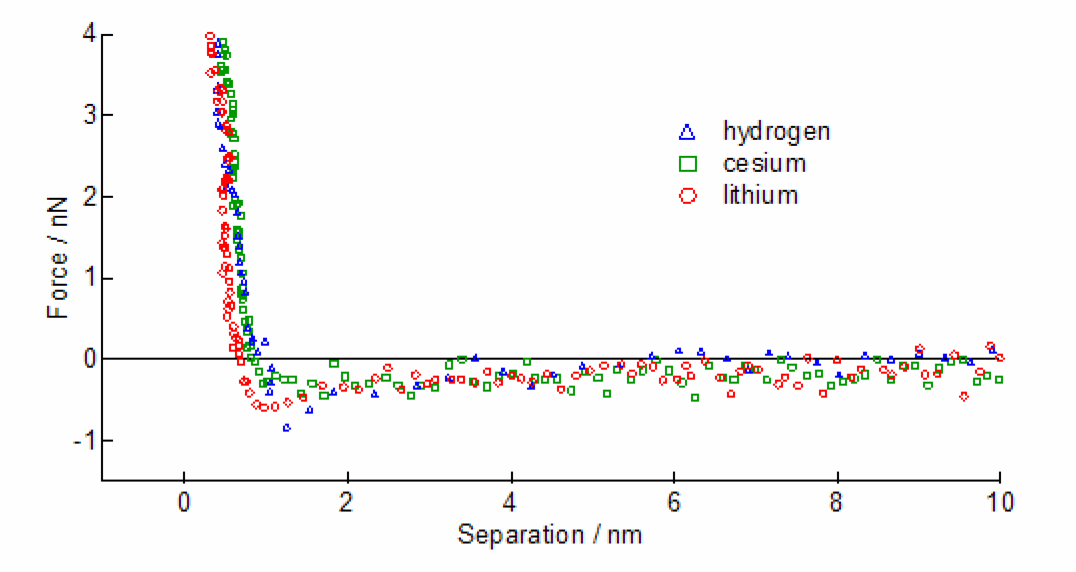

Figure 5.7. Comparison of the short range force in HCl (blue), LiCl (red), and CsCl (black).

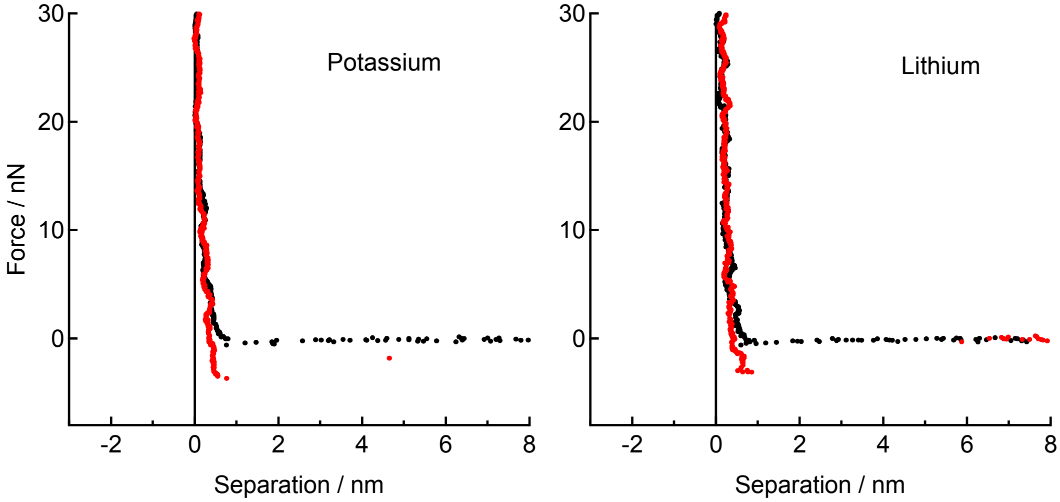

Figure 5.8. Approach (black) and withdrawal (red) curves for potassium and lithium. The withdrawal shows a slight adhesion. Sodium and cesium show similar adhesions. There is no adhesion measured in HCl solutions.

5.4 Discussion

These results confirm the existence of a short range repulsion between two hydrophilic surface in solution. The force does not depend on the ion in solution for 1M solutions of Group I metal chlorides. This suggests the force may be due to water structure or the properties of the glass or silicon nitride. It is reasonable to assume that the structure of water at a solid-liquid interface would be influenced by a dense layer of adsorbed hydrated ions, so I think that the disruption of an ordered water layer is an unlikely mechanism. The surface properties of glass and silicon nitride are less likely to be influenced by the ion in solution. The short range repulsion in this system is therefore likely due to the roughness of the surfaces, or a silica gel layer at the solid liquid interface.

One way in which we can model a gel layer is as a series of silica chains tethered to the solid, i.e. a polymer brush. Both experimental measurements and theory show that a polymer brush produces a force that is approximately exponential with separation, according to the following equation.[19]

$$F = 2\pi R\left[\frac{100kT}{\pi s^3}\exp\left(\frac{-\pi h}{L}\right)\right] \tag{5.2}$$

Where R is the radius of the tip, s is the spacing between polymer chains, h is the separation, and L is the length of the polymer chain. This equation is valid for surfaces with low surface coverage of polymer, and when the separation is less than 2 times the length of the polymer chain. According to equation 5.2 the length of the polymer chain that would give a decay length of 0.21 nm as observed in our experiments is ~0.66 nm. Using a silicon-oxygen bond length of 0.16 nm[20], these results are consistent with a polymer chain with approximately 3 units ($-Si(OH)_2-O-$).

It is important to note that an exponentially decaying force does not prove the short range interaction is due to compression of a polymer film. The force could also be described by elastic deformations of surface asperities at the glass-liquid or silicon nitride-liquid interface. In the limit of very small asperities this is the same mechanism as the compression of polymer chains, so it is difficult to distinguish the mechanism.

Evanescent wave scattering by the AFM tip shows that an adsorbed salt layer can be displaced by the AFM tip, which should lead to a match between the separation determined by traditional AFM analysis and the scattering analysis of separation. However, the force-separation profile determined by traditional AFM analysis is consistently shorter ranged than the scattering analysis (the magnitude of the difference is not always the same). The discrepancy is caused by an onset of constant compliance at a piezo displacement that is shorter ranged than the piezo displacement needed to achieve a constant value of the scattering intensity, I_o. The question is why is there a region of constant compliance when the tip is still approaching the surface? This result could be accounted for if a material or object is present on one, or both surfaces, which behaves as a simple spring (short polymer chain or surface asperity). A second spring (which obeys Hooke's law) in series with the cantilever would result in a region of constant compliance, while the tip is still approaching the rigid solid. The region of constant compliance is defined when the change is piezo position ΔP equals the distance moved by the two springs in series.

$$F = k_1 \Delta X_c = k_2 \Delta X_s \tag{5.3}$$

$$\Delta P = \Delta X_c + \frac{k_1}{k_2} \Delta X_c \tag{5.4}$$

Where ΔX_c is the distance moved by the cantilever, ΔX_s is the distance moved by a surface spring, and k_1 and k_2 are the spring constants of the cantilever and surface. By traditional AFM analysis, this region will become the zero of separation, even while the tip is still approaching the rigid underlying substrate.

Future work in this area should focus on making the system more symmetric, and increasing the area of interaction. The silicon nitride tip can be coated with a layer of silicon oxide by electron beam deposition, and colloid probes with glass particles can be attached. In addition studies on the concentration of the salt should be conducted.

5.5 Conclusions

The evanescent wave atomic force microscope was used to study the short range repulsive interactions between hydrophilic surfaces. For the glass-solution-silicon nitride system, there is a short-ranged (< 1nm) repulsive force and a long-ranged attraction in excess of the vdW's force. The short range repulsion does not depend on the type of cation in solution or if the cation is even present. This result, in addition to the difference between traditional analysis and scattering analysis of separation suggests the short-range force is due to a property of the solids. Finally I have shown that an error in separation determined by traditional AFM analysis can go unaccounted for without a secondary measure of the separation between surfaces.

5.6 Cited Literature

1. Pashley, R. M., Hydration Forces between Mica Surfaces in Aqueous Electrolyte Solutions. *J Colloid Interface Sci* **1981,** 80, (1), 153.
2. Israelachvili, J.; Pashley, R. M., Molecular layering of water at surfaces and origin of repulsive hydration forces. *Nature* **1983,** 306, 249-250.

3. Chapel, J. P., Electrolyte Species Dependent Hydration Forces between Silica Surfaces. *Langmuir* **1994,** 10, (11), 4237-43.
4. Vigil, G.; Xu, Z.; Steinberg, S.; Israelachvili, J., Interactions of silica surfaces. *Journal of Colloid and Interface Science* **1994,** 165, (2), 367-85.
5. Horn, R. G.; Smith, D. T.; Haller, W., Surface Forces aand Viscosity of Water Measured Between Silica Sheets. *Chemical Physics Letters* **1989,** 162, 404-408.
6. Higashitani, K.; Ishimura, K., Evaluation of interaction forces between surfaces in electrolyte solutions by atomic force microscope. *Journal of Chemical Engineering of Japan* **1997,** 30, (1), 52-58.
7. Valle-Delgado, J. J.; Molina-Bolivar, J. A.; Galisteo-Gonzalez, F.; Galvez-Ruiz, M. J.; Feiler, A.; Rutland, M. W., Hydration forces between silica surfaces: Experimental data and predictions from different theories. *Journal of Chemical Physics* **2005,** 123, (3), 034708/1-034708/12.
8. Marcelja, S.; Radic, N., Repulsion of interfaces due to boundary water. *Chemical Physics Letters* **1976,** 42, (1), 129-30.
9. Jonsson, B.; Wennerstrom, H., *J Chem Soc Faraday Trans 2* **1983,** 79, 19.
10. Kjellander, R., On the image-charge model for the hydration force. *Journal of the Chemical Society, Faraday Transactions 2: Molecular and Chemical Physics* **1984,** 80, (11), 1323-48.
11. Attard, P.; Patey, G. N., Continuum Electrostatic Interactions Between Planar Lattices of Dipoles and the Possible Relevance to the Hydration Force. *Phys Rev Lett A* **1991,** 43, 2953-2962.
12. Paunov, V. N.; Kaler, E. W.; Sandler, S. I.; Petsev, D. N., A Model for Hydration Interactions between Apoferritin Molecules in Solution. *Journal of Colloid and Interface Science* **2001,** 240, (2), 640-643.
13. Manciu, M.; Ruckenstein, E., Oscillatory and Monotonic Polarization. The Polarization Contribution to the Hydration Force. *Langmuir* **2001,** 17, (24), 7582-7592.
14. Manciu, M.; Ruckenstein, E., Role of the Hydration Force in the Stability of Colloids at High Ionic Strengths. *Langmuir* **2001,** 17, (22), 7061-7070.
15. Ruckenstein, E.; Manciu, M., The Coupling between the Hydration and Double Layer Interactions. *Langmuir* **2002,** 18, (20), 7584-7593.
16. Attard, P.; Batchelor, M. T., A mechanism for the hydration force demonstrated in a model system. *Chemical Physics Letters* **1988,** 149, (2), 206-11.
17. Clark, S. P.; Walz, J. Y.; Ducker, W. A., AFM Colloid-Probe Measurements with Explicit Measurement of Particle-Solid Separation. *Langmuir* **2004,** 20, 7616-7622.
18. Bergstrom, L., Hamaker constants of inorganic materials. *Advances in Colloid and Interface Science* **1997,** 70, 125-169.
19. de Gennes, P. G., Polymers at an interface; a simplified view. *Adv. Colloid Interface Sci.* **1987,** 27, 189.
20. Warren, B. E., The Diffraction of X-Rays in Glass. *Phys Rev* **1934,** 45, 657-661.

Chapter 6

Summary

6.1 Summary

If we introduce an object with a refractive index contrast to the transmission medium of an evanescent wave, that object will scatter the evanescent wave. This thesis is an attempt to determine absolute changes in separation between an AFM probe and an interface, by observing changes in scattering intensity. The intensity of an evanescent wave in the absence of a probe is an exponential function of distance and is also a function of the refractive index. The traditional view has treated the scattering of evanescent waves by colloidal particles as directly proportional to the evanescent wave itself at all separations. I have shown in this thesis that this is not always the case for colloidal particles. I find that the scattering profile for objects of at least 1 micron in radius, attached to AFM cantilevers, is approximately fitted by a double exponential; where the long range scattering decay length can be described by the evanescent wave decay and the short range scattering decay depends on the radius of the particle. While this does not invalidate the use of scattered evanescent light as a useful tool, it does significantly complicate the analysis and suggests that TIRM work should be re-examined. Fortunately, I have found that the scattering profile generated from silicon nitride tips does depend directly on the decay length of the evanescent wave.

The first obvious application of scattered evanescent light was to measure the refractive index between two materials, which requires that the separation between the two objects be known. For rigid samples, traditional AFM analysis can be used consistently and reliably to measure the relative separation between a scattering tip and surface. I have demonstrated that the scattering of an evanescent wave, by an AFM tip, can be used to measure the bulk refractive index of a solution with a resolution of least 0.004. This technique was also used to measure separation-dependent changes in refractive index. I have directly measured the condensation of an organic material between two hydrophobic surfaces, which caused a long-range attraction. The fact that an organic material, when condensed between two microscopic hydrophobic surfaces, can cause a long-range attractive force is not a new experimental conclusion. The fact that I did not have to assume it was an organic material, or perform secondary experiments to infer that is was, is new to AFM measurements.

If the refractive index of the medium between a scattering object and surface is known (and assumed to be independent of separation) then the scattering intensity can be used to measure the absolute separation between a Si_3N_4 AFM tip and surface. This separation measurement was applied to AFM force measurements in the presence of an irreversibly adsorbed polymer film. A measure of the scattering intensity in contact prior to the adsorption of a polymer film is all that is required to know the absolute separation between the tip and surface at all subsequent times after the adsorption of a film. Direct contact between the tip and sample is no longer necessary. Although this was only shown for an AFM tip, this method should also apply to a colloid probe. This would require a calibration curve of the scattering as a function of separation obtained prior to film formation.

In addition to polymer studies, the scattering from an AFM tip was used to measure the absolute separation between hydrophilic surfaces in the presence of group I metals. These results confirmed the existence of a short-range force that did not depend on the salt between surfaces, or on whether the salt was present at all. The short-range repulsion (in these specific experiments) is therefore more likely due to the roughness of the surfaces, or a gel-like layer of silica at the solid liquid interface. These results also show that traditional AFM analysis can lead to errors in absolute separation and even the shape of the force-separation curve. This may be the reason for discrepancies in published results and perhaps incorrect conclusions on the mismatch between theory and experiment.

The obvious disadvantage of EW-AFM is the lack of a simple relationship between scattering intensity from colloidal particles and the intensity of the evanescent wave; or a theory that satisfactorily describes the profile. Despite this limitation, it is clear that new information can be obtained on the forces that exist between surfaces by observing scattered evanescent light. The work presented in this thesis has demonstrated that the evanescent wave atomic force microscope is a useful tool that can be used with the same precision as the atomic force microscope, with increased versatility in determining the separation and refractive index between surfaces.

6.2 Future Work

EW-AFM would be greatly enhanced if rigorous models were available to predict the scattering profile from tips in contact with solids coated with films or tips partially immersed in regions of phase separation. With these models, it may be possible to pursue work in proximity-induced phase separation studies. In addition, a model for predicting the scattering profile of spherical particles with varying radii would be particularly helpful.

Research will continue on the studies of hydration forces with the aim of deducing whether or not a polymeric material or surface asperity is the cause of the short-range force in the silicon nitride-glass system. In addition, more symmetric systems will be studied, and the effect of varying salt concentrations will also be looked at.

Finally, a dual beam EW-AFM has been designed and is being fabricated with applications for simultaneous measurement of the scattering profile for two wavelengths and two angles of incidence.